12-2002

Martian Xenon Components in Basaltic Shergottite Meteorites

Katherine Delene Ocker Stone
University of Tennessee - Knoxville

To the Graduate Council:

I am submitting herewith a dissertation written by Katherine Delene Ocker Stone entitled "Martian Xenon Components in Basaltic Shergottite Meteorites." I have examined the final electronic copy of this dissertation for form and content and recommend that it be accepted in partial fulfillment of the requirements for the degree of Doctor of Philosophy, with a major in Geology.

Harry Y. McSween, Major Professor

We have read this dissertation and recommend its acceptance:

Jamie D. Gilmour, Norbert Thonnard, Larry A. Taylor, Claudia L. Mora

Accepted for the Council:
Carolyn R. Hodges

Vice Provost and Dean of the Graduate School

(Original signatures are on file with official student records.)

To the Graduate Council:

I am submitting herewith a dissertation written by Katherine Delene Ocker Stone entitled "Martian Xenon Components in Basaltic Shergottite Meteorites." I have examined the final electronic copy of this dissertation for form and content and recommend that it be accepted in partial fulfillment of the requirements for the degree of Doctor of Philosophy, with a major in Geology.

Harry Y. McSween
Major Professor

We have read this dissertation and recommend its acceptance:

Jamie D. Gilmour

Norbert Thonnard

Larry A. Taylor

Claudia L. Mora

Acceptance for the Council:

Anne Mayhew
Vice Provost and Dean of Graduate Studies

(Original signatures are on file with official student records)

MARTIAN XENON COMPONENTS IN THE BASALTIC SHERGOTTITE METEORITES

A Dissertation Presented for the

Doctor of Philosophy Degree

The University of Tennessee, Knoxville

Katherine Delene Ocker Stone

December 2002

DEDICATION

This dissertation is dedicated to my parents, Darrell and Carrie Ocker, my husband, Chris Stone, my sisters, Dorothy Stillman and Vickie Hutchins, and the rest of my family, for giving me the desire, support and constant encouragement to overcome the obstacles in my path and achieve my goals.

ACKNOWLEDGEMENT

I wish to thank Dr. Jamie Gilmour for giving me the opportunity to work with him at the University of Manchester and his support in completing my Doctor of Philosophy in Geological Sciences. I thank Dr. Hap McSween for accepting the challenge of taking a physicist and turning her into a geochemist. I thank Dr. Norbert Thonnard for introducing me to the exciting world of resonance ionization and its research applications as well as generous financial support through a Graduate Research Assistantship by the Institute for Rare Isotope Measurements, funded in part by NASA Grants No. NAGW-4774 and NAG5-3464. I thank Dr. Larry Taylor and Dr. Claudia Mora for serving in my committee. I wish to acknowledge financial support through a Graduate Teaching Assistantship by the Department of Geological Sciences.

I wish to thank my family and friends, whose suggestions and encouragement made this work possible. I like to thank my mother, Carrie Ocker, for instilling in me the stubbornness to reach my goals. I thank my husband, Chris Stone, for supporting me through it all and still loving me even when things were rough. I thank the rest of my family for always being there with love, understanding and that extra push. I thank Rachel Lentz, Karen Stockstill, Valerie Slater, Josh Cahill, Alli Busfield, Vera Fernandes, Greg Holland, and Charles Joyner for their friendship, discussions and suggestions and help in this work. I thank Len Singleton, Clay and Jacene England, Adam and Tristy Berryhill, Ron Woo, and all my other friends for their encouragement and support.

ABSTRACT

Analyses of Chassigny, Nakhla, and ALH84001 reveal, in addition to a Xe component from the martian atmosphere, a second component loosely attributed to the martian "interior." This appears to be a mixture of solar- and fission- (^{244}Pu) derived xenon components. The proportions are consistent in each meteorite but vary from meteorite to meteorite. The working hypothesis is that this variation reflects different contributions of solar (mantle-derived) and fission (crustal-derived) xenon to each parent melt.

This study focused on mineral separates from two basaltic shergottites, Shergotty and EETA79001 Lithology-B (EETA), chosen to reflect, as far as possible, the extremes of crustal assimilation in the parent melt. Xenon analysis was performed revealing martian interior and atmospheric components. Of the mineral separates examined, the opaque phases in both meteorites have higher atmospheric gas concentrations than maskelynite and pyroxene separates. This is attributed to the adsorption of atmospheric gas on the grains and then shock implantation. The opaques, the smallest mineral phases in the meteorites, provided the most surface area and thus resulted in higher gas concentration.

The interior component is best defined in the pyroxene separates of both meteorites. This interior component is attributed to ambient xenon trapped upon crystallization of the mineral. The ^{129}Xe excess (^{129}Xe/^{132}Xe ~ 1.2) in the interior component of Shergotty is described as admixture of martian atmosphere to the melt,

while this component is absent for EETA. The fission-derived xenon of the two meteorites varies in that Shergotty has a higher $^{136}Xe^*$ concentration than that observed in EETA.

A model was constructed to reflect the isotopic evolution of xenon in the martian mantle, crust, and atmosphere during planetary differentiation, outgassing and atmospheric loss. An atmosphere is produced with elevated $^{129}Xe_{xs}/^{130}Xe$ and low radiogenic xenon to excess xenon ratio ($^{136}Xe^*/^{129}Xe_{xs}$), along with two interior reservoirs, one consisting of solar xenon with little or no radiogenic xenon and one with a high ratio of fissiogenic $^{136}Xe^*/^{130}Xe$ and a low $^{129}Xe_{xs}/^{136}Xe^*$ ratio. These latter ratios are qualitatively similar to those required to produce the interior components of the shergottites.

TABLE OF CONTENTS

LIST OF FIGURES

LIST OF TABLES

CHAPTER I

INTRODUCTION

Martian Meteorites

The meteorites historically referred as SNC's (*S*hergotty, *N*akhla, *C*hassigny), are petrologically diverse yet share a common parent body. The most compelling evidence for this is that the meteorites define a unique oxygen-isotope fractionation line that is displaced from the terrestrial mass fractionation line (Clayton and Mayeda, 1983; Franchi et al., 1999). Chemical fingerprints indicative of a common body, such as ratios of Fe/Mn, K/La, Co/(MgO + FeO) and Ni/Mg, are also consistent with this view (Dreibus and Wanke, 1985). These elements tend not to fractionate from each other during igneous processes; therefore, their ratios remain constant even though their absolute element abundances may change. The meteorites are a grouping of diverse igneous rocks: shergottites (basalts, gabbros and lherzolites), nakhlites (clinopyroxenites-wehrlites), Chassigny (dunite), and ALH84001 (orthopyroxenite).

The original suggestion that the SNC meteorites originated from Mars was based on their late crystallization ages and the difficulty of accounting for igneous activity on an asteroid-size body so late in solar system history (McSween, 1984 and references therein). This argument is based on the insulating capacity of large bodies, which could have retained heat from the decay of long-lived radioisotopes. Thus, crystallization ages of 1.3 Ga (nakhlites and chassignites) to 180 Ma (the suggested age for Shergotty) for

most SNC meteorites argue that the meteorites formed on a large parent body (but not specifically Mars). ALH84001 has a crystallization age of 4.5 Ga, and thus may represent an ancient sample of the parent body (Nyquist et al., 2001).

More definitive evidence matching the SNC meteorites to Mars was provided by the agreement between the isotopic and elemental compositions of gases trapped in shock-melted glass in the EETA79001 shergottite and the Viking measurements of the martian atmosphere (Becker and Pepin, 1984; Bogard and Johnson, 1983). Additional studies on the trapped component demonstrated that the molecular/atomic abundances and isotopic compositions of ^{20}Ne, ^{84}Kr, ^{36}Ar, ^{40}Ar, ^{132}Xe, N_2, and CO_2 accurately (to within the precision afforded by the Viking measurements) matched the martian atmosphere (Bogard et al., 2001 and references therein). Subsequently, shock experiments have demonstrated that ambient gases can be implanted during impact without elemental or isotopic fractionation (Bogard et al., 1986; Wiens and Pepin, 1988).

With the belief that these meteorites are martian rocks, we are provided with the possibility of extracting geologic information and history of this planet. Table I-1 lists the four distinct petrologic groups (shergottites, nakhlites, Chassigny, and ALH84001) and associated martian meteorites currently identified. Recent studies in the understanding of martian xenon components in Chassigny, nakhlites and ALH84001 have identified xenon components previously not described. The aim of this work is to determine and understand better the location of these martian xenon components, derived from the atmosphere and various "internal" sources (mantle and/or crustal), present in the

Table I-1. The SNC meteorites and respective petrologic grouping.

Shergottites		Nakhlites	Chassignites	ALH84001
Basaltic	**Lherzolitic**			
Shergotty	Allan Hills 77005	Nakhla	Chassigny	Allan Hills 84001
Zagami	Lewis Cliff 88516	Lafayette		
Los Angeles 001, 002	Yamato 793605	Governador Valadares		
Queen Alexandra Range 94201	Grove Mountains 99027	Yamato 000593, 000749		
Elephant Moraine 79001	Yamato 1075	Northwest Africa 998		
Dar al Gani 476, 489, 735, 670, 876		Northwest Africa 817		
Sayh al Uhaymir 005, 008, 051, 094, 060, 090				
Dhofar 019				
Dhofar 378				
Northwest Africa 480				
Northwest Africa 856				
Northwest Africa 1068, 1110				
Northwest Africa 1195				

shergottites. Furthermore, I will attempt to account for how these components came to be trapped, in the context of accepted models of crystallization and subsequent history for martian meteorites.

Basaltic Shergottites

The largest grouping of martian meteorites is the shergottites, which are subdivided into two lithologies: basalts and lherzolites. The basaltic shergottites are the focus of this study.

Basaltic shergottites are relatively fine-grained and predominantly consist of the clinopyroxenes pigeonite and augite (prisms up to 1 cm long) with lath-like and interstitial vitreous maskelynite, which was transformed from plagioclase by shock (Duke, 1968). Lesser amounts of titanomagnetite, ilmenite, pyrrhotite, whitlockite, and accessory apatite, quartz, baddeleyite, fayalite and mesostasis make up the rest of the meteorite (Smith and Hervig, 1979; Stöffler et al., 1986; Stolper and McSween, 1979). Most exhibit a foliated texture produced by preferential orientation of pyroxene prisms and maskelynite grains (Duke, 1968; Mikouchi et al., 2001; Stolper and McSween, 1979). The suggested crystallization history started with crystallization of homogeneous, Mg-rich pigeonite and augite grains. Next, the crystallization of Fe-rich pyroxene rims onto the magnesian pigeonite and augite cores occurred along with the interstitial, zoned plagioclase. The remaining trapped melt continued to crystallize, forming accessory phases and mesostasis (McSween, 1994).

Whole-rock Rb-Sr, U-Th-Pb and Hf-W data for shergottites suggest that martian global differentiation, including core formation, occurred near 4.5 Ga. and was, for the most part, concurrent with the completion of accretion (e.g. Halliday et al., 2001). This is consistent with planetary accretion models having time scales on the order of 100 Ma (Wetherill, 1986). The Rb-Sr, Pb-Pb and U-Pb systematics reflect a two-step evolution of the martian meteorite reservoir, the first being the ~4.5 Ga differentiation and the second a magmatic event that only slightly changed the Rb/Sr (Jagoutz, 1991). This necessitates a radioactive element-enriched crust (Breuer et al., 1993) and depleted mantle. Unlike the Earth where convective mixing has homogenized the mantle, variations of light rare Earth element (LREE) depletions observed in the martian meteorites indicate that Mars mantle source regions preserved ancient heterogeneities (Jagoutz et al., 1994).

The crystallization ages of the shergottites lie in the range of ~165-475 Myr (Nyquist et al., 2001). These young crystallization ages for meteorites were one of the first lines of evidence of their origin from a planetary sized body (McSween and Stolper, 1979; Nyquist et al., 1979a; Wasson and Wetherill, 1979). Unfortunately, earlier results showed discordant ages and showed considerable scatter about the best-fit isochron, leaving speculation about ~165 Myr age interpretation. The ambiguous Rb-Sr and ^{39}Ar-^{40}Ar ages were initially argued to be the result of resetting events such as thermal or shock metamorphism (Bogard et al., 1979; Nyquist et al., 1979b). However, it has been established that neither post-shock metamorphism nor shock transformation of mineral phases are adequate to reset these isotopic systems (Nyquist et al., 2001). Shih *et al*.

(1982) plotted several different shergottite whole-rock Sm-Nd data and interpreted the relation as an apparent isochron age of ~1.3 Gyr that agreed with the ages of the nakhlites (Shih et al., 1982).

However, a more favorable scenario suggests the relationship of the shergottites may represent a mixing between different mantle and/or crustal reservoirs on Mars (Jones, 1989; Longhi, 1991). The isotopic mixing model interprets the linear alignment of the Nd data as due to mixing more radiogenic Nd from the martian mantle with less radiogenic Nd from the martian crust and that the 1.3 Gyr is a coincidence (Jones, 1989; Longhi, 1991). Further results for the Nd isotopic compositions and other REE abundances in the shergottites also suggests a mixture between two sources – one component identified with the depleted martian mantle and one, relatively enriched in LIL elements, tentatively associated with the martian crust (Borg et al., 1997; Jones, 1986; Norman, 1999). The redox state of the meteorites additionally suggests a two-source mixture (Herd et al., 2001; Wadhwa, 2001). In each case Shergotty exhibits a higher contribution from the crustal component as seen in Figure I-1 (Herd and Papike, 2000). Shergotty has higher oxygen fugacity (close to the quartz-fayalite-magnetite oxygen buffer curve reflecting an evolved component) and lower epsilon neodymium ($\varepsilon_{Nd} \sim -7$, Jones, 1986) compared to QUE94201, which has oxygen fugacity close to iron-wüstite buffer (Herd and Papike, 2000) and ε_{Nd} of 0.92 ± 0.11 (Borg et al., 1997). The goal of this study is to seek evidence of such mixing in the xenon isotopic systematics of these meteorites.

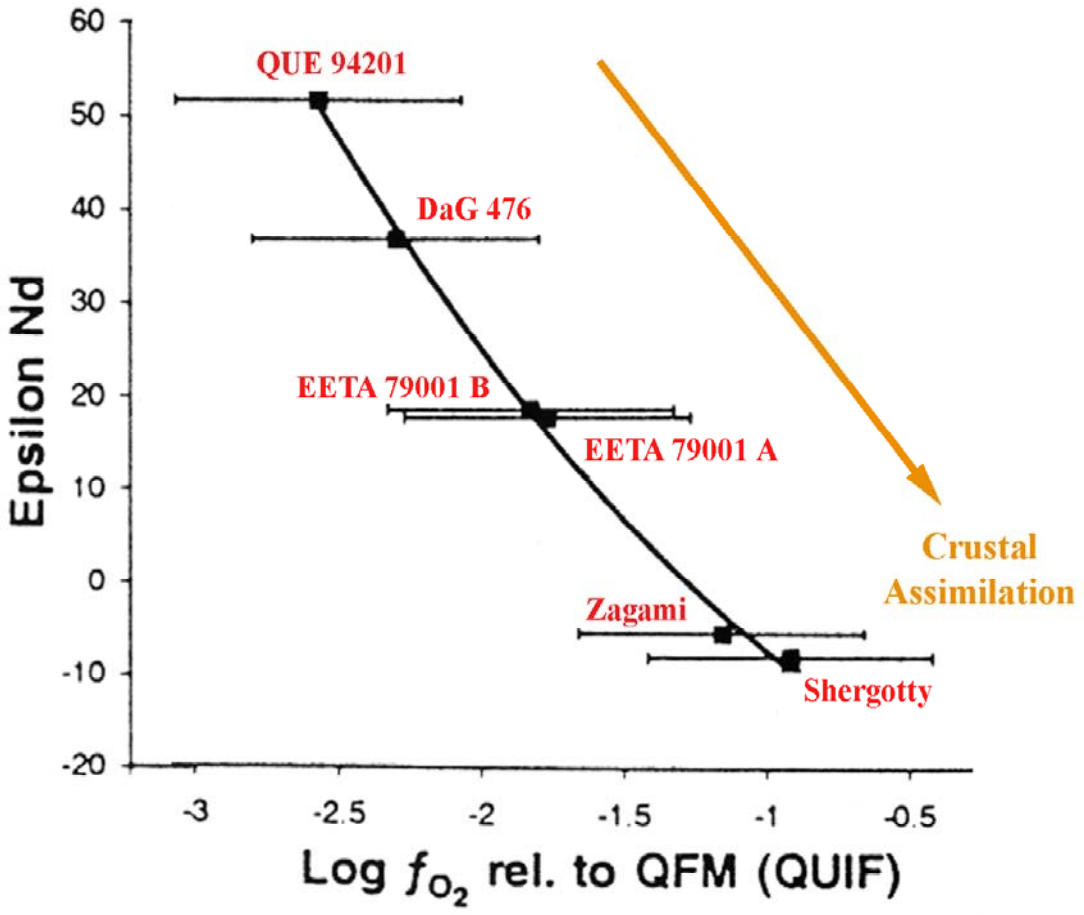

Herd C. D. K. and Papike J. J. (2000)

Figure I-1. The relationship of oxygen fugacity to epsilon neodymium for some of the known basaltic shergottites. Isotopic variations of neodymium and the redox state of the meteorites suggest a mixture between two sources – one component identified with the depleted Martian mantle and one, relatively enriched in LIL elements, tentatively associated with the Martian crust (Borg et al., 1997; Jones, 1986). This has lead researchers to believe that Shergotty crystallized from magma source that has more crustal contamination than that observed in QUE94201.

Noble Gases in SNC Meteorites and the Evolution of Martian Atmosphere

Noble gases are highly useful because of their low concentration in terrestrial and extraterrestrial rocks and their consequent susceptibility to isotopic modification through nucleogenic effects. Noble gas research is one of the most important means of determining the age of the atmosphere, the degree of degassing of the mantle and the sources and timing of fluid flows responsible for the secondary alteration of rocks here on Earth. Noble gases have already played a major role in the recognition of Mars as the parent body of the SNC meteorites. By analyzing the martian meteorites, similar advances in understanding the preserved record of interactions between atmosphere, hydrosphere and lithosphere on Mars, including the origin of the atmosphere and the timing of its collapse, may be achieved (Pepin, 1994).

Several groups have reported krypton and xenon measurements for the SNC meteorites (refer to figure text for references). Unique patterns of the trapped noble gases found in the SNC meteorites show that the gas concentrations as well as elemental abundance ratios differ from meteorite to meteorite (e.g. Ott, 1988). As previously discussed, a component found trapped in shocked glass of shergottite EET79001 is elementally and isotopically identical to the present-day martian atmosphere, as measured by Viking. Because better analytical precision is possible in the laboratory, this trapped component is now used to define the martian atmospheric signature (Becker and Pepin, 1984; Bogard and Johnson, 1983; Swindle et al., 1986). A second component is found in the dunite Chassigny and is thought to represent the martian interior (Ott, 1988). This

component has the isotopic signature of solar xenon and its presence in a mantle rock has led to its association with the martian interior (mantle). This, in part, mirrors terrestrial findings of noble gases that have shown a preservation of near-solar isotopic signatures (Dixon et al., 2000; Honda et al., 1993), although a solar xenon component has yet to be identified in the Earth's interior. The $^{36}Ar/^{132}Xe$ (~5) and $^{84}Kr/^{132}Xe$ (~1.1) elemental ratios measured in this mantle component represent a heavily elementally fractionated solar system reservoir (Mathew and Marti, 2001).

Martian heavy noble gas components are illustrated in Figure I-2, which plots $^{129}Xe/^{132}Xe$ ratios versus $^{84}Kr/^{132}Xe$ ratios. The martian atmospheric signature of EET79001 shock glass has elevated $^{129}Xe/^{132}Xe$ and $^{84}Kr/^{132}Xe$ compared to solar. The mantle component identified in the dunite meteorite Chassigny has a solar $^{129}Xe/^{132}Xe$ ratio accompanied by an $^{84}Kr/^{132}Xe$ ratio of ~1. This is noteworthy since it shows that drastic elemental fractionation has occurred with no detectable effect on the isotopic signature, possibly due to an equilibrium process. Shergottite bulk compositions, except for one analysis of Zagami (Ott et al., 1988), define an array that is broadly consistent with a mixing between the martian atmosphere and a interior/mantle endmember (e.g. Ott, 1988). Nakhlites and analyzed samples of ALH84001 broadly define a second mixing line between an interior/mantle component and an elementally fractionated martian atmosphere, krypton being depleted relative to xenon (Ott et al., 1988). The nakhlites differ from ALH84001 by a lower $^{84}Kr/^{132}Xe$ ratio.

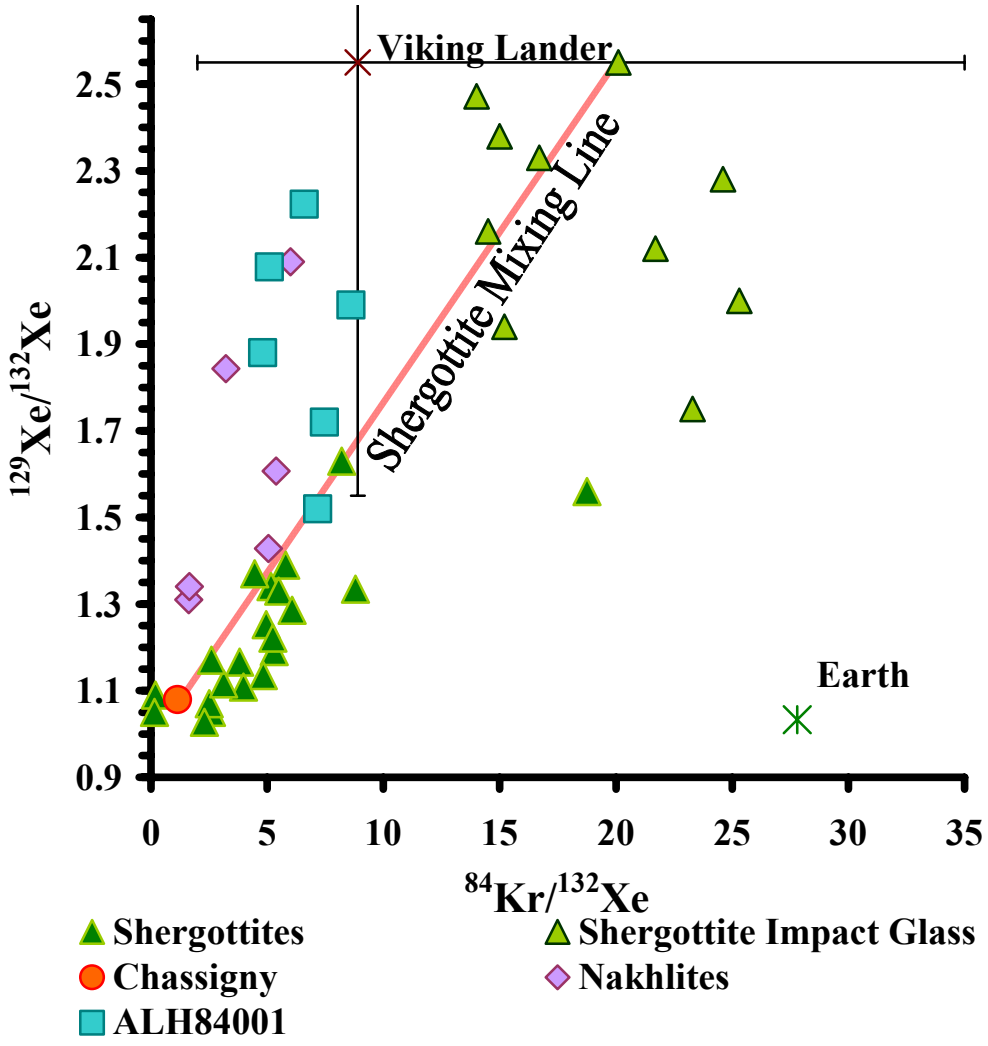

Figure I-2. $^{84}Kr/^{132}Xe$ *vs.* $^{129}Xe/^{132}Xe$ for some SNC meteorites. Most shergottites define a mixing between Martian interior (Chassigny) and Martian atmosphere (EET79001-Glass) as seen in this graph. Falling off this mixing line are the nakhlites and ALH84001 due to mass fractionation or the possible existence of a third high $^{129}Xe/^{132}Xe$ reservoir (see text for further discussion). Impact glass shows a mixing of a component identified in crushed samples that yield a low $^{129}Xe/^{132}Xe$ ratio (Ott, 1988). Data is from literature (Bart et al., 2001; Becker and Pepin, 1984; Bogard and Garrison, 1998b; Bogard et al., 1984; Drake et al., 1994; Garrison and Bogard, 2000; Miura et al., 1995; Mohapatra and Ott, 2000; Murty and Mohapatra, 1997; Ott, 1988; Ott and Lohr, 1992; Ott et al., 1988; Owen et al., 1977; Ozima and Pososek, 1983; Swindle et al., 1986; Swindle et al., 1995; Swindle et al., 1989; Swindle et al., 2000; Terribilini, 2000; Wiens, 1988).

There are several models to account for the origin of this elementally fractionated component. Direct incorporation of atmospheric gases into martian weathering products with fractionation controlled by water solubility has been suggested (Bogard and Garrison, 1998a; Drake et al., 1994), though this is now demonstrably false since this component is not dominated by gas associated with weathering products in either Nakhla or ALH84001 (Gilmour et al., 1998b; Gilmour et al., 1999). Gilmour et al. (1998) suggested a mechanism involving adsorption of atmospheric gases onto mineral surfaces followed by shock implantation to account for the component in ALH84001, and adopted to account for that in the nakhlites (Gilmour et al., 2001; Swindle et al., 2000). A third interpretation implies the variation is not a result of fractionation before or in the process of incorporation into the rock. Instead the variation reflects actual differences in the Kr/Xe ratio of the martian atmosphere at the time of the incorporation of the meteorites and that the varying elemental composition of the martian atmosphere results from temperature-controlled variations in partitioning of the global atmospheric into carbon dioxide clathrates in the polar caps of Mars (Musselwhite and Swindle, 2001). As of yet, no such clathrates have been identified, so this model remains speculative.

The nature of the martian atmosphere component in the martian meteorites has provided invaluable constraints on models of the evolution of the martian atmosphere. These generally require partial loss of the planetary atmosphere either very early in Mars' history or over extended geological time. Most models (Jakosky and Jones, 1997; Pepin, 1991, 1994) attribute the mass-dependent isotopic fractionation of xenon observed in the present-day martian atmosphere to hydrodynamic escape prior to 4.0 Ga ago. This

process also resulted in the complete loss of all noble gases lighter than xenon. The light noble gases in the atmosphere today then represent subsequent outgassing from the crust or mantle and/or were produced by decay of radiogenic elements. ALH84001, which in contrast to the other young martian meteorites is a sample of the ancient martian crust, is believed to contain a sample of the ancient martian atmosphere. This xenon component has a lower $^{129}Xe/^{132}Xe$ ratio than the present-day martian atmosphere, suggesting that outgassing of ^{129}Xe from ^{129}I decay from the crust to the atmosphere was incomplete when the component was trapped. More controversially, Mathew and Marti (2001) argue that this xenon component is isotopically unfractionated, suggesting that the hydrodynamic escape that 'set' the fractionation of xenon isotopes in the modern atmosphere had yet to occur. The observations clearly restrict models of the ancient atmosphere of Mars (Gilmour et al., 1998b; Mathew et al., 1998; Murty and Mohapatra, 1997). The $^{129}Xe/^{132}Xe$ ratio of the trapped component is lower than that of the present-day martian atmosphere, thus suggesting the trapped gas sampled the atmosphere, at least 4 Ga before the xenon isotopic ratios had evolved to their present values (Gilmour et al., 1998a). Further outgassing of the atmosphere is due to atmospheric erosion by impacts, sputtering, and photochemical escape to produce the present martian atmosphere (Jakosky and Jones, 1997; Pepin, 1991, 1994; Swindle and Jones, 1997).

The particular interest in this proposed work is the relationship between $^{136}Xe/^{132}Xe$ ratios and $^{129}Xe/^{132}Xe$ ratios as shown in Figure I-3. This graph shows the processes that evolve solar xenon to the present-day accepted xenon signature of the martian atmosphere identified in the glass phase of EET79001 (Becker and Pepin, 1984;

Podosek and Huneke, 1971). These processes include the decay of ^{129}I (16 Ma half-life) to ^{129}Xe, fission of ^{244}Pu and ^{238}U producing ^{136}Xe, and mass fractionation resulting from dissolution, crystallization, and other physical processes. This proposed work builds on more recent data in an attempt to decipher the evolution of the martian xenon components.

Martian Evolution of Xe Components

Several models that have been suggested to describe the isotopic evolution of martian xenon components (Pepin, 1994; Swindle and Jones, 1997; Swindle and Kring, 1997). Swindle and Jones (1997) utilized solar wind xenon as the primordial martian Xe and demonstrated an atmospheric evolution model that considered martian geochemical evolution and degassing history. This model showed that the martian atmosphere could be derived from mass fractionated solar xenon with an addition of fission Xe from ^{244}Pu and ^{238}U and ^{129}Xe from ^{129}I decay. Although ^{129}I decays with a half life of 16 Ma, contrasting with ^{244}Pu half life of 82 Ma, elemental fractionation during the formation of the crust and control of atmospheric evolution by rates of degassing of crustal reservoirs means that the order of the processes – isotopic fractionation, outgassing of iodine, and outgassing of fission products – is not well constrained. The ancient atmospheric signature identified in ALH84001 is enriched in ^{129}Xe from iodine decay but isotopically unfractionated and has little or no ^{244}Pu fission xenon (Mathew and Marti, 2001). This reflects the build up of ^{129}Xe before ~4.0 Ga ago when ALH84001 was shocked on the surface of Mars. The development of interior xenon evolving to atmospheric xenon includes three processes: 1) chemical fractionation--the differentiation of Pu and I into

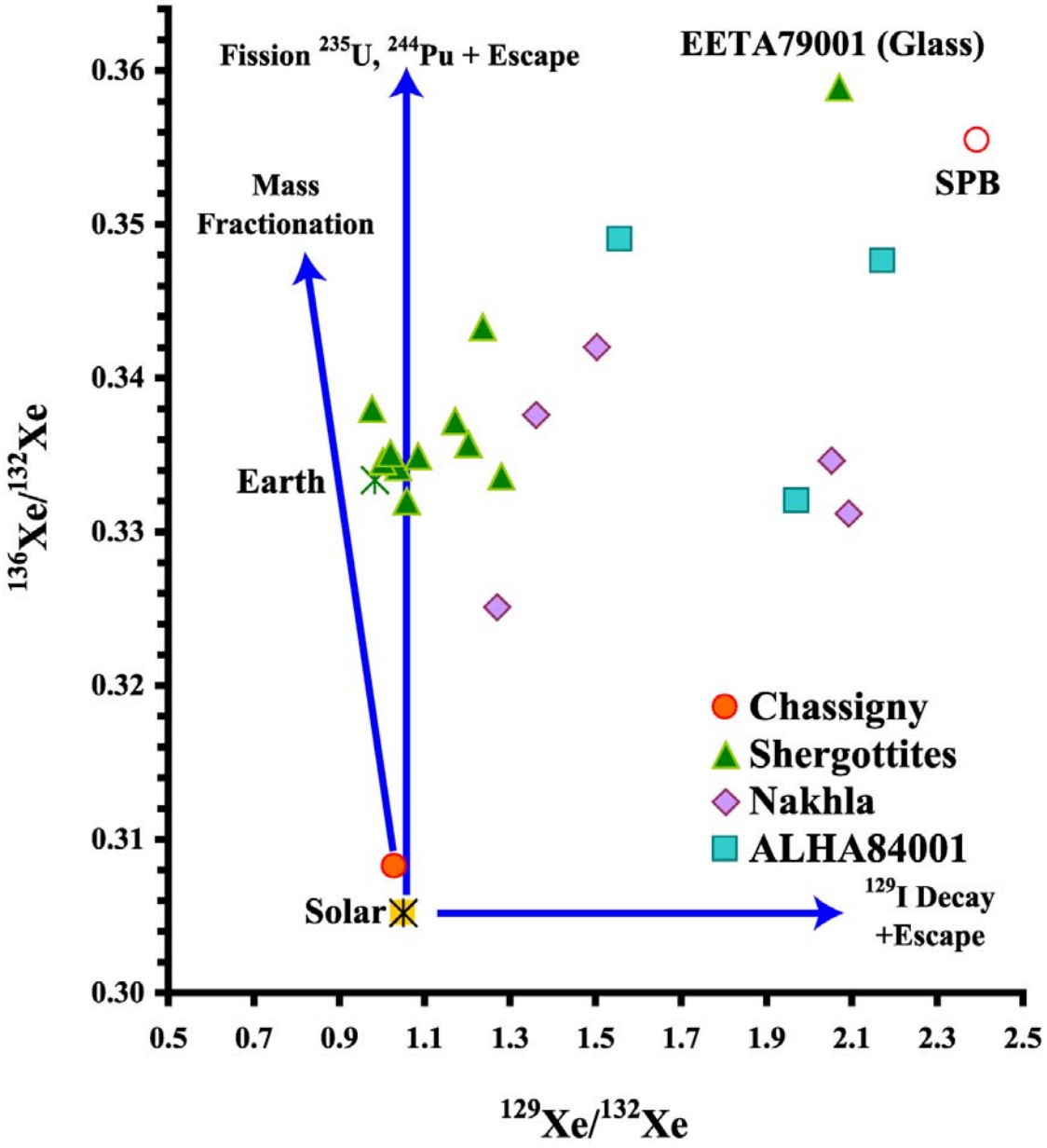

Figure I-3. The $^{136}Xe/^{132}Xe$ ratio *vs.* $^{129}Xe/^{132}Xe$ ratio for some SNC meteorites. SPB (Swindle, 1986) represents the Martian atmosphere component while Chassigny represents the Martian mantle component because of its similarity to solar xenon (Podosek et al., 1971). The arrows show the processes that evolve solar xenon, mass fraction (M. F.), ^{129}I decay plus escape and ^{244}Pu and ^{235}U fission plus escape. Data is from literature (Becker and Pepin, 1984; Gilmour, 2000b; Murty and Mohapatra, 1997; Ott, 1988; Swindle et al., 1986; Swindle et al., 1995; Terribilini, 2000).

the crust, 2) in situ decay--^{129}I half-life = 16 Ma, ^{244}Pu half-life = 80.8 Ma and ^{238}U half-life = 4.47 Ga, and 3) outgassing of the crust to the atmosphere--possibly released by impacts or another mechanism to regenerate the surface. Using published isotopic data, possible evolution path(s) of the martian atmosphere is illustrated in Figure I-4.

In trying to understand martian evolution, researchers are trying to understand the possible different xenon reservoirs. The solar component is suggested to originate from the mantle while geochemistry suggests Pu and I were concentrated in the crust. But how the different reservoirs and parent isotope half-lives interacted to produce the atmosphere is unclear. While investigating the early evolution of martian volatiles, Mathew and Marti (2001) described a new component in Chassigny. This component, Chass-E, has a similar ^{129}Xe/^{132}Xe ratio as the accepted martian interior component; however, its ^{136}Xe/^{132}Xe ratio reflects an addition of ^{244}Pu fission Xe. This defines an evolved uniform trapped signature and implies that the fission Xe component was well mixed with the solar Xe component, ruling out *in situ* decay of ^{244}Pu (Mathew and Marti, 2001). Chass-E xenon suggests a late entrapment and also different carriers than the solar-derived component. The estimated interior xenon components of ALH84001 and Nakhla also indicate various proportions of fission xenon mixed with solar xenon as shown in Figure I-4 (Mathew, 2000). It appears that the bulk analysis of the shergottites reflects a mixture between some solar (mantle?) plus fission (crustal?) interior components and modern martian atmosphere, but this interior component in the shergottites is not yet well characterized.

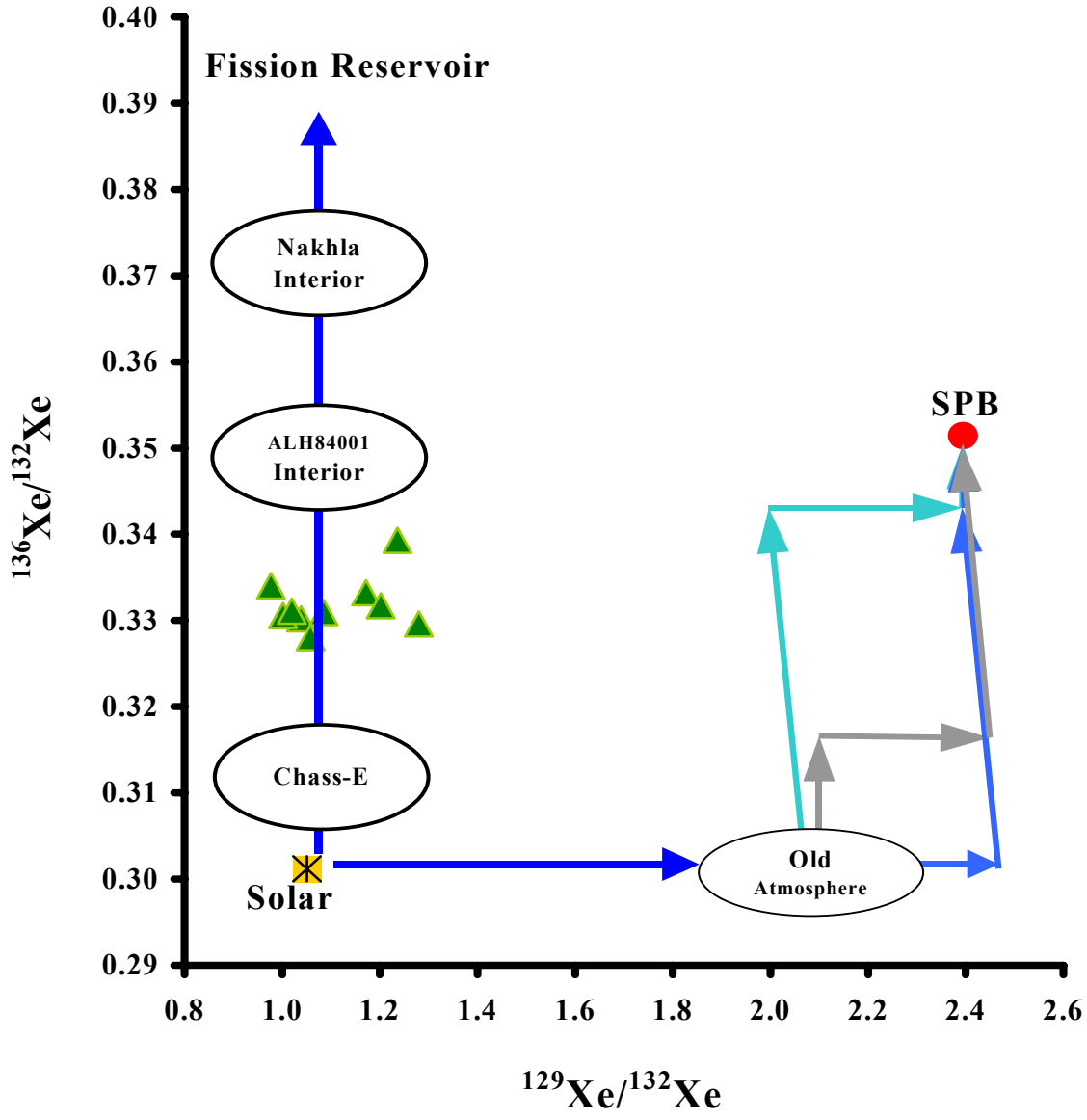

Figure I-4. Possible evolutions of solar xenon to the present day martian atmosphere, SPB. Unfractionated solar xenon found in ALH84001 is symbolized by Old Atm (Mathew and Marti, 2001). From this point, addition of various ^{129}Xe that escaped from the crust, ^{136}Xe from ^{244}Pu and escaped and mass fractionation occur (order unknown) to evolve the present day Martian atmosphere. The interior xenon components thus far identified for ALH84001, Chass-E, and Nakhla are shown as solar with various proportions of ^{244}Pu (Gilmour, 2000a; Mathew and Marti, 2001). Currently, the interior xenon component is poorly defined for the shergottites; published "bulk" samples of the shergottites are shown for comparison (Becker and Pepin, 1984; Ott, 1988; Swindle et al., 1986; Terribilini, 2000).

Present Work

The research here identifies the presence and sites of the xenon components in the basaltic shergottites.

With the laser probe and analyses of mineral and glass separates, a search for identifiably distinct martian components and location of these martian Xe component(s) was performed. The goal was to answer several questions:

- ✧ What are the host phases of the martian interior and atmospheric xenon?
- ✧ Does the interior xenon component identified support the model of a solar-derived "mantle" reservoir or "crustal" reservoir?
- ✧ Do the components appear as pure components or are they "mixed" and to what extent in individual host phases?
- ✧ How can the existence of the xenon component within its host phase be explained (trapped upon crystallization, assimilation, absorption, shock implanted, etc.)?
- ✧ What is the extent of fission contribution to the martian interior component in the shergottites? Is it consistent with ideas about a crustal contribution to the shergottite parent melt?

CHAPTER II

PRINCIPLES OF RESONANCE IONIZATION AND EXPERIMENTAL PROCEDURE

Principles and Operation of Resonance Ionization

Resonance ionization utilizes lasers tuned to specific atomic energy levels of a selected element and produces only ions of that element. Ionization is achieved by exciting the target species through one or more energy levels with laser light tuned to the transition frequencies, the final step being to the continuum directly or through an auto-ionizing state. Above a certain laser intensity, the ionization efficiency of the selected element becomes unity for atoms in the laser beam. Thus resonance ionization is potentially much more efficient than conventional methods such as electron bombardment, thermal ionization, or sputtering. In addition, as ionization depends on the presence of the resonant step or steps, interfering ions from the other major sample constituents are severely reduced or eliminated. This leads to significant improvements in the detection limits of minute quantities of a particular element in the presence of an overwhelmingly larger background (Payne et al., 1994). Utilizing a cryogenic sample concentrator, a static noble gas resonance ionization spectroscopy time-of-flight mass spectrometer (RIS-TOF) has demonstrated a detection limit of ~ 100 ^{85}Kr atoms (Thonnard et al., 1992). This results in an extremely fast analyzer, ~ 3 min. detection half-life versus ~ 60 min. for conventional systems. The short analysis time reduces the

effect of build up from out gassing in the mass spectrometer, which is one of the most important performance-limiting parameters for a static mass spectrometer.

This project employs the Refrigerator Enhanced Laser Analyzer for Xenon (RELAX) housed at the University of Manchester (Gilmour et al., 1994). This system, similar to and based on the RIS-TOF system originally housed at Atom Sciences and now under renewed development at the University of Tennessee (Appendix A), employs a laser tuned to a specific atomic energy level of xenon, thus producing only ions of xenon. This involves a two-photon excitation at 249.6 nm of the $^2P_{3/2}6p[1/2]_0(j_1l$ coupling) level of the xenon atom followed by a one-photon ionization at the same wavelength. The light at 249.6 nm is produced by a commercial system, Spectron Laser Systems SL803, based on a pulsed Nd:YAG laser. The fundamental light of the Nd:YAG (1064 nm) is frequency doubled (532 nm) to pump a dye laser (an oscillator and two amplifier cells using DCM) thus producing light in the 650 nm region. This light is then frequency doubled, and then mixed in a deuterated di-hydrogen phosphate crystal with residual light at the fundamental Nd:YAG wavelength to generate light in the 250 nm region. Varying the dye laser wavelength allows tuning to the precise wavelength needed for the xenon transition.

A 25 cm focal length lens (~22cm at 249.6 nm due to wavelength dependence of the refractive index) focuses the ionizing light into the ion source region of the time-of-flight mass spectrometer. To enhance the sensitivity of the spectrometer, a cryogenic sample concentrator, an idea conceived at Oak Ridge National Laboratory (Hurst et al., 1984), and refined on the system in Tennessee (Thonnard et al., 1984), creates a localized

cold spot in the source region of the mass spectrometer onto which the sample condenses. Immediately before the ionization laser is fired another laser pulse is directed onto the cold spot, heating it and releasing the sample into the ionization region of the spectrometer. This is provided by a small Q-switched Nd:YAG laser of 5 ns pulse duration and 3 mJ pulse energy, heating the cold spot. The delay between the two lasers is adjusted to optimize the concentration of sample in the ionization region at the arrival of the ionization laser in the spectrometer. After passing through the ion source, the ionizing laser pulse is detected by a photodiode that triggers the data acquisition system.

An einzel lens focuses the ions from the ion source region down a 65 cm flight tube onto a chevron-mounted microchannel plate detector. The output signal from the detector is passed through an x10 pulse amplifier and recorded on a digital oscilloscope sampling at 400 MHz. Flight times between 8.8 and 9.8 μs, the xenon region of the time spectrum, are monitored and signals from a sequence of laser shots are transferred to a personal computer and stored on disc.

Sample Preparation and Xenon Extraction

Sample Preparation

Untreated milligram-size samples that had not been exposed to water were requested for this work. Shergotty was received from the Natural History Museum, London, England, and EETA79001 Lithology-B was supplied from the meteorite group at Johnson Space Center, Houston, Texas. The main sample preparation needed was to physically divide identifiable mineral separates for individual xenon analysis. This was

accomplished in two ways: (1) creating major-element composition maps from thick sections of the sample that were then physically separated, and (2) using distinctive optical traits under reflective light to separate mineral grains micro to millimeter in size.

Thick sections (~100 μm) were prepared from portions of the samples taking care to use a dissolvable adhesive for mounting to glass slides. The thick sections were analyzed using the fully automated CAMECA SX-50 electron microscope at the University of Tennessee, which employs an accelerating voltage of 15 kV, a beam current of 20-30 nA and full ZAF (PAP) correction. Analysis provided major-element compositions (Ca, Al, Mg and Fe) maps through the use of backscatter images and EDS analysis. These provided confirmation of the different minerals present in the thick sections and determine where the thick section could be cut with a 100 μm-thick diamond saw to isolate individual minerals. After removing the carbon coating needed for electron microscope analysis by washing the sample with acetone, the thick section was removed from the glass slide. The sections were then cut and physically separated into "bulk" pyroxene, augite, pigeonite, and maskelynite.

Portions of the samples were crushed into millimeter size grains. The grains were then physically separated by hand picking the grains that were visually identified as dominantly consisting of pyroxene (yellow to light brown), maskelynite (clear glass) and opaques phases (black and with magnetite responding to a weak magnet). The categorization of the individual minerals grains was based on the dominant mineral phase present. A bulk sample from each meteorite sample was also separated for analysis.

Samples of maskelynite and pyroxene were further divided into subsamples and washed with 1% HCl for at least 19.5 hours to remove phosphates that could not be removed physically by hand. The acid solution removed from the grains was analyzed by ion chromatography to determine the weight percent of phosphate removed from the subsamples.

Xenon Extraction

Samples were loaded into the sample chamber of RELAX where laser stepped heating was performed. The chamber was evacuated and baked at ~200°C for at least 12 hours to remove terrestrial contamination. Upon cooling, the pressure in the sample chamber was allowed to reach the low 10^{-9} Torr regime before opening to the rest of the extraction line on RELAX.

The sample gas was extracted by use of a continuous wave Nd:YAG laser at its fundamental wavelength (1064 nm). The sample was illuminated for two minutes at constant power with an unfocused beam whose cross-section is larger than the sample diameter. Laser step heating temperatures can be estimated by assuming that radiated power was equal to the laser power (Gilmour et al., 1998b). During the laser heating of the sample, the sample chamber was exposed to a getter to remove evolved active gases. After an additional minute of gettering, the sample gas was admitted to the mass spectrometer and xenon isotopic analysis quickly followed. Upon removal of each sample, it was seen to have melted and flowed, so peak temperatures in excess of the

melting point of the mineral analyzed must have been achieved. Any samples not fully melted were returned to the sample chamber for further laser step heating.

Data Acquisition and Reduction

RELAX is a time-of-flight mass spectrometer. Data acquisition is triggered by the ionization laser pulse and proceeds for five minutes. Data acquired over 10 seconds (100 individual complete spectra) are summed to produce a composite spectrum. Thus, by summing 100 individual spectra, 30 consecutive summed spectra are generated in each five minutes of analysis. However, during the analysis, the measured $^{129}Xe/^{132}Xe$ ratio declines due to the build-up of the terrestrial atmosphere derived xenon in the isolated spectrometer. The isotopic signature and rate of build-up are measured during separate "spectrometer blank" analyses that intersperse sample data acquisition, and are used for data corrections. The data is transferred to a personal computer for calculation of abundances.

Data reduction is performed with a custom application (Gilmour et al., 1994) and is only briefly described here. Each summed spectrum is recorded and a sequence of peaks is fitted. These are spaced according to the masses of the xenon isotopes and the theoretical time-of-flight mass relationship; peak widths are assumed to vary with mass as predicted by the same theory. Amplitudes are free parameters of the fit, which accordingly produces a separate amplitude for each xenon isotope from each summed spectrum. These amplitudes are converted to relative abundances by ratioing to the abundance of a nominated reference isotope, which was ^{132}Xe in this project. The blank-

corrected evolution of these ratios with time (in the sequence of summed spectra) is used to determine the final analytical ratio for each analysis. The reference isotope is converted to an absolute gas amount by comparison with intervening analyses of a sample of air xenon, which is also used to correct for instrumental discrimination, including systematic variations due to changes in the laser pulse energy over the course of an analysis. The absolute peak height of the reference isotope is fitted with a simple decay curve and extrapolated to time zero. Errors in the isotope ratios are calculated from the distribution of the ratios of the summed spectra around the best-fit line from which the final ratio is determined. The error on the reference isotope is calculated assuming proportionality of error to the square root of abundance, and the errors in the remaining isotopic abundance are corrected accordingly.

CHAPTER III

MARTIAN XENON COMPONENTS IN SHERGOTTY MINERAL SEPARATES: LOCATION, SOURCES, AND TRAPPING MECHANISMS

This chapter is a modified version of a paper by the same name to be submitted to the journal *Meteoritics and Planetary Science* by Katherine D. Ocker and Jamie D. Gilmour.

My contributions to this paper include (1) the physical hand-picking of the sample, (2) the electron microprobe analysis, (3) the acid washing of sample grains, (4) the xenon data analysis and (5) most of the writing.

Abstract

Isotopic signatures and concentrations of xenon have been measured in Shergotty mineral separates by laser step heating. Martian atmosphere and 'martian interior' xenon are present, as is a spallation component. Martian atmospheric xenon is 5-10x more concentrated in opaque minerals (magnetite, ilmenite and pyrrhotite) and maskelynite than in pyroxenes perhaps reflecting grain size variation. This is shown to be consistent with shock incorporation. A component consisting of solar xenon with a fission contribution, similar to components previously identified in martian meteorites and associated with the martian interior, is best defined in the pyroxene-dominate separates. This component exhibits a consistent ^{129}Xe excess ($^{129}Xe/^{132}Xe \sim 1.2$). We suggest that

gas present in the melt, perhaps a mixture of interior xenon and martian atmosphere, was incorporated into the pyroxenes in Shergotty as the minerals crystallized.

Introduction

The basaltic shergottites exhibit correlated variations in rare earth element fractionation and isotopic systematics of neodymium and strontium suggesting a mixture between two sources; one component identified with the depleted martian mantle and one, relatively enriched in large ion lithophile elements, tentatively associated with the martian crust (Borg et al., 1997; Jones, 1986). The redox state of the meteorites also suggests a two-source mixture. In each case, Shergotty is a representative of the highest contribution from a crustal component. Shergotty has the highest oxygen fugacity (close to the quartz-fayalite-magnetite oxygen buffer curve reflecting an evolved component) and lowest epsilon neodymium ($\varepsilon_{Nd} \sim -7$, Jones, 1986) in contrast to QUE94201, the meteorite with the lowest crustal component, which has oxygen fugacity close to iron-wüstite buffer (Herd and Papike, 2000) and ε_{Nd} of 0.92 ± 0.11 (Borg et al., 1997). Our work is the first stage to seek evidence of such mixing in the xenon isotopic systematics of these meteorites.

Figure III-1 uses literature data to illustrate the variations in bulk xenon isotope signatures of the basaltic shergottites (Mathew and Marti, 2001; Ott, 1988; Swindle et al., 1986; Terribilini, 2000). Xenon isotope systematics of martian meteorites typically reveal mixing between a martian atmospheric signature (**S**hergottite **P**arent **B**ody; Swindle et al., 1986) and one or more interior components. The xenon isotopic

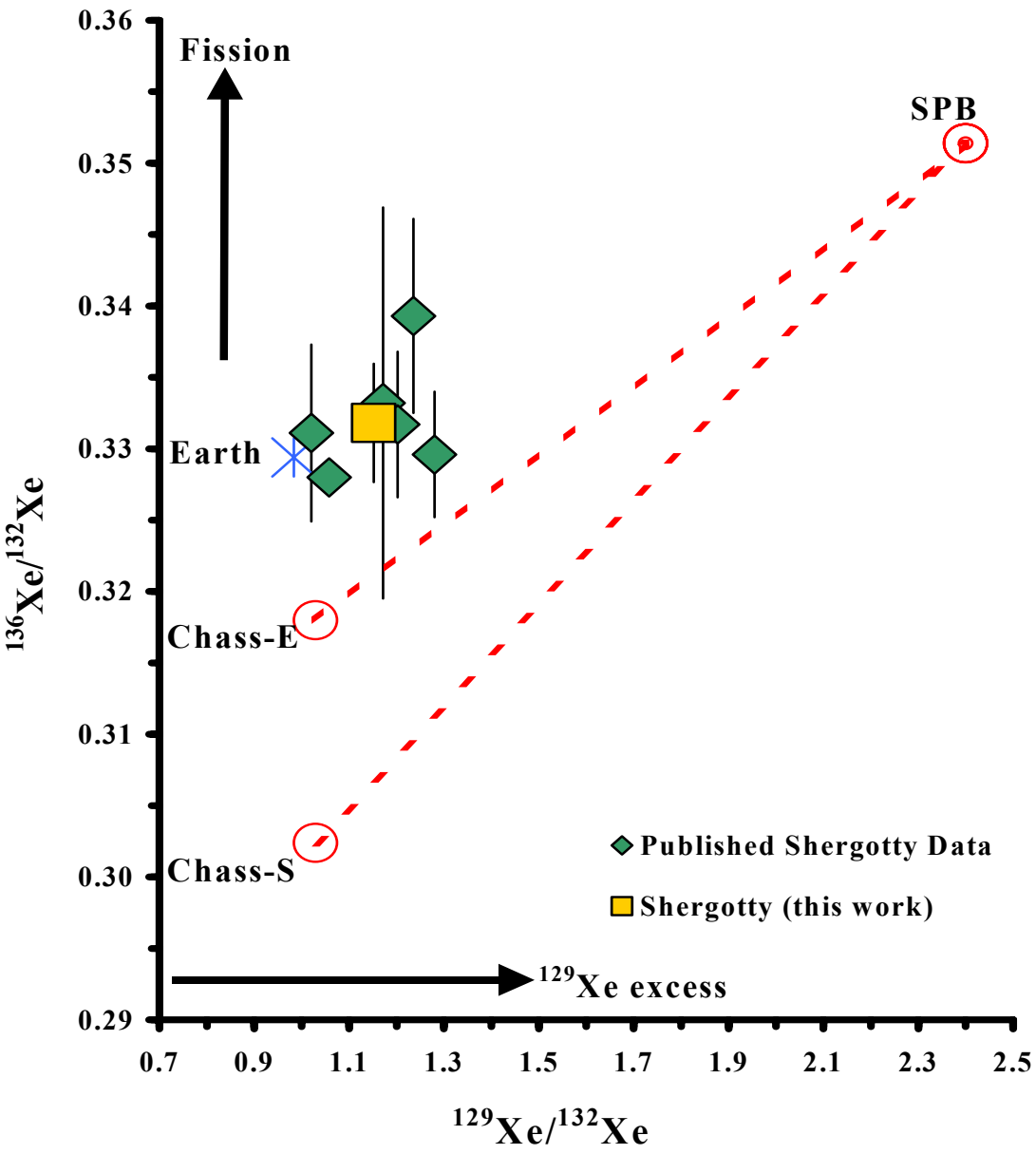

Figure III-1. The $^{136}Xe/^{132}Xe$ ratio *vs.* $^{129}Xe/^{132}Xe$ ratio for some basaltic shergottites. The xenon composition of the basaltic shergottites has been described as a mixture of a Martian atmosphere component, noted as SPB for Shergottite Parent Body (Swindle et al., 1986) and Martian mantle-like solar component found in Chassigny (Chass-S) (Ott, 1988). However, all the presented data lie above this simple two-component mixing line, suggesting three-component mixing or modification of the mantle-like component (see text). Published values of Shergotty are represented to show the agreement with our whole rock data (Mathew and Marti, 2001; Ott, 1988; Swindle et al., 1986; Terribilini, 2000).

signature of the martian atmosphere, identified in shergottite melt glass and in Nakhla, is distinguished by an elevated $^{129}Xe/^{132}Xe$ ratio of 2.40 ± 0.02. A pure solar xenon ($^{129}Xe/^{132}Xe \cong 1$) has been observed in the dunite Chassigny and is denoted here by Chass-S (Ott, 1988). Its presence in a dunite led to its association with the martian interior. Building on this identification, further components dominated by solar xenon but with varying proportions of fission xenon, are also identified with the martian interior. The fission source has been identified as ^{244}Pu (Mathew and Marti, 2001). There is some variation in the relative proportions of fission xenon and solar xenon in these components. One such component, also detected in Chassigny (Mathew and Marti, 2001) and denoted as Chass-E (Figure III-1) has similar $^{129}Xe/^{132}Xe$ ratio to Chass-S, the pure solar interior component. Chass-E is a well-defined component implying that fission and solar xenon were well mixed before incorporation into the meteorite, ruling out *in situ* decay (Mathew and Marti, 2001). The estimated interior component of ALH84001 and Nakhla analyses also indicate mixtures of fission and solar xenon (Mathew, 2000), albeit in distinctly different proportions from each other and from Chass-E. In these cases the components are constrained to lie on mixing lines between solar, ^{244}Pu source and the $^{129}Xe/^{132}Xe$ ratio in the interior component is not accurately known. In Figure III-1, literature data from bulk analyses of shergottites suggest the presence of an interior component containing some fission xenon as well as modern martian atmosphere. However, the proportions of fission and solar xenon in the interior component in the shergottites are not well constrained.

Xenon isotopic analyses of mineral separates from ALH84001 and Nakhla have been reported (Gilmour et al., 2001 and references therein). In these meteorites, the atmosphere-derived xenon component is associated with a lower Kr/Xe ratio than that of the martian atmosphere (as determined in the shergottite melt glass), an elemental fractionation most readily associated with the trapping mechanism. It was determined that the majority of trapped martian atmosphere xenon measured in ALH84001 was located in the orthopyroxenes and believed to have been incorporated into the surface of the grains by shock (Gilmour et al., 1998b). This component is isotopically distinct from the modern martian atmosphere leading to its identification with an ancient atmosphere trapped 4 Ga ago. In Nakhla, the highest concentration of martian atmospheric xenon is associated with the feldspathic mesostasis, though mass balance suggests pyroxene is an equally significant host in the bulk meteorite (Gilmour et al., 1999). Alteration products have also been shown to host martian atmospheric xenon in the nakhlite Lafayette, though they do not contribute significantly to the overall budget (Swindle et al., 2000). This distribution has been interpreted as a grain size effect consistent with shock incorporation of martian atmospheric noble gases adsorbed onto mineral surfaces, a process that seems capable of accounting for both the observed elemental fractionation and the distribution among host phases.

Studies on the basaltic shergottites to date have been limited to bulk analysis (Figure III-1). The data are consistent with a mixture of modern martian atmospheric xenon with a martian interior component consisting of fission xenon intimately mixed with solar xenon. Here we present a xenon isotopic study of mineral separates from

Shergotty to complement these bulk analyses. Our aim was to determine the location of the martian xenon components derived from the atmosphere and interior, and to characterize the proportions of fission and solar xenon present in the interior component. In the light of our results, we discuss how these components came to be incorporated into Shergotty in the context of accepted models of its crystallization and subsequent history. We also discuss wider implications for the noble gas geochemistry of Mars.

Experimental Procedure

A 50 mg sample of Shergotty (sample number: #1985, MFH) was prepared for analysis by the methods described in Chapter 2 under the section titled Sample Preparations with Figure II-2 showing a backscatter image of a thick section of Shergotty. Shergotty was divided into three dominant mineral separates of pyroxene, maskelynite and opaque phases. Base on the mineral mode of Stopler and McSween (1979), the pyroxene-dominate separates are composed of augite and pigeonite of equal proportions, and may contain possible trace amounts of fayalite. Maskelynite-dominate separates are composed of the diaplectic glass and may contain trace amounts of whitlockite that was removed in the acid-wash treated separate. The opaque-dominate separates compose of titanomagnetite, ilmenite and pyrrhotite. The summaries of the samples generated are summarized in Table III-1.

Samples were loaded into the laser port of the RELAX mass spectrometer (Gilmour et al., 1994) for laser step-heating as described in Chapter 2 under the section title Xenon Extraction.

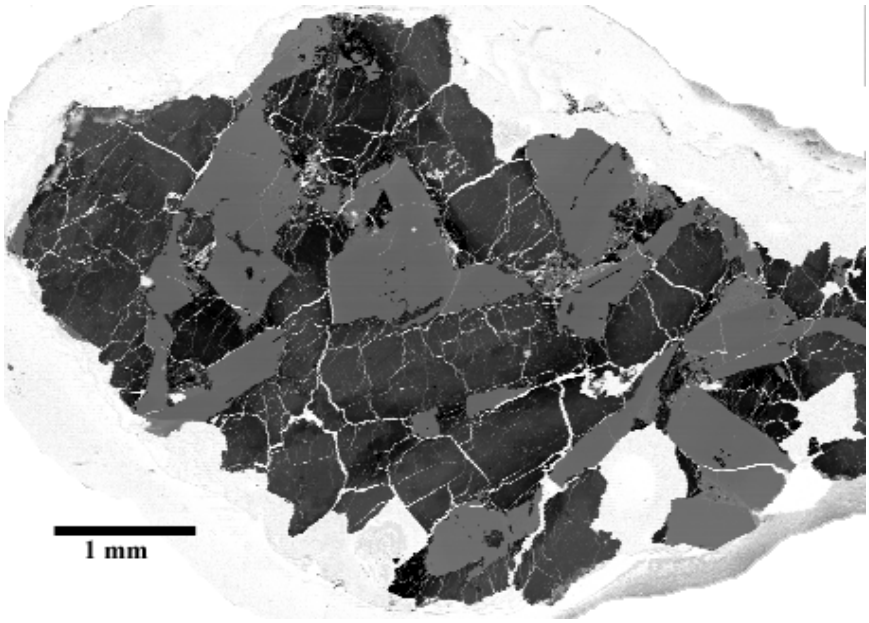

Figure III- 2. Inverted backscatter image of a thick section of Shergotty meteorite showing large pyroxene crystals separated by grey lathes of maskelynite.

Table III-1. Summary of Shergotty samples generated for xenon isotope study.

Sample	Mass	Preparation Treatment
WR-01	4.19 mg	Plucked from crushed grains
PYX-01	7.54 mg	Plucked from crushed grains
PYX-02	6.25 mg	Plucked from crushed grains
PYX-03	2.45 mg	Cut from thick section
AUG	1.55 mg	Cut from thick section
PIG	1.51 mg	Cut from thick section
MSK-01	7.28 mg	Plucked from crushed grains
MSK-02	1.58 mg	Plucked from crushed grains
MSK-HCl	1.33 mg	Acid washed
OPQ-01	1.06 mg	Plucked from crushed grains

Results

All xenon data acquired from the analyses are presented in Table III-2. Figure III-3A shows the laser step-heating data from the whole rock plotted with ^{129}Xe and ^{124}Xe normalized to ^{132}Xe. Elevated ^{129}Xe ratios are diagnostic of the martian atmosphere, while increased $^{124}Xe/^{132}Xe$ ratios are a result of spallation by cosmic rays during Shergotty's transit from Mars to Earth. Thus $^{124}Xe/^{132}Xe$ trace the presence of spallation target elements (Barium, light rare earth elements) in the mineral being degassed and allow releases from their major component minerals of Shergotty to be identified. The whole-rock data reveal a correlation between elevated $^{129}Xe/^{132}Xe$ and elevated $^{124}Xe/^{132}Xe$, showing that the host phase of the martian atmosphere is relatively rich in Ba and LREEs.

In Figure III-3B we present data from mineral separates on the same plot of $^{129}Xe/^{132}Xe$ ratio versus $^{124}Xe/^{132}Xe$ ratio for comparison with the whole-rock releases of Figure 3A. Three regions are defined by the three different mineral separates. The pyroxene data show on average low $^{124}Xe/^{132}Xe$ ratio indicative of the absence of spallation target elements. The correlation between spallation and $^{129}Xe_{xs}$ for the opaques and maskelynite grains show a positive slope. The steeper slope of the opaque data is due to concentration of the martian atmospheric xenon in the opaque grains (Table III-3). For comparison, the whole rock trend line from Figure III-3A has also been plotted and shows that the maskelynite signature dominates the whole rock data that have a high $^{129}Xe/^{132}Xe$ ratio.

Table III-2. Data from Shergotty samples. ^{132}Xe in 10^{-12} cm^3 STP g^{-1}, Ratios to $^{132}Xe = 100$.

	^{132}Xe	$\frac{^{124}Xe}{^{132}Xe}$	$\frac{^{126}Xe}{^{132}Xe}$	$\frac{^{128}Xe}{^{132}Xe}$	$\frac{^{129}Xe}{^{132}Xe}$	$\frac{^{130}Xe}{^{132}Xe}$	$\frac{^{131}Xe}{^{132}Xe}$	$\frac{^{134}Xe}{^{132}Xe}$	$\frac{^{136}Xe}{^{132}Xe}$
WR, bulk sample, 4.19 mg.									
1	0.189 ± 0.007	0.83± 0.54	1.34 ± 0.54	8.25 ± 0.74	117.01 ± 3.54	13.85 ± 0.92	81.31 ± 2.72	38.24 ± 1.65	34.89 ± 1.53
2	0.524 ± 0.010	1.22 ± 0.18	1.74 ± 0.19	9.40 ± 0.37	110.70 ± 1.71	15.50 ± 0.48	80.83 ± 1.35	38.29 ± 0.82	33.17 ± 0.74
3	0.216 ± 0.008	1.93 ± 0.51	3.50 ± 0.53	11.49 ± 0.80	117.17 ± 3.49	16.43 ± 0.96	85.05 ± 2.75	39.61 ± 1.64	32.86 ± 1.46
4	0.309 ± 0.011	4.08 ± 0.51	7.15 ± 0.59	14.22 ± 0.92	148.86 ± 4.72	17.92 ± 1.12	92.07 ± 3.33	39.36 ± 1.91	33.52 ± 1.72
5	0.422 ± 0.012	1.33 ± 0.31	1.51 ± 0.31	8.82 ± 0.53	109.47 ± 2.49	16.15 ± 0.71	80.49 ± 2.00	38.69 ± 1.22	33.31 ± 1.11
6	0.206 ± 0.008	1.94 ± 0.48	3.63 ± 0.50	11.08 ± 0.80	123.55 ± 3.79	16.07 ± 0.99	82.85 ± 2.84	38.81 ± 1.70	31.36 ± 1.49
7	0.628 ± 0.011	0.58 ± 0.14	1.01 ± 0.14	7.63 ± 0.30	104.21 ± 1.47	14.69 ± 0.42	78.76 ± 1.20	38.79 ± 0.74	33.15 ± 0.66
Total:	2.494 ± 0.026	1.48 ± 0.12	2.39 ± 0.12	9.61 ± 0.21	115.16 ± 0.98	15.68 ± 0.27	82.05 ± 0.76	38.76 ± 0.46	33.18 ± 0.42
MSK-01, maskelynite-dominate mineral separates, 7.28 mg.									
1	1.117 ± 0.011	0.36 ± 0.05	0.36 ± 0.05	7.76 ± 0.16	99.42 ± 0.77	14.60 ± 0.22	78.79 ± 0.64	39.27 ± 0.40	33.51 ± 0.36
2	0.191 ± 0.005	0.28 ± 0.29	0.26 ± 0.29	9.71 ± 0.51	103.49 ± 2.23	15.09 ± 0.64	80.48 ± 1.85	40.32 ± 1.15	34.00 ± 1.02
3	0.166 ± 0.006	0.06 ± 0.51	0.27 ± 0.51	9.67 ± 0.75	99.12 ± 3.17	14.44 ± 0.92	76.36 ± 2.62	38.27 ± 1.64	33.40 ± 1.50
4	0.374 ± 0.009	0.33 ± 0.26	0.60 ± 0.26	9.24 ± 0.46	105.17 ± 2.07	15.19 ± 0.59	79.37 ± 1.68	39.61 ± 1.05	34.08 ± 0.95
5	0.212 ± 0.005	0.38 ± 0.27	0.66 ± 0.27	7.53 ± 0.44	109.37 ± 2.20	14.80 ± 0.60	81.22 ± 1.76	40.03 ± 1.08	33.60 ± 0.97
6	0.774 ± 0.009	0.82 ± 0.08	1.15 ± 0.08	8.47 ± 0.20	110.06 ± 0.99	15.51 ± 0.28	80.17 ± 0.78	38.94 ± 0.48	33.52 ± 0.43
7	0.089 ± 0.004	0.54 ± 0.70	0.84 ± 0.70	8.74 ± 0.92	105.63 ± 4.16	14.41 ± 1.16	80.44 ± 3.41	37.81 ± 2.06	33.42 ± 1.88
8	0.147 ± 0.005	0.87 ± 0.46	1.54 ± 0.46	9.05 ± 0.69	111.41 ± 3.11	15.38 ± 0.87	82.76 ± 2.51	40.11 ± 1.52	33.00 ± 1.36
9	0.734 ± 0.008	1.43 ± 0.09	1.93 ± 0.10	9.33 ± 0.21	115.35 ± 1.02	16.05 ± 0.28	81.81 ± 0.79	39.09 ± 0.47	33.23 ± 0.42
10	0.189 ± 0.004	1.36 ± 0.26	2.50 ± 0.28	10.04 ± 0.47	115.99 ± 2.20	16.33 ± 0.60	82.93 ± 1.71	39.42 ± 1.03	33.75 ± 0.92
11	0.170 ± 0.004	2.65 ± 0.32	3.49 ± 0.34	12.25 ± 0.57	122.06 ± 2.55	16.82 ± 0.68	83.65 ± 1.92	39.51 ± 1.15	34.03 ± 1.04
12	0.288 ± 0.006	2.96 ± 0.29	4.05 ± 0.31	12.33 ± 0.50	130.40 ± 2.34	17.38 ± 0.61	85.06 ± 1.71	38.99 ± 1.01	33.33 ± 0.91
13	0.379 ± 0.011	1.80 ± 0.38	2.49 ± 0.39	12.48 ± 0.65	123.29 ± 2.91	17.01 ± 0.78	84.43 ± 2.21	38.72 ± 1.30	32.36 ± 1.16
Total:	4.831 ± 0.025	1.00 ± 0.06	1.40 ± 0.06	9.33 ± 0.11	110.45 ± 0.48	15.58 ± 0.13	80.95 ± 0.38	39.21 ± 0.23	33.45 ± 0.21
MSK-02, maskelynite-dominate mineral separates, 1.59 mg.									
1	0.478 ± 0.015	0.11 ± 0.45	-0.20 ± 0.45	6.81 ± 0.61	97.07 ± 2.72	14.84 ± 0.81	78.47 ± 2.32	38.60 ± 1.42	32.51 ± 1.29
2	0.701 ± 0.021	1.73 ± 0.42	3.00 ± 0.44	11.44 ± 0.69	147.11 ± 3.49	16.83 ± 0.82	82.19 ± 2.28	39.77 ± 1.38	32.28 ± 1.23
3	0.664 ± 0.022	4.55 ± 0.52	5.38 ± 0.55	15.02 ± 0.84	161.52 ± 4.10	18.73 ± 0.94	88.07 ± 2.61	39.26 ± 1.51	33.68 ± 1.38
4	0.414 ± 0.015	7.09 ± 0.81	12.74 ± 0.97	25.22 ± 1.40	180.65 ± 6.02	26.29 ± 1.46	99.10 ± 3.80	35.50 ± 1.98	32.54 ± 1.85
Total:	2.257 ± 0.037	3.15 ± 0.26	4.71 ± 0.28	13.90 ± 0.42	146.43 ± 1.97	18.60 ± 0.48	86.07 ± 1.33	38.63 ± 0.78	32.79 ± 0.71

Table III-2 continue. Data from Shergotty samples.

	^{132}Xe	$\frac{^{124}Xe}{^{132}Xe}$	$\frac{^{126}Xe}{^{132}Xe}$	$\frac{^{128}Xe}{^{132}Xe}$	$\frac{^{129}Xe}{^{132}Xe}$	$\frac{^{130}Xe}{^{132}Xe}$	$\frac{^{131}Xe}{^{132}Xe}$	$\frac{^{134}Xe}{^{132}Xe}$	$\frac{^{136}Xe}{^{132}Xe}$
MSK-HCL, acid washed maskelynite-dominate mineral separates, 1.33 mg.									
1	0.225 ± 0.014	0.58 ± 1.38	0.48 ± 1.38	7.59 ± 1.54	104.23 ± 6.67	15.53 ± 1.94	79.17 ± 5.50	42.79 ± 3.52	33.51 ± 3.19
2	0.222 ± 0.013	0.34 ± 1.23	-0.14 ± 1.23	8.67 ± 1.44	103.55 ± 6.06	15.26 ± 1.76	77.98 ± 4.98	40.10 ± 3.13	31.76 ± 2.85
3	0.171 ± 0.015	0.08 ± 1.91	0.58 ± 1.91	7.03 ± 2.11	104.34 ± 9.31	17.13 ± 2.69	77.24 ± 7.55	38.72 ± 4.79	34.50 ± 4.45
4	0.263 ± 0.016	0.47 ± 1.30	0.41 ± 1.30	7.38 ± 1.46	104.16 ± 6.18	16.78 ± 1.84	75.07 ± 4.97	37.58 ± 3.12	32.17 ± 2.91
5	0.387 ± 0.015	1.29 ± 0.63	1.31 ± 0.63	8.00 ± 0.81	111.37 ± 3.63	16.15 ± 1.02	82.25 ± 2.93	39.90 ± 1.79	34.20 ± 1.64
6	0.547 ± 0.016	1.54 ± 0.37	1.70 ± 0.37	9.86 ± 0.59	110.70 ± 2.67	16.48 ± 0.76	82.78 ± 2.15	39.26 ± 1.29	34.98 ± 1.20
7	0.308 ± 0.019	3.62 ± 1.41	5.31 ± 1.43	19.28 ± 1.96	140.99 ± 7.78	19.02 ± 2.03	93.74 ± 5.77	37.24 ± 3.25	32.05 ± 3.00
8	0.554 ± 0.025	6.08 ± 0.96	8.92 ± 1.05	18.89 ± 1.42	139.91 ± 5.61	23.30 ± 1.60	96.26 ± 4.24	37.38 ± 2.32	30.70 ± 2.10
Total:	2.676 ± 0.048	2.27 ± 0.35	3.04 ± 0.36	11.72 ± 0.46	117.84 ± 1.91	17.95 ± 0.55	84.84 ± 1.51	38.92 ± 0.90	33.00 ± 0.83
OPQ-01, opaque-dominate mineral separates, 1.06 mg.									
1	2.032 ± 0.036	0.37 ± 0.16	0.38 ± 0.16	7.07 ± 0.33	99.92 ± 1.47	14.83 ± 0.43	79.93 ± 1.24	39.27 ± 0.76	34.55 ± 0.70
2	0.617 ±0.023	0.12 ± 0.54	0.32 ± 0.54	5.71 ± 0.79	104.54 ± 3.38	14.05 ± 0.95	80.14 ± 2.77	40.54 ± 1.73	33.76 ± 1.54
3	0.550 ± 0.020	0.33 ± 0.50	0.20 ± 0.50	6.51 ± 0.76	107.67 ± 3.31	13.67 ± 0.90	79.23 ± 2.64	39.66 ± 1.63	33.53 ± 1.47
4	0.865 ± 0.026	0.69 ± 0.37	0.66 ± 0.37	7.20 ± 0.62	110.42 ± 2.73	14.39 ± 0.75	81.11 ± 2.17	41.00 ± 1.35	33.50 ± 1.19
5	1.750 ± 0.035	1.22 ± 0.20	1.43 ± 0.20	8.64 ± 0.41	124.68 ± 1.96	15.24 ± 0.50	80.53 ± 1.42	39.59 ± 0.87	34.48 ± 0.79
6	1.899 ± 0.039	1.98 ± 0.24	3.01 ± 0.26	10.33 ± 0.46	143.10 ± 2.26	15.88 ± 0.53	84.76 ± 1.52	39.83 ± 0.91	34.26 ± 0.82
7	2.439 ± 0.048	1.39 ± 0.19	2.25 ± 0.21	9.79 ± 0.41	161.22 ± 2.33	15.84 ± 0.50	82.52 ± 1.41	39.71 ± 0.85	33.94 ± 0.77
Total:	10.510 ± 0.089	1.07 ± 0.09	1.51 ± 0.10	8.50 ± 0.18	128.41 ± 0.89	15.18 ± 0.22	81.62 ± 0.63	39.78 ± 0.38	34.14 ± 0.35
PYX-01, pyroxene-dominate mineral separates, 7.84 mg.									
1	0.103 ± 0.003	0.15 ± 0.36	0.76 ± 0.36	12.45 ± 0.68	115.06 ± 2.84	14.26 ± 0.74	76.55 ± 2.11	40.05 ± 1.35	35.27 ± 1.24
2	0.165 ± 0.005	0.27 ± 0.39	0.45 ± 0.39	8.56 ± 0.61	122.05 ± 2.94	14.20 ± 0.76	78.96 ± 2.16	40.90 ± 1.36	34.07 ± 1.22
3	0.188 ± 0.004	0.50 ± 0.22	0.66 ± 0.22	7.45 ± 0.40	116.19 ± 2.06	14.72 ± 0.55	80.67 ±1.58	41.11 ± 0.99	34.16 ± 0.88
4	0.045 ± 0.002	0.37 ± 0.81	0.51 ± 0.81	5.88 ± 1.01	112.83 ± 4.92	13.34 ± 1.32	79.81 ± 3.86	39.98 ± 2.40	33.52 ± 2.15
5	0.552 ± 0.008	1.07 ± 0.09	1.40 ± 0.10	8.79 ± 0.24	118.76 ± 1.25	15.88 ± 0.33	81.26 ± 0.94	39.30 ± 0.58	33.54 ± 0.52
6	0.094 ± 0.008	0.94 ± 0.33	1.51 ± 0.33	9.31 ± 0.56	113.53 ± 2.61	15.72 ± 0.72	81.33 ± 2.04	41.05 ± 1.27	32.87 ± 1.11
7	0.159 ± 0.005	0.59 ± 0.38	1.12 ± 0.38	9.11 ± 0.62	117.14 ± 2.92	16.33 ± 0.81	80.24 ± 2.23	38.50 ± 1.35	33.58 ± 1.24
8	0.432 ± 0.008	0.90 ± 0.13	1.18 ± 0.14	9.16 ± 0.33	117.39 ± 1.62	15.31 ± 0.43	79.87 ± 1.21	39.77 ± 0.75	33.26 ± 0.67
Total:	1.738 ± 0.016	0.78 ± 0.08	1.11 ± 0.08	8.92 ± 0.15	117.49 ± 0.76	15.35 ± 0.20	80.27 ± 0.57	39.86 ± 0.35	33.63 ± 0.32

Table III-2 continue. Data from Shergotty samples.

	^{132}Xe	$\frac{^{124}Xe}{^{132}Xe}$	$\frac{^{126}Xe}{^{132}Xe}$	$\frac{^{128}Xe}{^{132}Xe}$	$\frac{^{129}Xe}{^{132}Xe}$	$\frac{^{130}Xe}{^{132}Xe}$	$\frac{^{131}Xe}{^{132}Xe}$	$\frac{^{134}Xe}{^{132}Xe}$	$\frac{^{136}Xe}{^{132}Xe}$
PYX-02, pyroxene-dominate mineral separates, 6.25 mg.									
1	0.573 ± 0.009	0.27 ± 0.13	1.35 ± 0.14	52.39 ± 0.82	101.35 ± 1.35	16.18 ± 0.41	76.41 ± 1.10	37.87 ± 0.68	30.96 ± 0.60
2	0.099 ± 0.004	0.11 ± 0.74	0.79 ± 0.74	7.25 ± 1.09	129.08 ± 4.93	12.69 ± 1.18	79.96 ± 3.50	39.82 ± 2.17	34.79 ± 1.98
3	0.122 ± 0.004	0.53 ± 0.44	1.00 ± 0.45	7.79 ± 0.73	122.88 ± 3.31	14.73 ± 0.85	81.21 ± 2.45	39.67 ± 1.50	34.31 ± 1.36
4	0.102 ± 0.004	0.97 ± 0.50	2.37 ± 0.50	7.70 ± 0.79	124.06 ± 3.60	14.26 ± 0.91	81.77 ± 2.66	39.74 ± 1.62	34.33 ± 1.47
5	0.193 ± 0.005	0.97 ± 0.32	1.61 ± 0.32	7.39 ± 0.55	120.63 ± 2.61	14.14 ± 0.66	82.00 ± 1.97	40.15 ± 1.20	33.65 ± 1.08
6	0.263 ± 0.006	1.23 ± 0.26	1.44 ± 0.26	7.95 ± 0.48	126.35 ± 2.35	15.50 ± 0.60	81.04 ± 1.69	40.52 ± 1.05	34.68 ± 0.95
7	0.111 ± 0.005	0.52 ± 0.69	0.53 ± 0.69	6.96 ± 0.97	116.58 ± 4.16	13.83 ± 1.10	77.94 ± 3.12	40.93 ± 1.98	33.36 ± 1.76
8	0.266 ± 0.008	0.57 ± 0.45	1.08 ± 0.45	6.29 ± 0.67	123.74 ± 3.11	14.83 ± 0.81	81.26 ± 2.30	41.24 ± 1.43	34.74 ± 1.28
Total:	1.730 ± 0.017	0.60 ± 0.12	1.30 ± 0.12	22.33 ± 0.31	116.07 ± 0.94	15.07 ± 0.25	79.41 ± 0.71	39.58 ± 0.44	33.20 ± 0.39
PYX-03, pyroxene-dominate mineral separates, 2.45 mg.									
1	0.081 ± 0.006	0.06 ± 1.74	-0.32 ± 1.74	7.05 ± 1.92	122.09 ± 8.46	11.86 ± 2.15	77.97 ± 6.25	39.76 ± 3.91	35.62 ± 3.62
2	0.321 ± 0.012	0.39 ± 0.51	0.24 ± 0.51	0.97 ± 0.84	116.89 ± 3.66	12.96 ± 0.95	81.64 ± 2.83	39.59 ± 1.73	36.12 ± 1.60
3	0.498 ± 0.020	1.01 ± 0.40	1.48 ± 0.40	8.60 ± 0.78	117.54 ± 3.92	14.13 ±1.01	82.07 ± 3.04	39.39 ± 1.86	33.48 ± 1.68
4	0.214 ± 0.011	0.89 ± 0.85	0.42 ± 0.85	7.58 ± 1.13	116.20 ± 5.57	14.72 ± 1.47	80.71 ± 4.30	40.52 ± 2.70	33.12 ± 2.40
5	0.278 ± 0.012	0.34 ± 0.70	0.20 ± 0.70	7.22 ± 0.96	128.64 ± 5.01	15.16 ± 1.24	80.90 ± 3.63	38.87 ± 2.23	35.09 ± 2.05
Total:	1.392 ± 0.029	0.65 ± 0.29	0.64 ± 0.29	6.21 ± 0.44	119.62 ± 2.14	14.01 ± 0.55	81.25 ± 1.63	39.55 ± 1.01	34.51 ± 0.92
AUG, augite-dominate mineral separates, 1.55 mg.									
1	0.065 ± 0.009	2.05 ± 2.37	2.56 ± 2.37	14.58 ± 2.81	126.71 ± 11.58	12.36 ± 2.90	81.45 ± 8.50	42.08 ± 5.36	35.57 ± 4.81
2	0.396 ± 0.017	1.41 ± 0.83	1.97 ± 0.83	8.68 ± 1.04	124.98 ± 5.06	15.88 ± 1.31	81.76 ± 3.76	37.82 ± 2.26	32.52 ± 2.03
3	0.244 ± 0.012	0.66 ±1.02	2.77 ± 1.02	10.59 ± 1.31	129.23 ± 6.07	15.76 ± 1.53	80.79 ± 4.39	38.90 ± 2.69	33.77 ± 2.42
4	0.197 ± 0.011	0.28 ± 1.13	1.17 ± 1.13	7.83 ± 1.32	137.20 ± 6.87	12.31 ± 1.54	79.95 ± 4.74	38.83 ± 2.92	34.77 ± 2.66
Total:	0.902 ± 0.026	1.05 ± 0.57	2.07 ± 0.57	9.72 ± 0.70	128.95 ± 3.30	14.63 ± 0.82	81.07 ± 2.39	38.85 ± 1.46	33.71 ± 1.32
PIG, pigeonite-dominate mineral separates, 1.51 mg.									
1	0.260 ± 0.016	0.35 ± 1.23	1.26 ± 1.23	8.36 ± 2.05	124.06 ± 6.71	17.45 ± 1.92	78.45 ± 4.87	43.51 ± 3.20	35.64 ± 2.78
2	0.263 ± 0.011	1.31 ± 0.77	1.50 ± 0.77	8.34 ± 0.95	125.41 ± 4.32	15.04 ± 1.10	84.05 ± 3.21	38.06 ± 1.92	33.96 ± 1.75
3	0.237 ± 0.011	1.37 ± 0.94	2.14 ± 0.94	10.29 ± 1.17	120.36 ± 4.79	17.18 ± 1.34	81.20 ± 3.60	36.82 ± 2.17	33.44 ± 1.99
4	0.279 ± 0.013	1.36 ± 0.87	1.55 ± 0.88	8.53 ± 1.21	118.76 ± 4.89	16.61 ± 1.35	83.93 ± 3.80	40.07 ± 2.30	33.10 ± 2.06
5	0.303 ± 0.014	1.19 ± 0.89	2.10 ± 0.90	7.80 ± 1.20	127.32 ± 5.20	16.03 ± 1.36	83.74 ± 3.84	38.39 ± 2.28	32.16 ± 2.07
6	0.241 ± 0.013	0.20 ± 1.04	3.24 ± 1.07	9.45 ± 1.43	142.46 ± 6.36	13.10 ± 1.44	81.11 ± 4.26	40.76 ± 2.65	32.69 ± 2.36
Total:	1.583 ± 0.032	0.98 ± 0.39	1.97 ± 0.39	8.76 ± 0.55	126.42 ± 2.19	15.86 ± 0.58	82.22 ± 1.61	39.55 ± 0.99	33.44 ± 0.88

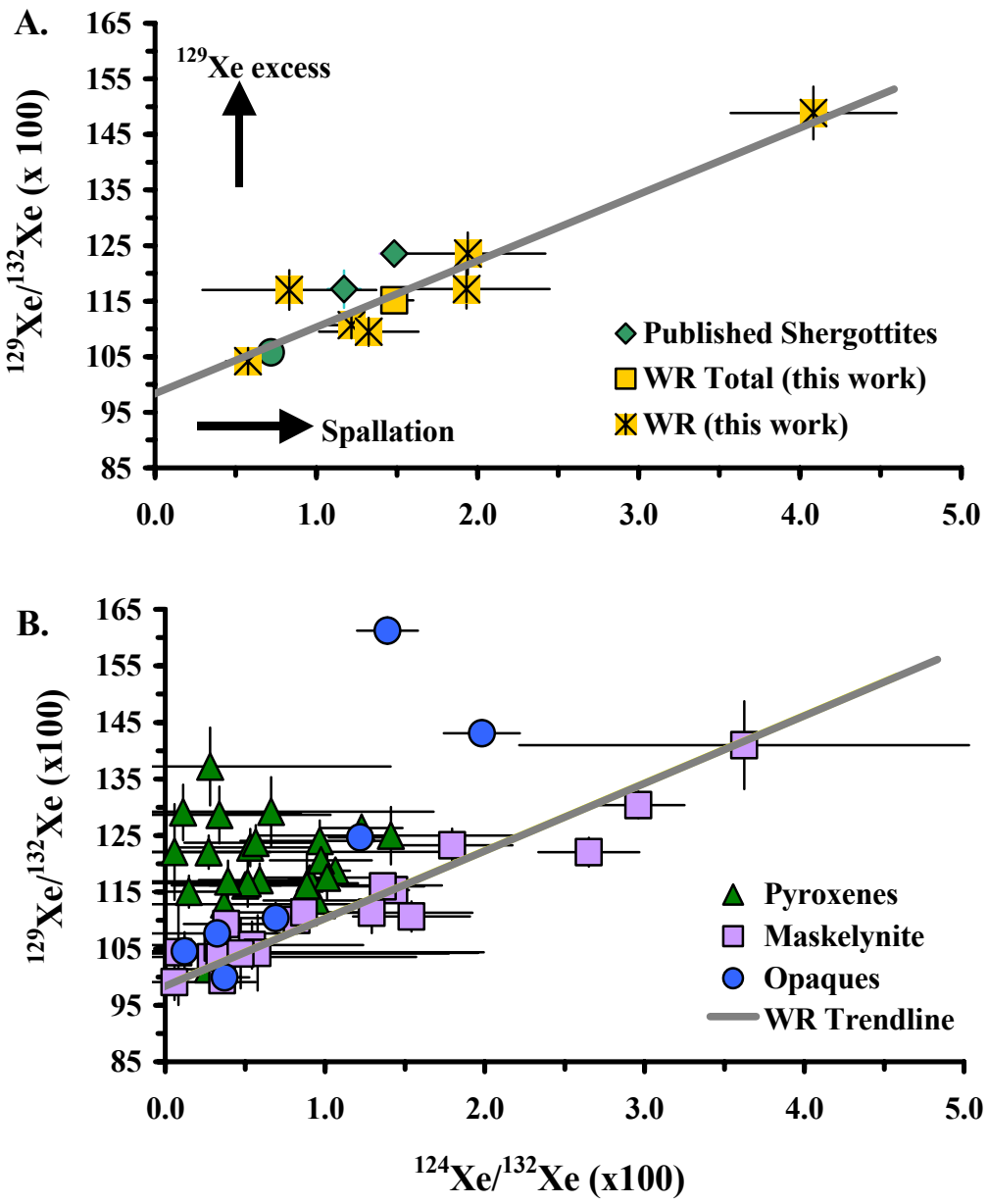

Figure III- 3. ^{129}Xe/^{132}Xe ratio versus ^{124}Xe/^{132}Xe ratio plot of published whole rock data (Ott, 1988; Terribilini, 2000). The whole rock observed in this experiment defines a trend line that is illustrated in both plots (A and B). In plot B, the pyroxene-dominate separates reflect a low ^{124}Xe/^{132}Xe ratio due to the lack of target elements for spallation. The opaque-dominate separates show a steep, positive correlation between spallation and excess ^{129}Xe/^{132}Xe representing a concentration of atmospheric xenon in the opaque grains. The maskelynite correlation illustrates that maskelynite grains define the whole rock trend.

Table III-3. Spallation Corrected Xenon Components in Shergotty. Concentrations in 10^{-12} cm3 STP g-1

	$^{132}Xe_{total}$	$^{129}Xe/^{132}Xe$	$^{129}Xe_{xs}$	$^{132}Xe_{interior}$
WR (bulk sample, 4.19 mg.)	2.494 ± 0.026	1.153 ± 0.011	0.311 ± 0.007	2.291 ± 0.213
MSK-01 (maskelynite-dominate mineral separates, 7.28 mg.)	4.831 ± 0.025	1.105 ± 0.007	0.353 ± 0.007	4.405 ± 0.203
MSK-02 (maskelynite-dominate mineral separates, 1.59 mg.)	2.257 ± 0.037	1.473 ± 0.021	0.931 ± 0.024	1.421 ± 0.291
MSK-HCL (acid washed maskelynite-dominate mineral separates, 1.33 mg.)	2.676 ± 0.048	1.180 ± 0.020	0.393 ± 0.012	2.309 ± 0.494
OPQ-01 (opaque-dominate mineral separates, 1.06 mg.)	10.150 ± 0.089	1.285 ±0.010	2.617 ± 0.056	8.315 ± 0.712
PYX-01 (pyroxene-dominate mineral separates, 7.84 mg.)	1.738 ± 0.016	1.175 ± 0.008	0.269 ± 0.005	1.650 ± 0.111
PYX-02 (pyroxene-dominate mineral separates, 6.25 mg.)	1.730 ± 0.017	1.161 ± 0.009	0.231 ± 0.005	1.584 ± 0.133
PYX-03 (pyroxene-dominate mineral separates, 2.45 mg.)	1.393 ± 0.029	1.196 ± 0.021	0.219 ± 0.006	1.153 ± 0.261
AUG (augite-dominate mineral separates, 1.55 mg.)	0.902 ± 0.026	1.290 ± 0.033	0.252 ± 0.009	0.783 ± 0.313
PIG (pigeonite-dominate mineral separates, 1.51 mg.)	1.583 ± 0.032	1.264 ± 0.022	0.385 ± 0.011	1.358 ± 0.347

The evolutions of the $^{129}Xe/^{132}Xe$ ratio with cumulative ^{132}Xe release for the individual mineral separates are plotted in Figure III-4. Both the opaque (Figure III-4A) and maskelynite-dominate separates (Figure III-4B) show increasing $^{129}Xe_{xs}$ with increasing release steps, with the opaque-dominate separates being more gas-rich. The variation in $^{129}Xe_{xs}$ with release steps could be accounted for if the different minerals present (magnetite, ilmenite and pyrrhotite) have different xenon isotopic signatures and released gas at different temperatures. However, no such explanation can account for the similar evolution observed during analysis of the maskelynite-dominate separates since even removal of phosphate by the acid treatment (Msk-HCl), showed no affect on the data. The pyroxene-dominate separates show a consistent low $^{129}Xe/^{132}Xe$ ratio of ~1.2 over all temperature steps (Figure III-4C) except for the first steps in which a ratio close to that of the Earth's atmosphere is observed that we attributed to a release of adsorbed xenon. Further division of the pyroxenes into augite and pigeonite show no distinguishable differences in this ratio.

The consistently low $^{129}Xe_{xs}$ in the pyroxene data indicate that the xenon component is not dominated by the martian atmospheric component as in the opaque and maskelynite-dominate separates. To further understand this component the data were corrected for a spallation contribution so that they could be compared to predicted isotopic variations if the elevated $^{136}Xe/^{132}Xe$ ratio is due to fractionation of addition of fission xenon. Using the $^{124}Xe/^{132}Xe$ ratio from each release, ^{132}Xe was partitioned between a spallation component with $^{124}Xe/^{132}Xe = 0.664 \pm 0.023$ (calculated from the proportion of Ba and light rare Earth elements expected for Shergotty (Lodders, 1998)

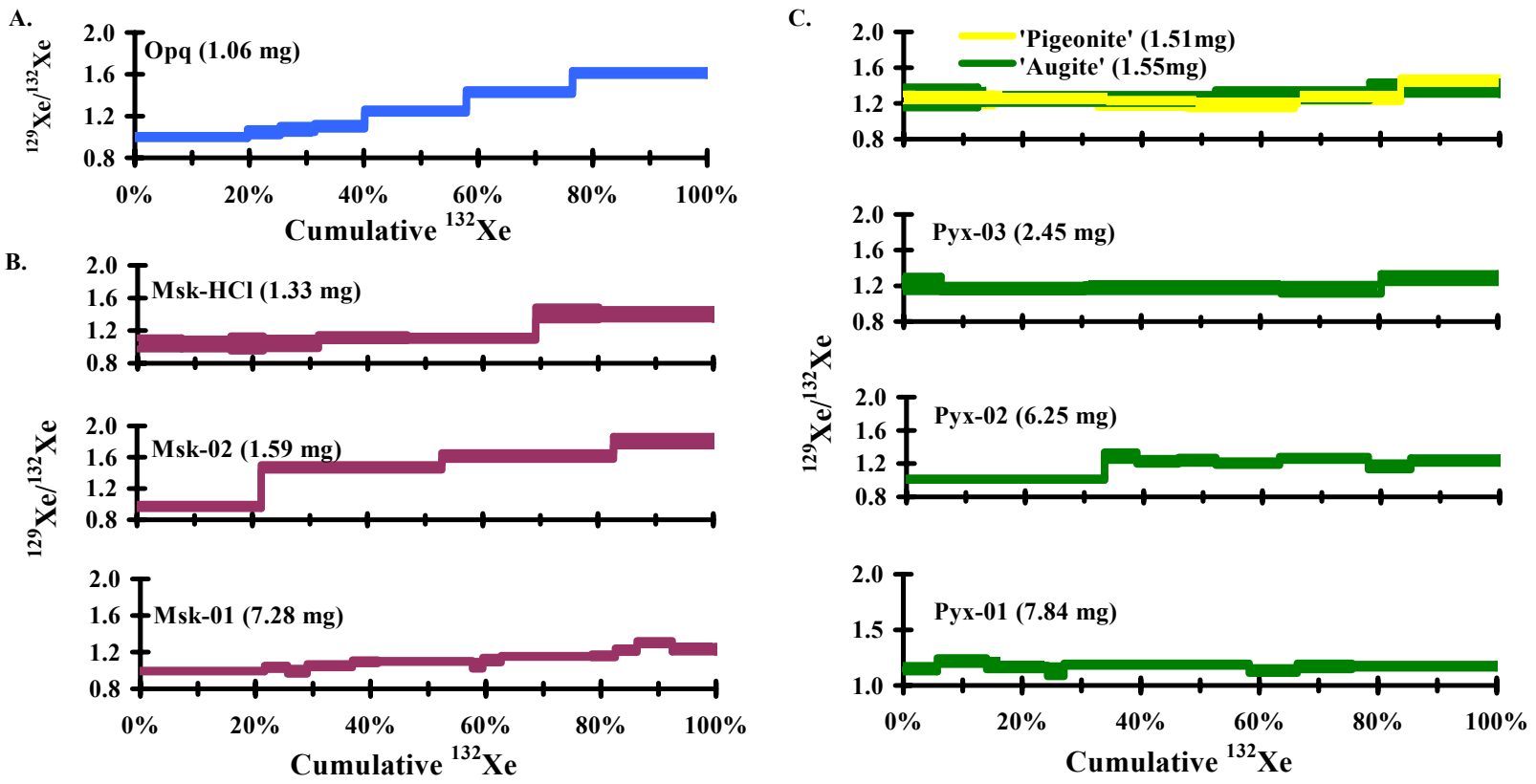

Figure III- 4. The evolution of the $^{129}Xe/^{132}Xe$ ratio with temperature for the individual mineral separates: opaques (A), maskelynite (B) and pyroxene (C). The opaques and maskelynite show an increase in excess $^{129}Xe/^{132}Xe$ (opaques more gas-rich) while the pyroxene show a consistent $^{129}Xe/^{132}Xe$ ~1.2. See text for further details.

and using the spallation components (Hohenberg et al., 1981)) and a trapped component with $^{124}Xe/^{132}Xe = 0.0043 \pm 0.0005$ (the value and errors being chosen to encompass both solar and martian atmospheric values of this ratio). ^{129}Xe and ^{136}Xe were then corrected in proportion to the calculated concentration of spallation ^{132}Xe and summed over the high temperature steps. The near absence of spallation in the pyroxene analyses rendered all corrections minor.

The comparison with spallation-corrected data is made in Figure III-5. The trend obtained by adding fission-xenon to Chassigny solar xenon is illustrated as well as the average of spallation corrected pyroxene data. Fractionation of the interior xenon gives a ratio similar to atmospheric xenon as shown in the two-component mixing line of martian interior (Chassigny solar xenon) to martian atmosphere (SPB), with further fractionation resulting in Earth's atmosphere. A mass fractionation of the pyroxene data confirms that the interior component identified in the pyroxene is of martian origin and not of terrestrial contamination.

Discussion

By analyzing mineral separates we have been able to identify two martian components that can be associated with identifiable mineral hosts.

The martian atmosphere component is more concentrated in the opaque-dominate mineral separates than in the maskelynite-dominate separates, and more concentrated in both than in the pyroxene-dominate separates. This is in turn consistent with the model

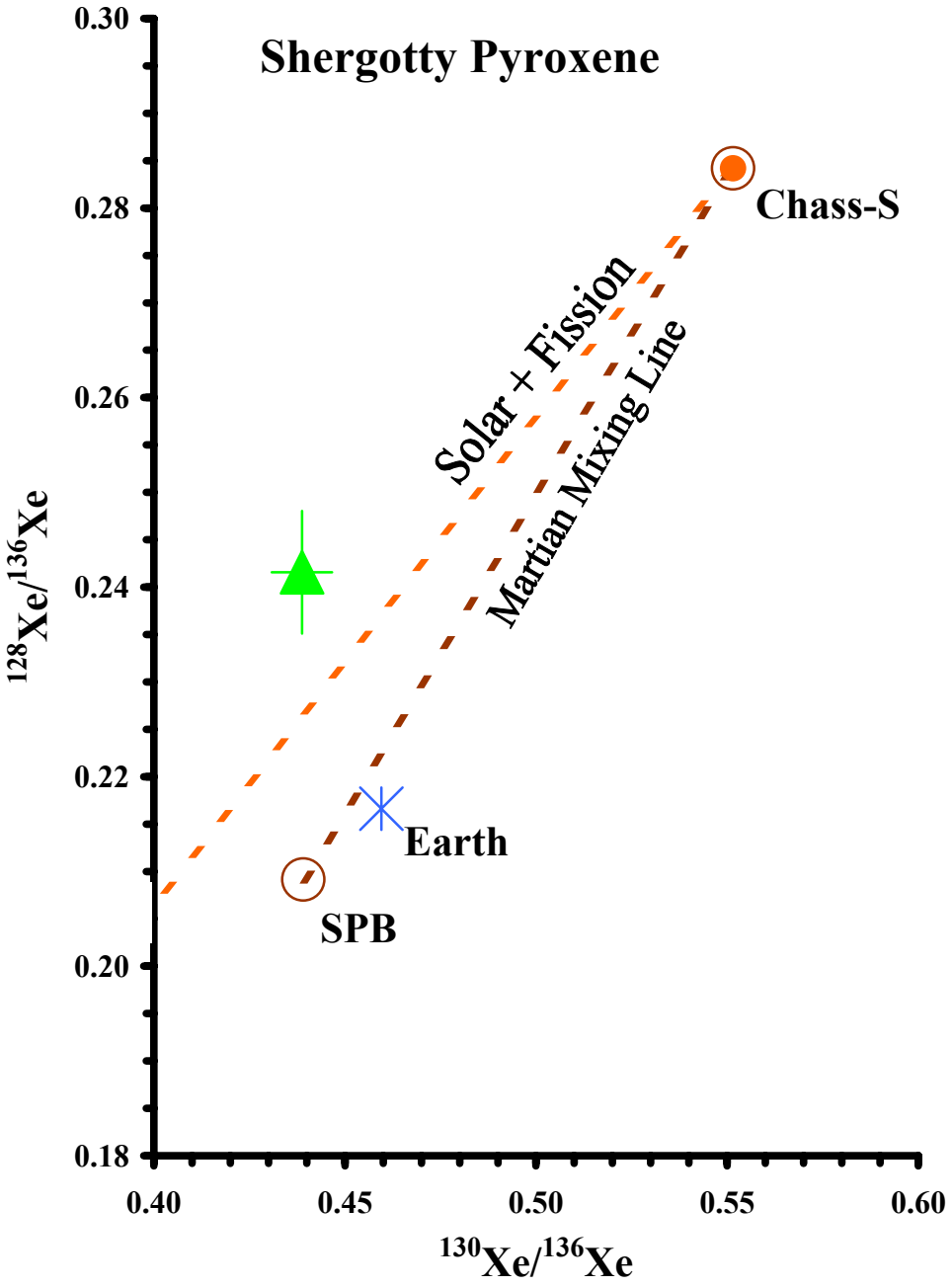

Figure III- 5. $^{128}Xe/^{136}Xe$ versus $^{130}Xe/^{136}Xe$ graph of the average of spallation-corrected pyroxene data. The interior component defined by the pyroxene mineral separates lies on the line illustrating the addition of fission-xenon to solar xenon, as measured in Chassigny. Also drawn is the mixing line between Martian interior and Martian atmosphere. The location of the pyroxene data point illustrates that the interior component is product of solar with a fission contribution and is of Martian origin.

of shock incorporation of adsorbed atmospheric gas invoked for the nakhlites and for ALH84001 (Gilmour et al., 1998b). The smaller the grain size, the more surface area per unit mass and higher the concentration of xenon after shock incorporation. From our mineral separates, the smallest grain sizes are the opaques (<400 μm) followed by the maskelynite (~1 mm) and then pyroxenes (>3 mm). This broadly corresponds to the trend in atmospheric concentration observed in the mineral separates such that the opaque-dominate separates have a higher gas concentration followed by maskelynite-dominate separates and lastly the pyroxene-dominate separates. The combination of absorbed atmospheric gas that is shock implanted seems to be the most viable explanation of the observed gas concentration in the mineral separates. Consideration of shock implantation as the only mechanism would lead to the speculation that maskelynite, diaplectic glass formed from plagioclase that has experienced shock, would have higher emplacement of gases than the opaques.

The process that led to the incorporation of xenon from the martian atmosphere is also implicated in the elemental fractionation that decreased the Kr/Xe ratio observed in the martian meteorites. Reports (Drake et al., 1994; Musselwhite and Swindle, 2001) suggest that the shergottites define an array that is broadly consistent with mixing between a martian atmosphere-like component and a martian mantle-like component. The nakhlites and shergottites noble gas data in fact are consistent with the atmosphere's elemental composition (Musselwhite and Swindle, 2001). On the other hand, nakhlites and ALH84001 have a lower $^{84}Kr/^{132}Xe$ ratio for their high $^{129}Xe/^{132}Xe$ ratio to be consistent with the same simple mixing array as the shergottites in Figure I-2. Studies of

the nakhlites and ALH84001 suggest that the Kr/Xe ratio observed is due to an elemental fractionation of the atmospheric reservoir during the adsorption of atmospheric gases onto mineral surfaces, followed by shock implantation (Gilmour et al., 2001). Adsorption of xenon on mineral surfaces is significant at the temperatures characteristic of the martian surface – calculations (Fanale et al., 1978) suggest that, in these conditions, adsorbed xenon dominates ambient xenon when surfaces are separated by less than ~30 μm. This implies that some degree of elemental fractionation enhancing Xe in the trapped component is to be expected and re-emphasizes that trapping without fractionation is the exception rather than the rule. It is interesting to note that the measurement of Lithology C of EETA79001 (Becker and Pepin, 1984; Bogard and Johnson, 1983; Bogard et al., 1984) and later calculated as SPB (Swindle et al., 1986) is at one extreme of the proposed mixing array that represent the shergottites while whole rock analysis are at the other, making definitive comments about the Kr/Xe ratio difficult. It is accepted that shergottite glass acquired its budget of martian atmospheric gases as a result of shock trapping and that shock can result in the trapping of ambient gases without elemental fractionation (Bogard et al., 1986; Wiens and Pepin, 1986). We propose that the signature seen in Shergotty resulted from shock incorporation of martian atmosphere that had been adsorbed on grain surfaces (and hence elementally fractionated) as explained in the fractionated components of ALH84001 (Gilmour et al., 1998b), Nakhla (Gilmour et al., 1999; Gilmour et al., 2001), and in iddingsite from Lafayette (Swindle et al., 2000).

The consistent $^{129}Xe/^{132}Xe$ ratio observed in the pyroxene-dominate separates across all temperature steps suggest that it is our best choice to define the interior component. The $^{136}Xe/^{132}Xe$ ratio is found to be similar to the other documented martian interior components that contain fission xenon in that it is consists of a mixture of solar xenon and fission xenon, possibly from ^{244}Pu as in ALH84001 and Chass-E (Mathew and Marti, 2001). The uniformity of the mixture in the pyroxene-dominate separates suggests that this is the signature of the ambient xenon present in the magma from which they crystallized, and notably that this had an elevated $^{129}Xe/^{132}Xe$ ratio. It remains unclear whether the elevated $^{129}Xe/^{132}Xe$ ratio observed in this component is evidence of an admixture of martian atmosphere to the melt perhaps consistent with a high assimilated crustal contribution, or if the elevated $^{129}Xe/^{132}Xe$ is preserved in the source region of the interior component such as a fission anomaly from ^{244}Pu.

However, the preservation of a fission anomaly from ^{244}Pu in the young meteorites suggests degassing that ceased early in martian history. This allowed xenon components with elevated $^{136}Xe/^{132}Xe$ ratios to form as ^{244}Pu decayed and subsequently to conserve these components. In the extreme, Marty and Marti (2002) have argued that data from the nakhlites, where the interior component is preserved in the mesostasis (Gilmour et al., 1999) and hence correlates with large ion lithophiles, demonstrate that xenon behaves as an incompatible element in a closed system during nakhlites crystallization and interprets the relatively low ratio of $^{136}Xe^*/Pu$ as evidence of degassing of the source region for the first 170 Ma to 330 Ma of formation and subsequent closure.

This interpretation, however, highlights in an extreme form an outstanding problem in the identification of anomalies due to ^{244}Pu decay in martian meteorites: the absence of identifiable excess of parentless ^{40}Ar from ^{40}K decay. A source region with substantial fission anomalies from ^{244}Pu decay must have closed to xenon loss within 500 Ma of the origin of the solar system, suggesting that ^{40}Ar should have accumulated over ~2.7 Ga before the formation event of the nakhlites. Nakhla has a well defined ^{40}Ar-^{39}Ar age of 1.33 ± 0.03 Ga and a bulk K-Ar age of 1.36 ± 0.03 Ga (Podosek, 1973). These are both identical to the accepted crystallization age of Nakhla, and indicate that the parent melt was substantially degassed on formation. Preservation of ^{136}Xe fission anomalies in the nakhlites and other young martian meteorites thus requires partition of xenon away from argon at some point during or shortly before formation of the meteorite, a process that we feel is unlikely to have preserved total fission xenon contents in a way that allows ^{136}Xe/Pu ratios to be interpreted chronologically as closure ages of the source region.

Another suggestion for the anomalous fission ^{136}Xe is to consider the assimilation of a crustal component in Shergotty's melt. Because of their comparable ionic radii, Pu can behave similarly to the LREE in igneous fractionation process (Shukolyukov and Begemann, 1996). Thus Pu could reside in a more evolved component such as the martian crusts, and become assimilated into the parent melt before crystallization. This follows the similar indications of epsilon Nd and the oxygen fugacity and that Shergotty reflects a high mixing of a crustal component in its parent melt.

Summary

Maskelynite-, opaque-, and pyroxene-dominate mineral separates that were physically divided from Shergotty contain uniquely identified martian atmospheric and interior xenon components. Martian atmospheric xenon (^{129}Xe excess over ^{129}Xe/^{132}Xe=1) is 5-10x more concentrated in opaque-dominate minerals separates and maskelynite-dominate separates than in pyroxene-dominate separates. Gas concentrations are argued to be related to the grain size in that the smallest grains present greater surface area for adsorption before shock incorporation of martian atmospheric xenon. This is the same mechanism said to account for the incorporation of martian atmospheric xenon in Nakhla. Thus the measured bulk Kr/Xe ratio in the shergottites may be the same elemental fractionations between EETA79001 melt glass and nakhlites and not a simple mixing of martian mantle and martian atmosphere.

The interior component consists of solar xenon with a fission contribution similar to that suggested by Chass-E, but with a higher fission contribution (Mathew and Marti, 2001). Though present in all minerals analyzed, it is best defined in pyroxene-dominate separates. The pyroxene-dominate separates exhibit a consistent $^{129}Xe_{xs}$ (^{129}Xe/^{132}Xe ~ 1.2) that contrasts with the maskelynite- and opaque-dominate minerals separates where ^{129}Xe/^{132}Xe increased with increasing release temperature. This interior component in the pyroxene-dominate separate is thought to be ambient xenon, which is a mixture of solar, fission and atmospheric components, present in the magma in which the pyroxenes formed before incorporation. The fission contribution in the interior component is evidence of either an admixture of martian atmosphere to the melt with a high crustal

contribution, or a preservation of a fission anomaly from ^{244}Pu in the source region of the interior component. Further investigation of the interior component in other basaltic shergottites may help in understanding the fission contribution and its origin.

CHAPTER IV

MARTIAN XENON COMPONENTS IN EETA79001 LITHOLOGY B MINERAL SEPARATES

This chapter is a paper by the same name to be submitted to the journal *Earth and Planetary Science Letters* by Katherine D. Ocker and Jamie D. Gilmour.

My contributions to this paper include (1) physical hand-picking of the sample, (2) xenon data analysis, (3) most of the development of the model and (5) the writing.

Abstract

The isotopic signature and concentration of xenon in mineral separates of EETA79001 Lithology B have been measured. Martian atmospheric xenon, as in Shergotty, is more concentrated in opaque minerals (magnetite, ilmenite and pyrrhotite) than in maskelynite and pyroxene. We have previously suggested this reflects grain size variation.

The interior component consists of solar xenon with a fission contribution and is thus similar to that observed in Chassigny, ALH84001, and Nakhla (Mathew and Marti, 2001). As in Shergotty (Ocker and Gilmour, 2001), it is best defined in pyroxene-dominate separates but in contrast to Shergotty, the interior component in EETA79001 Lithology B exhibits no excess ^{129}Xe ($^{129}Xe/^{132}Xe = 1.02 \pm 0.004$) and a lower fission

contribution. This may be a consequence of EETA79001 Lithology B parent magma having had a lesser contribution from a crustal component than Shergotty, as has been suggested to account for differences in isotopic systematics, LREE fractionation and redox state between these two meteorites and among the basaltic shergottites in general.A simple model is constructed of the isotopic evolution of xenon in the martian mantle, crust, and atmosphere investigating the circumstances of rate of differentiation, duration and rate of crustal degassing, and extent of atmospheric loss of Mars to evolve to the required xenon isotopic signatures to serve as the endmembers that then mix together to explain the isotopic systematics of the meteorites. The atmosphere is required to have elevated iodine-derived xenon ($^{129}Xe^*/^{130}Xe$) and low fission-derived to iodine-derived xenon ratio ($^{136}Xe^*/^{129}Xe^*$), along with two interior reservoirs, one consisting of solar xenon with little or no radiogenic xenon and one with a high fissiogenic ratio ($^{136}Xe^*/^{130}Xe$) and a high $^{136}Xe^*/^{129}Xe^*$ ratio. These latter are qualitatively similar to those required to produce the interior components of the shergottites.

Introduction

Literature data suggest some variations in the bulk xenon isotope signatures of the basaltic shergottites (e.g. Mathew and Marti, 2001). Most studies are consistent with a mixture of modern martian atmospheric xenon (SPB) with a martian interior component consisting of fission xenon intimately mixed with solar xenon (refer to figure text in Chapter I and III for references). Presented here is a xenon isotopic study of mineral separates from EETA79001 Lithology-B (hereafter EETA) to complement previous bulk analyses and a mineral separates study of Shergotty (Ocker and Gilmour, 2001). This

study will determine the number and location of the martian xenon components, characterize the proportions of fission and solar xenon present in the interior component, and discuss how these components came to be incorporated into EETA in the context of accepted models of its petrogenisis.

Analyses of mineral separates of Shergotty have previously been presented in Chapter III. The interior component was identified in the pyroxene-dominate separate that had significant excesses of ^{129}Xe and fission isotopes over solar xenon. It was speculated that this component's radiogenic character resulted from the admixture of a 'crustal' component to the parent melt of Shergotty. Such a component has been invoked to explain variations in oxygen fugacity and epsilon neodymium (Borg et al., 1997; Herd and Papike, 2000; Jones, 1986). It is not clear whether the $^{129}Xe_{xs}$ (^{129}Xe/^{132}Xe over 1.03) is a radiogenic component developed in this reservoir or a product of atmospheric contamination, while fission isotopes are clearly not associated with atmospheric contamination. The aim here is to test this hypothesis through analysis of EETA, for which a smaller crustal contribution is required by other geochemical indicators.

Xenon isotopic signatures might also serve as a tracer of planetary processes. Relative proportions of radiogenic xenon isotopes, especially those produced from extinct radionuclides, and stable xenon isotopes can be used to constrain the history of a planet. Terrestrial interior and atmospheric xenon has varying proportions of xenon from the decay of ^{129}I and fission (of ^{244}Pu or ^{238}U or both), and this has been used to estimate the time of Earth's formation and to constrain the degassing history of the planet (Ozima and Pososek, 1983; Porcelli and Wasserburg, 1995). Based on xenon isotope signatures

identified in the martian meteorites, several models of volatile evolution on Mars have been proposed (Bogard et al., 2001 and references therein). To explain the differences observed in the identifiable interior component of Shergotty and EETA, a simple model was designed to track xenon isotopically through differentiation, outgassing and atmospheric loss of Mars. This allows us to test under what circumstances the proposed crustal and mantle reservoirs would evolve xenon with isotopic signatures today similar to those required to explain the meteorite interior components by mixing. Requirements for this model include an atmosphere with excess ^{129}Xe (^{129}Xe*/^{130}Xe > 6.3) and low fissiogenic xenon to iodine-derived ratio (^{136}Xe*/^{129}Xe*); in addition, we attempt to produce two interior reservoirs, one consisting of solar xenon with no radiogenic xenon and one with a high ^{136}Xe*/^{130}Xe ratio and a low ^{129}Xe*/^{136}Xe* ratio to account for the variable interior components.

Experimental Procedure

A portion of a 90 mg chip of EETA79001 Lithology B was prepared for analysis by the methods described in Chapter 2 under the section titled Sample Preparations. EETA was separated into three main mineral separates; pyroxene-dominate, maskelynite-dominate and opaque-dominate phases. Utilizing the published mineral modes (McSween and Jarosewich, 1983), the pyroxene-dominate separates are identified as being composed mostly of pigeonite with lesser proportions of augite. Maskelynite-dominate separates are composed of the diaplectic glass with the possibility of whitlockite and mesostasis, which are found in trace amounts in EETA79001 Lithology-B.

Titanomagnetite, ilmenite, and pyrrhotite make up the opaque-dominate mineral separates. The summaries of the samples generated are summarized in Table III-1.

Samples were loaded into the laser port of the RELAX mass spectrometer (Gilmour et al., 1994) for laser step-heating as described in Chapter 2 under the section title Xenon Extraction.

Results

All xenon data acquired from the analyses are presented in Table IV-2. The evolutions of the $^{129}Xe/^{132}Xe$ ratio with cumulative ^{132}Xe release for the individual mineral separates are plotted in Figure IV-1. The pyroxene-dominate separates show a consistent low $^{129}Xe/^{132}Xe$ ratio of ~1.0 over all temperature steps (Figure IV-1A and B). Both the maskelynite- (Figure IV-1C) and opaque-dominate separates (Figure IV-1D) have increasing excess xenon ($^{129}Xe_{xs}$) with increasing release steps, with the opaque-dominate separates reaching as high as 1.381×10^{-13} ccSTPg^{-1} of $^{129}Xe_{xs}$. The variation in $^{129}Xe_{xs}$ with the opaque release steps could be accounted for if the different minerals present (magnetite, ilmenite and pyrrhotite) have different xenon isotopic signatures and released gas at different temperatures. However, no definitive explanation can account for the similar evolution observed during analysis of the maskelynite-dominate separates. One hypothesis is that maskelynite adsorbs air easily, explaining why it managed to trap a lot of martian atmosphere and why at low temperature it releases a lot of terrestrial atmosphere.

Table IV- 1. EETA79001 Lithology-B samples for xenon isotope study.

Sample	Mass	Preparation Treatment
PYX-01	4.76 mg	Plucked from crushed grains
PYX-02	5.87 mg	Plucked from crushed grains
MSK-01	5.52 mg	Plucked from crushed grains
OPQ-01	0.38 mg	Plucked from crushed grains

Table IV- 2. Data from EETA79001 Lithology-B.

	^{132}Xe	$\frac{^{124}Xe}{^{132}Xe}$	$\frac{^{126}Xe}{^{132}Xe}$	$\frac{^{128}Xe}{^{132}Xe}$	$\frac{^{129}Xe}{^{132}Xe}$	$\frac{^{130}Xe}{^{132}Xe}$	$\frac{^{131}Xe}{^{132}Xe}$	$\frac{^{134}Xe}{^{132}Xe}$	$\frac{^{136}Xe}{^{132}Xe}$
PYX-01, pyroxene-dominate mineral separates, 4.758 mg.									
1	1.059± 0.013	0.26± 0.09	0.65± 0.09	8.03± 0.23	99.45± 1.03	14.84± 0.30	79.02± 0.87	39.61± 0.54	33.58± 0.49
2	0.200± 0.005	0.16± 0.38	0.06± 0.38	7.00± 0.53	99.88± 2.43	14.95± 0.72	79.14± 2.05	39.14± 1.27	33.54± 1.15
3	0.033± 0.003	0.19± 2.50	1.81± 2.50	10.80± 2.72	107.37± 10.11	12.55± 2.82	80.16± 8.23	38.79± 5.12	35.11± 4.77
4	0.031± 0.003	0.19± 2.13	0.28± 2.13	6.51± 2.23	107.47± 8.87	13.16± 2.48	78.22± 7.12	35.31± 4.33	33.77± 4.12
5	0.067± 0.003	0.04± 1.12	0.04± 1.12	7.00± 1.23	116.03± 5.60	14.16± 1.49	75.75± 4.18	40.29± 2.72	33.14± 2.43
6	0.161± 0.005	0.35± 0.48	0.86± 0.48	7.85± 0.63	106.03± 2.87	14.77± 0.81	77.97± 2.30	39.44± 1.45	33.46v 1.31
7	0.225± 0.006	0.25± 0.36	0.10± 0.36	7.20± 0.51	102.93± 2.37	14.39± 0.67	78.47± 1.94	38.41± 1.20	32.46± 1.09
8	0.318± 0.007	0.21± 0.27	0.17± 0.27	7.25± 0.42	105.21± 2.04	14.55± 0.57	78.86± 1.65	39.58± 1.04	33.76± 0.94
9	0.763± 0.011	0.31± 0.11	0.37± 0.11	7.37± 0.24	104.59± 1.20	14.58± 0.34	79.02± 0.98	39.18± 0.61	33.68± 0.55
10	0.007± 0.002	1.12± 6.81	3.88± 6.86	29.27± 8.68	114.47± 25.64	11.11± 7.25	73.74± 19.39	39.99± 12.74	30.89± 11.34
11	0.048± 0.003	0.22± 1.58	1.47± 1.58	9.73± 1.77	104.52± 6.84	13.81± 1.95	78.17± 5.58	41.35± 3.60	33.05± 3.19
Total:	2.912± 0.022	0.26± 0.09	0.48± 0.09	7.74± 0.15	102.75± 0.66	14.62± 0.19	78.80± 0.54	39.35± 0.34	33.51± 0.31
PYX-02, pyroxene-dominate mineral separates, 5.866 mg.									
1	0.795± 0.009	0.29± 0.08	0.07± 0.08	7.41± 0.21	99.77± 1.01	14.94± 0.30	79.16± 0.85	38.92± 0.52	33.17± 0.47
2	0.589± 0.010	0.06± 0.16	-0.07± -0.16	7.43± 0.32	97.36± 1.47	14.48± 0.44	78.39± 1.25	39.78± 0.79	32.92± 0.70
3	0.298± 0.006	0.41± 0.20	0.45± 0.21	6.91± 0.36	99.36± 1.67	14.41± 0.49	78.73± 1.40	39.62± 0.88	33.18± 0.78
4	0.129± 0.004	0.46± 0.46	0.18± 0.46	7.32± 0.65	101.33± 2.78	14.53± 0.81	79.79± 2.33	39.48± 1.45	33.37± 1.31
5	0.147± 0.004	0.48± 0.41	0.67± 0.41	8.42± 0.62	104.77± 2.64	14.43± 0.75	78.57± 2.14	39.42± 1.34	33.92± 1.22
6	0.375± 0.007	0.39± 0.18	0.46± 0.18	7.69± 0.34	104.06± 1.58	14.64± 0.45	79.39± 1.29	39.34± 0.80	33.81± 0.72
7	0.167± 0.005	0.41± 0.40	0.33± 0.40	7.03± 0.65	105.09± 2.67	14.02± 0.75	79.88± 2.17	39.11± 1.35	33.84± 1.23
8	0.679± 0.009	0.31± 0.10	0.37± 0.10	7.07± 0.25	99.23± 1.15	14.73± 0.34	79.35± 0.97	39.67± 0.60	33.70± 0.54
9	0.298± 0.007	0.22± 0.24	0.35± 0.25	9.26± 0.48	98.47± 1.85	14.75± 0.55	80.15± 1.58	39.21± 0.97	34.02± 0.89
10	0.333± 0.007	0.30± 0.22	0.67± 0.22	8.78± 0.45	101.53± 1.81	14.60± 0.52	78.62± 1.49	39.31± 0.93	33.54± 0.84
11	0.419± 0.007	0.26± 0.15	0.44± 0.15	7.55± 0.31	104.72± 1.48	14.89± 0.42	78.82± 1.20	39.76± 0.75	33.70± 0.68
12	0.090± 0.004	-0.07± -0.72	0.36± 0.72	7.31± 0.94	112.07± 4.07	13.71± 1.10	77.16± 3.14	40.66± 2.03	33.41± 1.82
13	0.013± 0.002	-2.77± -5.87	5.43± 5.92	21.96± 7.49	129.67± 25.16	13.78± 6.65	87.60± 19.21	48.36± 12.43	23.93± 9.86
14	0.029± 0.003	-1.00± -2.80	1.42± 2.80	9.88± 3.26	124.88± 12.68	13.72± 3.32	74.67± 9.09	41.48± 6.01	32.91± 5.40
Total:	4.361± 0.024	0.27± 0.06	0.32± 0.06	7.67± 0.11	101.19± 0.48	14.64± 0.14	79.06± 0.40	39.48± 0.25	33.45± 0.22

Table IV-1 continue. Data from EETA79001 Lithology-B

	^{132}Xe	$\frac{^{124}Xe}{^{132}Xe}$	$\frac{^{126}Xe}{^{132}Xe}$	$\frac{^{128}Xe}{^{132}Xe}$	$\frac{^{129}Xe}{^{132}Xe}$	$\frac{^{130}Xe}{^{132}Xe}$	$\frac{^{131}Xe}{^{132}Xe}$	$\frac{^{134}Xe}{^{132}Xe}$	$\frac{^{136}Xe}{^{132}Xe}$
MSK-01, maskelynite-dominate mineral separates, 5.519 mg.									
1	0.295± 0.007	0.06± 0.28	0.47± 0.28	7.66± 0.44	97.82± 1.96	14.89± 0.59	77.93± 1.66	40.10± 1.05	32.79± 0.93
2	0.119± 0.005	0.31± 0.83	0.93± 0.83	8.90± 1.00	102.23± 4.07	15.31± 1.21	78.28± 3.36	42.39± 2.20	32.04± 1.88
3	0.084± 0.003	0.40± 0.78	-0.14± -0.78	6.76± 0.86	102.71± 3.59	15.15± 1.11	79.96± 3.00	39.57± 1.86	33.24± 1.68
4	0.046± 0.003	0.15± 1.52	-0.23± -1.52	8.59± 1.60	111.83± 6.02	14.58± 1.79	79.13± 4.75	40.01± 2.99	32.02± 2.66
5	0.272± 0.006	0.45± 0.28	0.35± 0.28	8.35± 0.44	112.61± 2.06	14.32± 0.56	78.81± 1.59	39.71± 1.00	33.46± 0.89
6	0.143± 0.005	0.27± 0.53	0.43± 0.53	7.38± 0.70	126.42± 3.36	14.77± 0.86	79.94± 2.42	39.29± 1.50	34.37± 1.37
7	0.221± 0.006	0.33± 0.40	0.66± 0.40	7.61± 0.57	137.40± 2.99	14.88± 0.72	81.11± 2.03	40.52± 1.27	35.17± 1.15
8	0.020± 0.002	0.58± 3.59	-0.78± -3.59	6.86± 3.71	146.57± 15.32	10.59± 3.78	78.43± 10.08	35.46± 6.20	33.02± 5.86
9	0.103± 0.005	0.69± 1.01	0.56± 1.01	7.07± 1.17	143.65± 5.56	15.94± 1.39	79.30± 3.66	39.03± 2.29	32.70± 2.07
Total	1.303± 0.015	0.32± 0.19	0.42± 0.19	7.79± 0.25	116.51± 1.11	14.79± 0.30	79.21± 0.84	39.98± 0.53	33.45± 0.48
OPQ-01, opaque-dominate mineral separates, 0.379 mg.									
1	1.145± 0.098	0.18± 1.86	0.15± 1.86	10.44± 2.35	102.53± 10.14	13.87± 2.89	82.72± 8.62	42.96± 5.36	33.94± 4.75
2	0.234± 0.026	-1.30± -2.72	-1.98± -2.72	1.30± 2.85	117.10± 12.27	10.41± 3.17	75.50± 9.18	34.01± 5.67	31.04± 5.18
3	1.134± 0.039	0.02± 0.54	0.79± 0.54	8.22± 0.76	150.42± 4.16	13.72± 0.90	78.73± 2.60	38.40± 1.61	35.46± 1.50
4	0.416± 0.025	-0.81± -1.14	0.53± 1.14	8.90± 1.42	137.04± 6.67	13.07± 1.56	82.08± 4.65	41.76± 2.94	33.78± 2.57
5	0.268± 0.039	-0.58± -3.83	-0.32± -3.83	10.19± 4.98	163.83± 26.24	16.79± 5.80	80.84± 16.33	35.38± 9.85	28.34± 8.84
6	0.408± 0.039	0.59± 2.01	-0.54± -2.01	7.90± 2.55	115.11± 11.13	15.87± 3.07	70.81± 8.20	36.41± 5.29	32.56± 4.88
Total	3.604± 0.124	-0.17± -0.61	0.20± 0.61	8.39± 0.77	132.53± 3.75	13.79± 0.91	79.25± 2.66	39.26± 1.65	33.79± 1.50

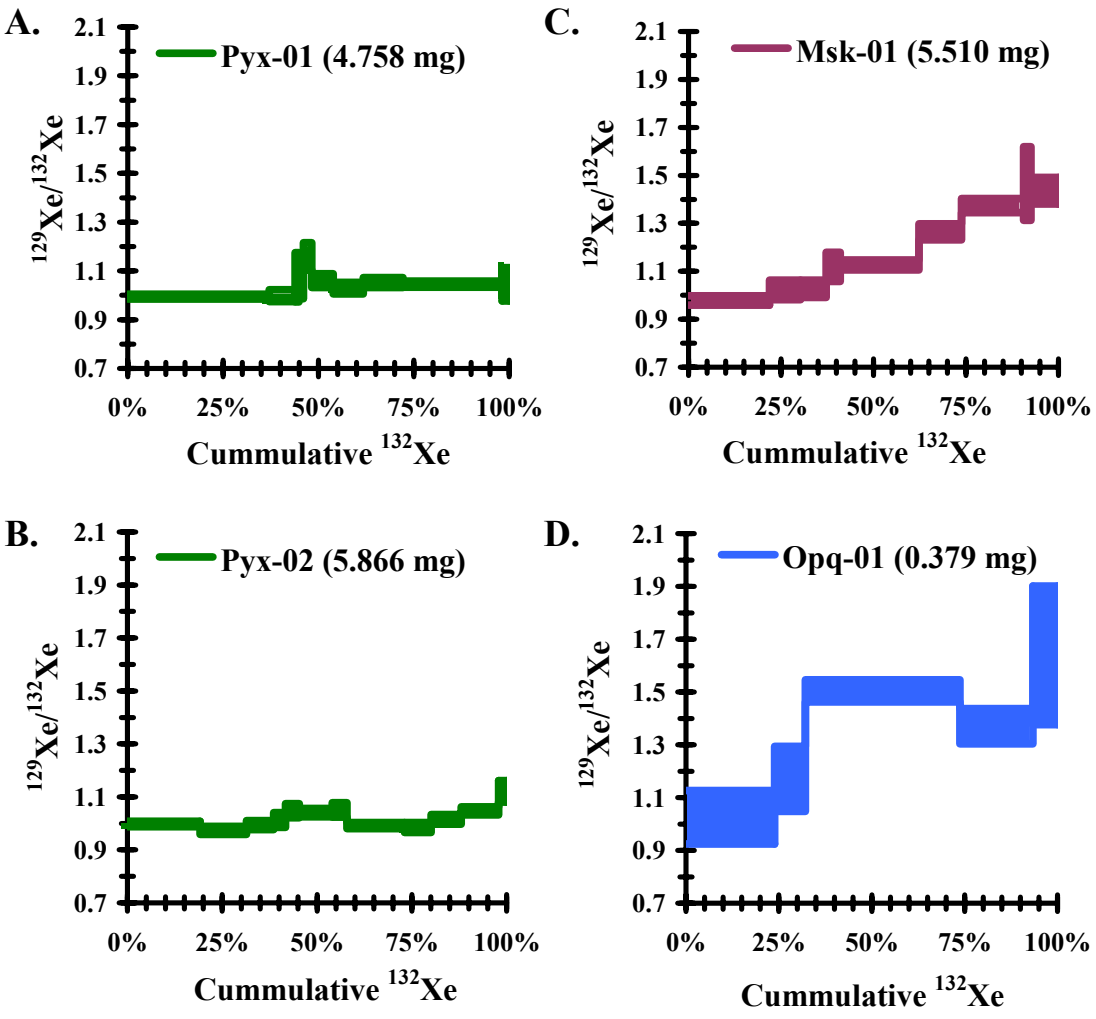

Figure IV-1. The evolutions of the $^{129}Xe/^{132}Xe$ ratio with temperature for the individual mineral separates: pyroxene- (A and B), maskelynite- (C) and opaque-dominate separates(D). The opaques- and maskelynite-dominate separates show an increase in excess $^{129}Xe/^{132}Xe$ (opaques more gas-rich) while the pyroxene-dominate separates show a consistent $^{129}Xe/^{132}Xe$ ~1.2. See text for further details.

The consistently low $^{129}Xe_{xs}$ in the pyroxene data indicate that the xenon martian atmospheric component is absent, unlike the component in the opaque- and maskelynite-dominate separates (Figure IV-2). There are two candidate components that could account for this low ratio: martian interior xenon (solar plus fission) or terrestrial xenon (related to solar xenon by mass fractionation). To determine which endmember is present, in Figure IV-3, the trends obtained by adding fission-xenon to solar xenon and mass-fractionated solar xenon are compared with the average of spallation-corrected pyroxene data. Using the $^{124}Xe/^{132}Xe$ ratio from each release, ^{132}Xe was partitioned between a spallation component with $^{124}Xe/^{132}Xe = 17.933 \pm 3.638$, calculated from the proportion of Ba and LREE expected for EETA79001 (Lodders, 1998) and using the spallation components of Hohenberg et al. (1981) and a trapped component with $^{124}Xe/^{132}Xe = 0.0043 \pm 0.0005$ (the value and errors being chosen to encompass both solar and martian atmospheric values of this ratio). ^{129}Xe and ^{136}Xe were then corrected in proportion to the calculated concentration of spallation ^{132}Xe and summed over the high-temperature steps. The near absence of spallation in all the sample analyses rendered all corrections minor. In Figure IV-3, the pyroxene data are consistent with a mixture of solar xenon and fission xenon rather than mass fractionation of solar xenon. We conclude that the component is of martian origin and not terrestrial contamination.

Table IV-3 shows the spallation-corrected concentrations from the mineral separates from both meteorite samples. As seen in Shergotty (Ocker and Gilmour, 2001), there is a trend of the smallest minerals, opaques in both meteorites, exhibiting the highest gas concentration. The pyroxene-dominate separates are identified as the interior

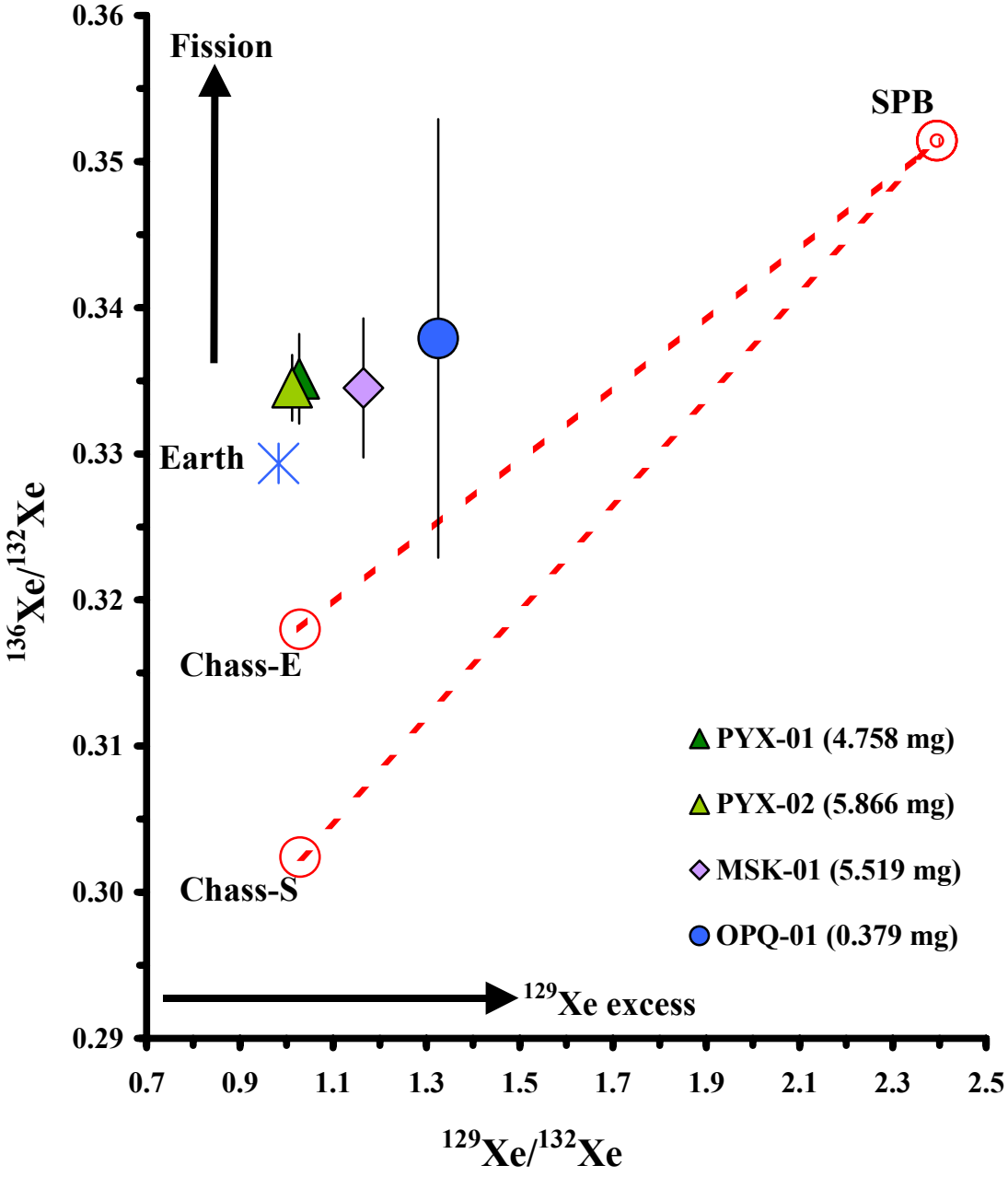

Figure IV-2. The xenon composition of the mineral separates of EETA79001 Lithology-B. The opaques are measured with a higher $^{129}Xe_{xs}$ as well as higher fission xenon contribution than that observed in the other mineral separates. SPB (Shergottite Parent Body), and martian mantle-like components (Chass-S and Chass-E) are shown for comparison (Mathew et al., 1998; Ott, 1988; Swindle et al., 1986).

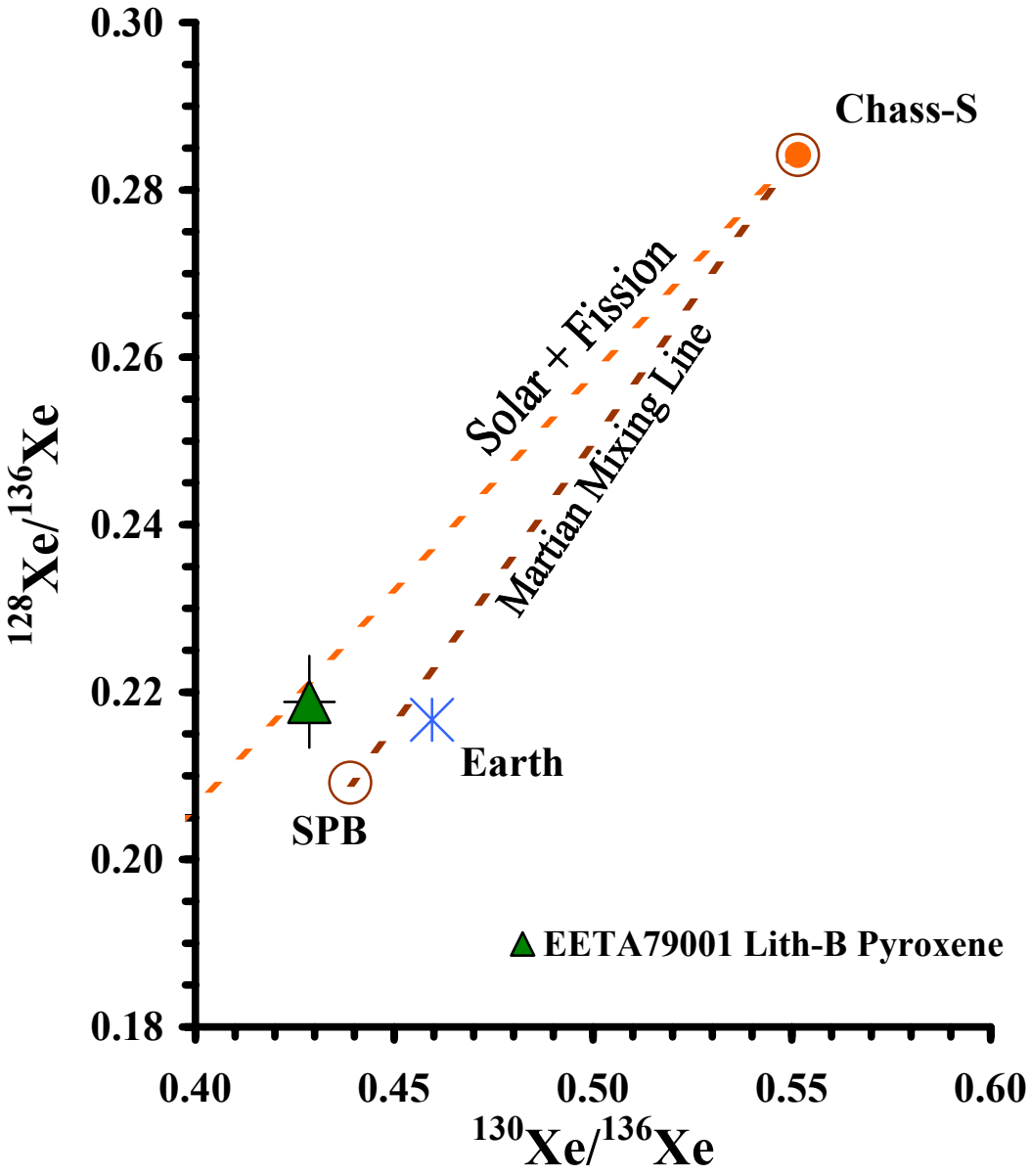

Figure IV-3. $^{128}Xe/^{136}Xe$ versus $^{130}Xe/^{136}Xe$ graph of the average of spallation corrected pyroxene data. The interior component defined by the pyroxene-dominate separates lie on the line illustrating the addition of fission-xenon to solar xenon, as measured in Chassigny. Also drawn is the mixing line between Martian interior and Martian atmosphere. The location of the pyroxene data illustrates that the interior component is a product of solar with a fission contribution and is of Martian origin.

Table IV- 3. Spallation Corrected Xenon Components in EETA79001 Lithology-B and Shergotty.

$^{132}Xe_{total}$[a]	$^{129}Xe_{xs}$[a]	$^{132}Xe_{interior}$[a]	$^{129}Xe/^{136}Xe$	$^{129}Xe_{xs}/^{136}Xe$*
EETA79001-Litholgy B Pyroxene (observed grain size: 1-2 mm)				
3.636 ± 0.016	---[b]	3.608 ± 0.148	3.07519 ± 0.02300	---
Shergotty Pyroxene (observed grain size: 3-4.5 mm)				
1.469 ± 0.011	0.271 ± 0.004	1.305 ± 0.112	3.63230 ± 0.04069	5.28253 ± 2.40556
EETA79001-Litholgy B Maskelynite (observed grain size: up to 0.6 mm)				
1.303 ± 0.015	0.182 ± 0.004	1.196 ± 0.134	3.51927 ± 0.05268	4.73176 ± 0.15655
Shergotty Maskelynite (observed grain size: up to about 1.0 mm)				
3.248 ± 0.022	1.257 ± 0.024	6.823 ± 0.434	3.49569 ± 0.05519	17.26850 ± 3.48732
EETA79001-Litholgy B Opaques (observed grain size: ~0.2 mm)				
3.604 ± 0.124	1.132 ± 0.048	2.977 ± 1.316	3.96436 ± 0.18704	9.21741 ± 0.65556
Shergotty Opaques (observed grain size: ~0.4 mm)				
10.150 ± 0.089	2.616 ± 0.054	8.355 ± 0.662	3.79273 ± 0.05295	7.01919 ± 7.02154

[a]Concentrations in 10^{-12} cm^3 STP g^{-1}. [b]No $^{129}Xe_{xs}$ measured.

xenon component exhibiting little to no atmospheric xenon in EETA. Figure IV-4 compares the observed xenon component in the pyroxene of the two meteorites. The two unique signatures show the possibility that the interior component may reflect a mixture of a mantle (solar) component with a crustal component (fission xenon with, in this case, little or no $^{129}Xe_{xs}$).

Discussion

Xenon Components in EETA79001 Lithology B

As observed in Shergotty, mineral separates of EETA have two identifiable martian components that can be associated with particular mineral hosts.

The martian atmosphere component is more concentrated in the opaque-dominate separates than in the maskelynite-dominate separates, and more concentrated in both than in the pyroxene. This mimics the results of Shergotty mineral separates and is consistent with the model of shock incorporation of adsorbed atmospheric gas. The smaller the grain size, the more surface area per unit mass and higher the concentration of xenon after shock incorporation (Gilmour et al., 1998b). From EETA mineral separates, the smallest grain sizes are the opaques (less than ~ 200 μm) followed by maskelynite (up to about ~ 600 μm) and then pyroxenes (1-2 mm). This broadly corresponds to the trend perceived in Shergotty, with the atmospheric component sited in the mineral separates such that the opaque-dominate separates have a higher gas concentration followed by maskelynite-dominate separates and lastly the pyroxene-dominate separates. Adsorption

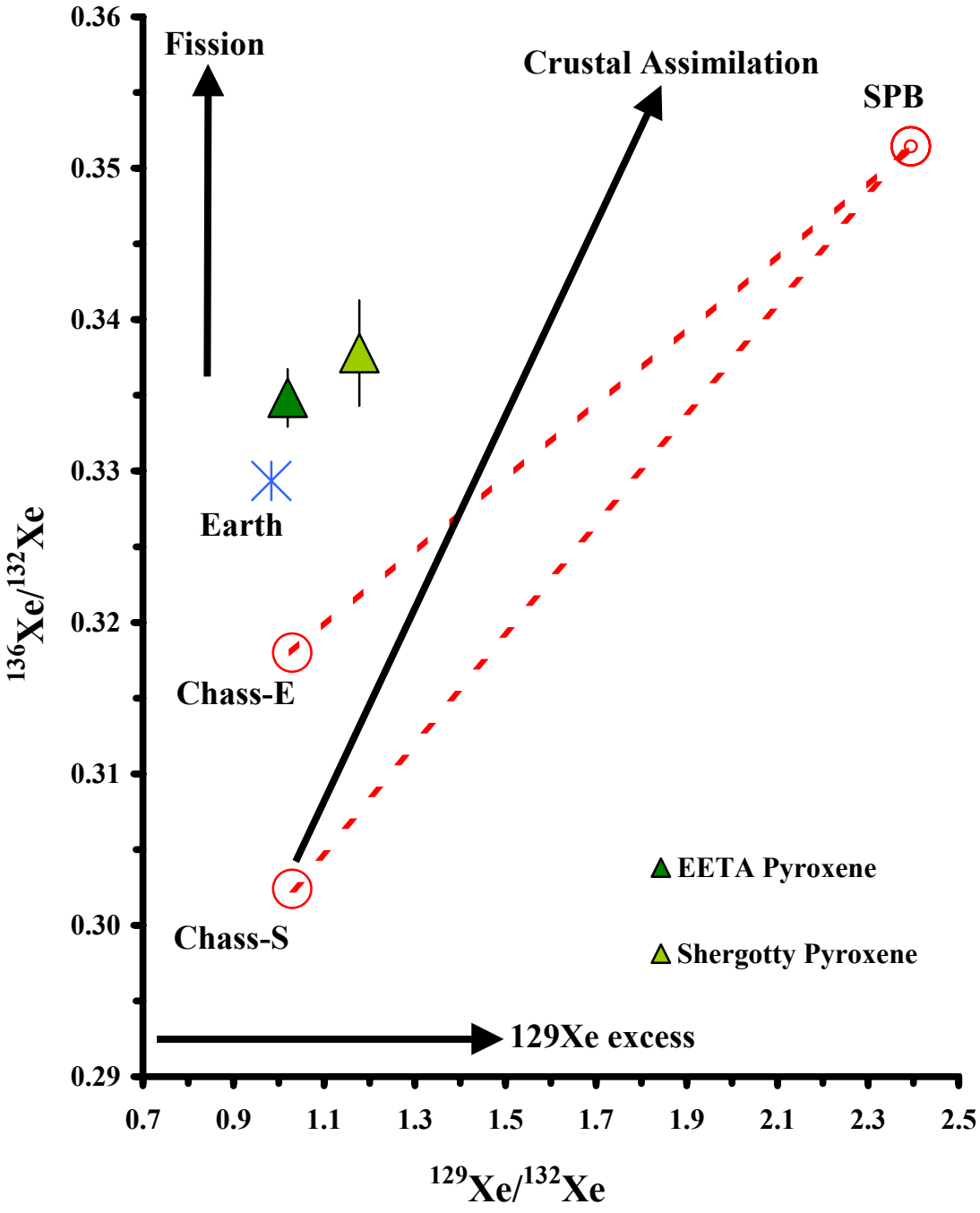

Figure IV-4. Comparison of interior components of Shergotty and EETA79001 Lithology-B. Shergotty has a higher fission component as well as a mixture from the martian atmosphere compared to EETA79001 Lithology-B. This relationship may reflect isotopic systematics seen in neodymium and strontium, rare Earth fractionation and oxygen fugacity in that Shergotty assimilated more crust in its parent melt than EETA79001 Lithology-B. The endmember components are the same as in Figure IV-2.

of xenon onto mineral surfaces is not independent of the chemical composition of the surface, so a perfect correlation is not to be expected. The combination of absorbed atmospheric gas that is shock implanted seems to be the best explanation presented to date of the observed gas concentration in the mineral separates. Consideration of shock implantation as the only mechanism (i.e. without including the effect of adsorption) would lead to the speculation that maskelynite, a diaplectic glass formed from plagioclase that has experienced shock, should have a higher concentration of gases than the opaques. The data illustrate that this is not the case.

It is important to note that the process that led to the incorporation of xenon from the martian atmosphere is also implicated in the elemental fractionation that decreased the Kr/Xe ratio observed in the martian meteorites. Nakhlites and ALH84001 have a lower $^{84}Kr/^{132}Xe$ ratio for their high $^{129}Xe/^{132}Xe$ ratio and thus are not consistent with the same simple mixing array of a martian atmosphere-like component and a martian interior component as the shergottites. The signature seen in EETA, as well as Shergotty, is proposed to be the result from shock incorporation of martian atmosphere that had been adsorbed on grain surfaces and hence was elementally fractionated. Adsorption of xenon on mineral surfaces is significant at the temperatures characteristic of the martian surface, and calculations of Fanale *et al*. (1978) illustrated that adsorbed xenon dominates ambient xenon, implying that some degree of elemental fractionation enhancing Xe in the trapped component is to be expected.

As found in Shergotty, the consistent $^{129}Xe/^{132}Xe$ ratio observed in the pyroxene-dominate separates across all temperature steps suggests that it is the best choice to define

the interior component for EETA. The $^{136}Xe/^{132}Xe$ ratio contains xenon that consists of a mixture of solar xenon and fission xenon, possibly from ^{244}Pu, and is found to be similar to the other documented martian interior components in ALH84001 and Chass-E (Mathew and Marti, 2001). The uniformity of the mixture in pyroxene-dominate separates suggests that this is the signature of the ambient xenon present in the magma from which EETA crystallized. $^{129}Xe_{xs}$ is notably absent from EETA while present in Shergotty. The elevated $^{129}Xe/^{132}Xe$ ratio observed in Shergotty's interior component could be evidence of an admixture of martian atmosphere to the melt perhaps, consistent with the higher crustal contribution seen in Shergotty (Borg et al., 1997; Herd and Papike, 2000; Herd et al., 2001; Jones, 1986).

Both basaltic meteorites have interior xenon that is a mixture of two components: solar ("unradiogenic") and radiogenic. The differences observed in the interior component can be attributed to unique source regions for the meteorites: Shergotty, with an elevated $^{129}Xe/^{132}Xe$ ratio and high $^{136}Xe/^{132}Xe$ ratio preserved in its source region, while EETA's source region, the $^{129}Xe/^{132}Xe$ ratio is absent and has a lower $^{136}Xe/^{132}Xe$ ratio. These possible scenarios are addressed in the xenon model discussed below. However, instead of suggesting two unique source regions from which these meteorites formed, a model was constructed to explain the interior xenon as reflecting a different mixture of mantle (solar, unradiogenic) and crust (radiogenic) components.

Modeling of Interior Xenon in the Basaltic Shergottites

From the same starting material, two reservoirs (crust and mantle) separated early in geological time by differentiation and each may experience some degassing. The

model uses a simple rate equation approach to trace the passage of xenon and its parent radiogenic isotopes ^{129}I ($t_{1/2}$ = 16 Myr), ^{244}Pu ($t_{1/2}$ = 82 Myr), and ^{238}U ($t_{1/2}$ = 4.47 Gyr) between the reservoirs and radioactive decay. It is assumed that Mars accreted from material having initial ratios of $^{129}I/^{127}I$ (1×10^{-4}) and $^{244}Pu/^{238}U$ (6.8×10^{-3}), and total abundance of I (1.97×10^{-14} moles/gram), U (1.05×10^{-10} moles/gram), and Xe (5.38×10^{-13} moles/gram), based on given chemical compositions of Mars (Dreibus and Wanke, 1987) but adjusted to the mass of the entire planet. The degassing from these two reservoirs creates a third reservoir, the atmosphere. This provides an exterior constraint on the model in that the atmosphere created must be somewhat like Mar's. Atmospheric loss is then included into the model as suggested by atmosphere evolution models (Pepin, 1991, 1994; Swindle and Jones, 1997).

Rates of differentiation, degassing and atmospheric loss can be varied as free parameters to investigate under what circumstances the isotopic signatures of the reservoirs are qualitatively similar to those necessary to explain martian meteorite xenon components. Mantle evolution is governed by a set of coupled differential equations

$$d/dt(^{132}Xe) = {}^{132}Xe_o(1 - \alpha - \beta) \quad (1)$$

$$d/dt(^{129}I) = {}^{129}I_o(1 - \alpha - \lambda_{129}) \quad (2)$$

$$d/dt(^{244}Pu) = {}^{244}Pu_o(1 - \alpha - y_1\lambda_{244}) \quad (3)$$

$$d/dt(^{238}U) = {}^{238}U_o(1 - \alpha - y_2\lambda_{238}) \quad (4)$$

$$d/dt(^{129}Xe) = {}^{129}Xe_o(1 - \alpha - \beta) + {}^{129}I_o\lambda_{129} \quad (5)$$

$$d/dt(^{136}Xe) = {}^{136}Xe_o(1- \alpha - \beta) + {}^{244}Pu_o\, y_1\lambda_{244} + {}^{238}U_o\, y_2\lambda_{238} \quad (6)$$

The mantle is assumed to lose constituents by the transport coefficient α during differentiation. After differentiation, the model allows gaseous species to be lost from the mantle to the atmosphere, not to the crust, with degassing coefficient β. λ_{129}, λ_{244}, and λ_{238} are the decay constants of ^{129}I (4.08×10^{-2} Myr^{-1}), ^{244}Pu (8.45×10^{-3} Myr^{-1}), and ^{238}U (1.55×10^{-4} Myr^{-1}), respectively, and y_1 and y_2 is the fraction of ^{136}Xe produced by the decay of ^{244}Pu (7.05×10^{-5}) and ^{238}U (3.50×10^{-8}), respectively. For the proposed shergottite relationship, the mantle retains high Xe/(Pu+U) and Xe/I ratios so that xenon ratios do not evolve away from solar. This xenon ratio decreases if the mantle degasses, but only affects xenon ratios if Pu, U and I are still alive at the time of degassing. This ratio can only increase if xenon is more compatible than the other elements.

Crustal evolution is governed by

$$d/dt(^{132}Xe) = {}^{132}Xe_c(1 - \chi) + {}^{132}Xe_o\alpha \quad (7)$$

$$d/dt(^{129}I) = {}^{129}I_c(1 - \lambda_{129}) + {}^{129}I_o\alpha \quad (8)$$

$$d/dt(^{244}Pu) = {}^{244}Pu_c(1 - y_1\lambda_{244}) + {}^{244}Pu_o\alpha \quad (9)$$

$$d/dt(^{238}U) = {}^{238}U_c(1 - y_2\lambda_{238}) + {}^{238}U_o\alpha \quad (10)$$

$$d/dt(^{129}Xe) = {}^{129}Xe_c(1 - \chi) + {}^{129}I_c\lambda_{129} + {}^{129}Xe_o\alpha \quad (11)$$

$$d/dt(^{136}Xe) = {}^{136}Xe_c(1- \chi) + {}^{244}Pu_c\, y_1\lambda_{244} + {}^{238}U_c\, y_2\lambda_{238} + {}^{136}Xe_o\alpha \quad (12)$$

The crust accumulates constituents from the mantle and loses gaseous species to the atmosphere with the degassing coefficient χ. For application to the crustal/mantle model of the shergottites, the resultant $^{136}Xe^*/^{130}Xe$ crustal ratio should be greatly elevated above the mantle reservoir.

Atmospheric evolution is then governed by

$$d/dt(^{132}Xe) = {}^{132}Xe_A(1 - \mu) + {}^{132}Xe_o\beta + {}^{132}Xe_c\chi \quad (7)$$

$$d/dt(^{129}Xe) = {}^{129}Xe_A(1 - \mu) + {}^{129}Xe_o\beta + {}^{129}Xe_c\chi \quad (11)$$

$$d/dt(^{136}Xe) = {}^{136}Xe_A(1- \mu) + {}^{136}Xe_o\beta + {}^{136}Xe_c\chi \quad (12)$$

The atmosphere is derived by the influx of gases species from the mantle β, after differentiation, and from the crust χ. The atmosphere is also affected from gas loss events μ such as hydrodynamic escape, sputtering and impact erosion. The $^{129}Xe^*/^{130}Xe$ is expected to be elevated above the mantle reservoir to apply to the atmospheric model of the shergottites.

The model traces the martian mantle, crust, and atmospheric reservoirs through five stages that represent identifiable processes which Mars has experienced throughout geological history.

1. The period of accretion and differentiation of Mars from planetesimals. The duration, $0<t<20$ Myr, is based on consideration of ^{182}Hf-^{182}W isotopic systematics (Lee and Halliday, 1997) and not varied as a free parameter. Any Xe produced by decay of ^{129}I, ^{244}Pu and ^{238}U before $t = 0$ is assumed to have been lost. Data from the nakhlites,

where the interior component is preserved in the mesostasis (Gilmour et al., 1999) and hence correlates with large ion lithophiles, demonstrate that xenon behaves as an incompatible element in a closed system during nakhlites crystallization (except that it can partition into a gas phase) (Marty and Marti, 2002). Based on the study of Angra dos Reis mineral separates, plutonium was shown to behave geochemically in a way similar to the LREE (Lugmair and Marti, 1977). This coherence of Pu and LREE is the result of the similarity of their ionic radii and valences (+3). From studies of solubility of iodine (Musselwhite and Drake, 2000; Musselwhite et al., 1991), it has been proposed that the high $^{129}Xe/^{132}Xe$ ratio of the martian atmosphere is the result of transfer of iodine early to the martian crust. Therefore, for this model, all constituents are assumed to have behaved as incompatible elements during differentiation and to have been transported to the crust at the same rate. Figure IV-5 illustrates the evolution of the radiogenic ratios through two scenarios for the mantle: evolution with only transport affecting the loss of constituents, and evolution with transport affecting the loss of constituents during differentiation and then degassing of the mantle after the period of differentiation. Note that even initial concentration ratios preserve some evolution of xenon isotopes occurrence, implying either xenon is more compatible (retained better during differentiation) or the initial Xe/(Pu+U) and Xe/I was higher.

2. Continual early atmosphere formation beyond differentiation by degassing fractions of the primordial xenon, ^{129}Xe produced by ^{129}I decay, and Pu+U-derived ^{136}Xe. The requirement to produce a crust with elevated $^{136}Xe/^{130}Xe$ and low $^{129}Xe/^{130}Xe$, and with significant concentrations of $^{136}Xe^{*}$, imposes quite stringent constraints on its

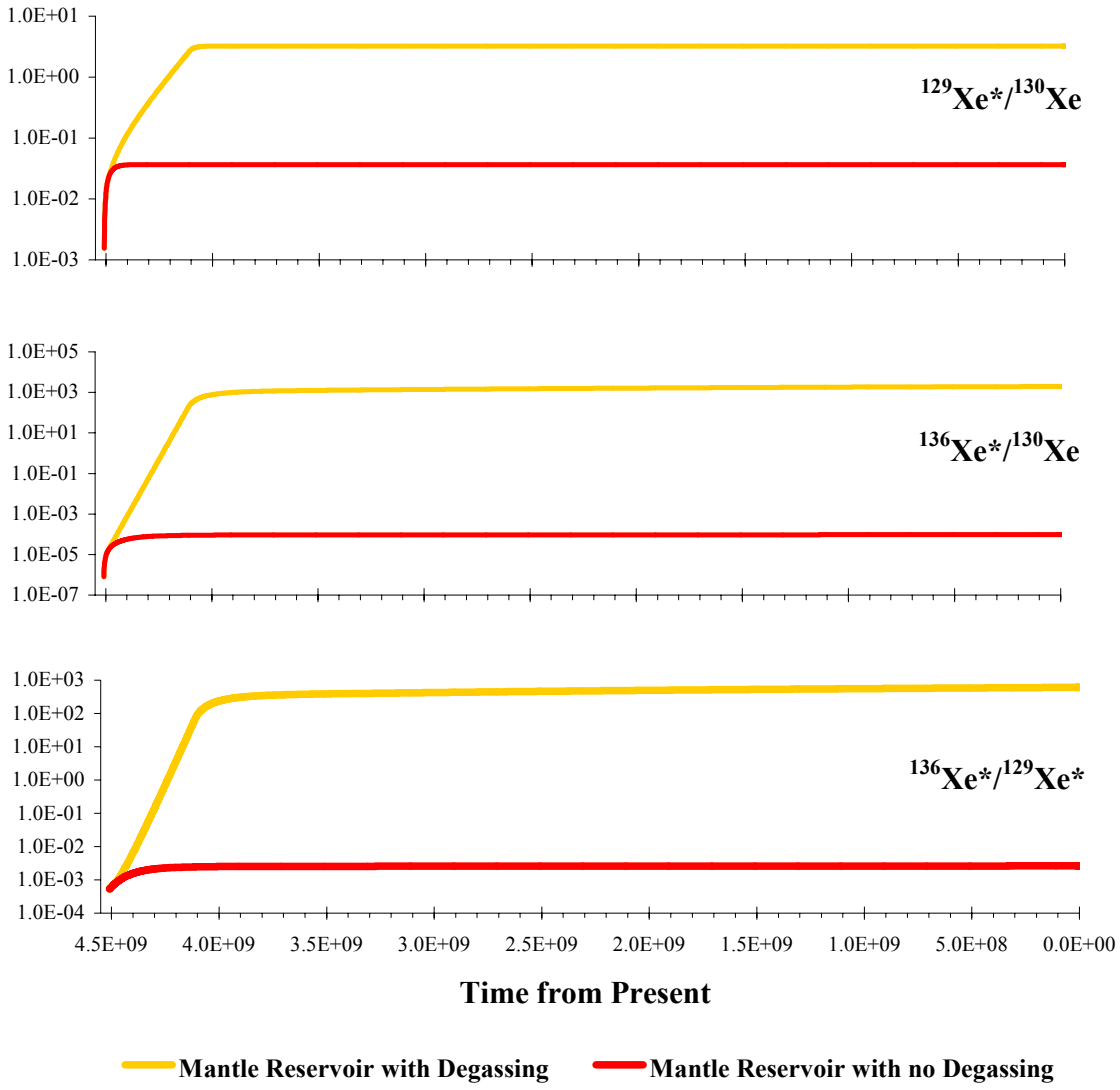

Figure IV- 5. Comparison of mantle evolution with and without degassing. Note that even initial concentration ratios preserve some evolution of xenon isotopes occurrence, implying either xenon is more compatible (retained better during differentiation) or the initial Xe/(Pu+U) and Xe/I was higher.

degassing history. Early major loss of ^{130}Xe is required to allow the $^{136}Xe/^{130}Xe$ ratio to evolve upwards subsequently. This loss must have continued on timescales long compared to that characteristic of ^{129}I decay (>~100Ma) to allow high $^{136}Xe^*/^{129}Xe^*$ ratios.

3. Atmospheric loss by hydrodynamic escape and erosion (Pepin, 1991, 1994) at a time 100 Myr after accretion. The gas is depleted from the early atmosphere and xenon isotopic compositions are set by the hydrodynamic escape and thereafter preserved (Pepin, 1991, 1994).

4. Continual degassing, releasing fractions of gas that either remain in the crust after the atmospheric loss or are produced by decay. The preservation of a fission anomaly from ^{244}Pu in the young meteorites suggests this degassing rate must have declined drastically on timescales short compared to that characteristic of ^{244}Pu decay (<~800 Ma), thus allowing xenon components with elevated $^{136}Xe/^{132}Xe$ ratios to form as ^{244}Pu decayed and subsequently conserve these components.

5. Late erosion of the atmosphere. Based on observations of impact erosion and fluvial features on the martian surface, a profound change in the atmospheric state is suggested (Pepin, 1994 and references within).

Table IV-4 summarizes a variety of solutions, with Figures 6-9 illustrating the xenon ratios evolution observed for some of the various parameters. In most of the models, α is chosen to move at least 50% of the constituents into the crust where it is available to participate in outgassing from the crust, the believed major source of

atmospheric gas. Note that the mantle reservoir slightly evolves to become radiogenic as a result of the transport coefficient being chosen to partition Xe and I from the mantle at the same rate. The ratio is the result in the build-up of radiogenic xenon in the mantle over time from the decay of ^{238}U isotopes remaining in the mantle. Figures 6 and 7 illustrate two different differentiation rates, $3.4x10^{-8}$ yr^{-1}, which moves ~50% of the constituents into the crust, and $1.0x10^{-7}$ yr^{-1}, which moves roughly 90% of the constituents into the crust. The concentration of the component is affected by the differing differentiation rates, but not the ratios of interest.

Degassing of the mantle, β, is chosen to be zero during the period of differentiation as transport to the crust is assumed to dominate the loss. After differentiation, any degassing from the mantle affects only the concentration of constituents but not the resulting ratios of interest.

Degassing of the crust, χ, is the most restrictive parameter as discussed above. For the models illustrated, χ is assumed to change after ~400 Myr and close ~2.0 Gyr. Listed in Table IV-4 are the various degassing rates before 400Myr (χ_{early}) and the various late degassing rates (χ_{late}). Comparison of Figure 6 and Figure 8 (and consequently Figure 9; however, χ_{late} and μ also differ between the two models) shows how the requirement of an early major loss of ^{130}Xe is needed, thus allowing the $^{136}Xe^*/^{130}Xe$ ratio to consequently evolve upwards. This early loss allows high $^{136}Xe^*/^{130}Xe$ ratio for the crust and a high $^{129}Xe^*/^{130}Xe$ ratio for the atmosphere. For degassing rates slower than $1.0x10^{-8}$ yr^{-1}, the atmospheric reservoir does not obtain the characteristically high $^{129}Xe^*/^{130}Xe$ ratio that defines the martian atmosphere. The time

Table IV- 4. Workable models of martian xenon evolution.

	α (yr^{-1})	χ_{Early} (yr^{-1})	χ_{Late} (yr^{-1})	μ_{Escape} (yr^{-1})	$\mu_{Erosion}$ (yr^{-1})	$\frac{^{136}Xe^*}{^{129}Xe^*}$ Mantle	$\frac{^{136}Xe^*}{^{129}Xe^*}$ Crust	$\frac{^{136}Xe^*}{^{129}Xe^*}$ Atmosphere
1)	$1.0x10^{-7}$	$1.0x10^{-7}$	$1.0x10^{-8}$	$5.0x10^{-7}$	$1.0x10^{-9}$	$2.63x10^{-3}$	$3.76x10^{+9}$	$8.43x10^{-2}$
2)	$6.7x10^{-8}$	$1.0x10^{-7}$	$1.0x10^{-8}$	$5.0x10^{-7}$	$1.0x10^{-9}$	$2.63x10^{-3}$	$3.75x10^{+9}$	$8.41x10^{-2}$
3)	$3.4x10^{-8}$	$1.0x10^{-7}$	$1.0x10^{-8}$	$5.0x10^{-7}$	$1.0x10^{-9}$	$2.63x10^{-3}$	$3.74x10^{+9}$	$8.40x10^{-2}$
4)	$3.4x10^{-8}$	$1.0x10^{-7}$	$1.0x10^{-8}$	$5.0x10^{-7}$	$1.0x10^{-8}$	$2.63x10^{-3}$	$3.74x10^{+9}$	$2.65x10^{+1}$
5)	$3.4x10^{-8}$	$1.0x10^{-7}$	$1.0x10^{-8}$	$1.0x10^{-6}$	$1.0x10^{-8}$	$2.63x10^{-3}$	$3.74x10^{+9}$	$2.77x10^{+1}$
6)	$3.4x10^{-8}$	$1.0x10^{-7}$	$5.0x10^{-9}$	$1.0x10^{-6}$	$1.0x10^{-8}$	$2.63x10^{-3}$	$1.37x10^{+6}$	$2.90x10^{+1}$
7)	$3.4x10^{-8}$	$5.0x10^{-8}$	$1.0x10^{-8}$	$5.0x10^{-7}$	$1.0x10^{-8}$	$2.63x10^{-3}$	$1.33x10^{+9}$	$1.12x10^{+1}$
8)	$3.4x10^{-8}$	$5.0x10^{-8}$	$1.0x10^{-8}$	$1.0x10^{-6}$	$1.0x10^{-8}$	$2.63x10^{-3}$	$1.33x10^{+9}$	$1.16x10^{+1}$
9)	$3.4x10^{-8}$	$5.0x10^{-8}$	$5.0x10^{-9}$	$1.0x10^{-6}$	$1.0x10^{-8}$	$2.63x10^{-3}$	$4.57x10^{+5}$	$1.22x10^{+1}$
10)	$3.4x10^{-8}$	$1.0x10^{-8}$	$5.0x10^{-9}$	$1.0x10^{-6}$	$1.0x10^{-8}$	$2.63x10^{-3}$	$6.19x10^{0}$	$2.28x10^{-1}$

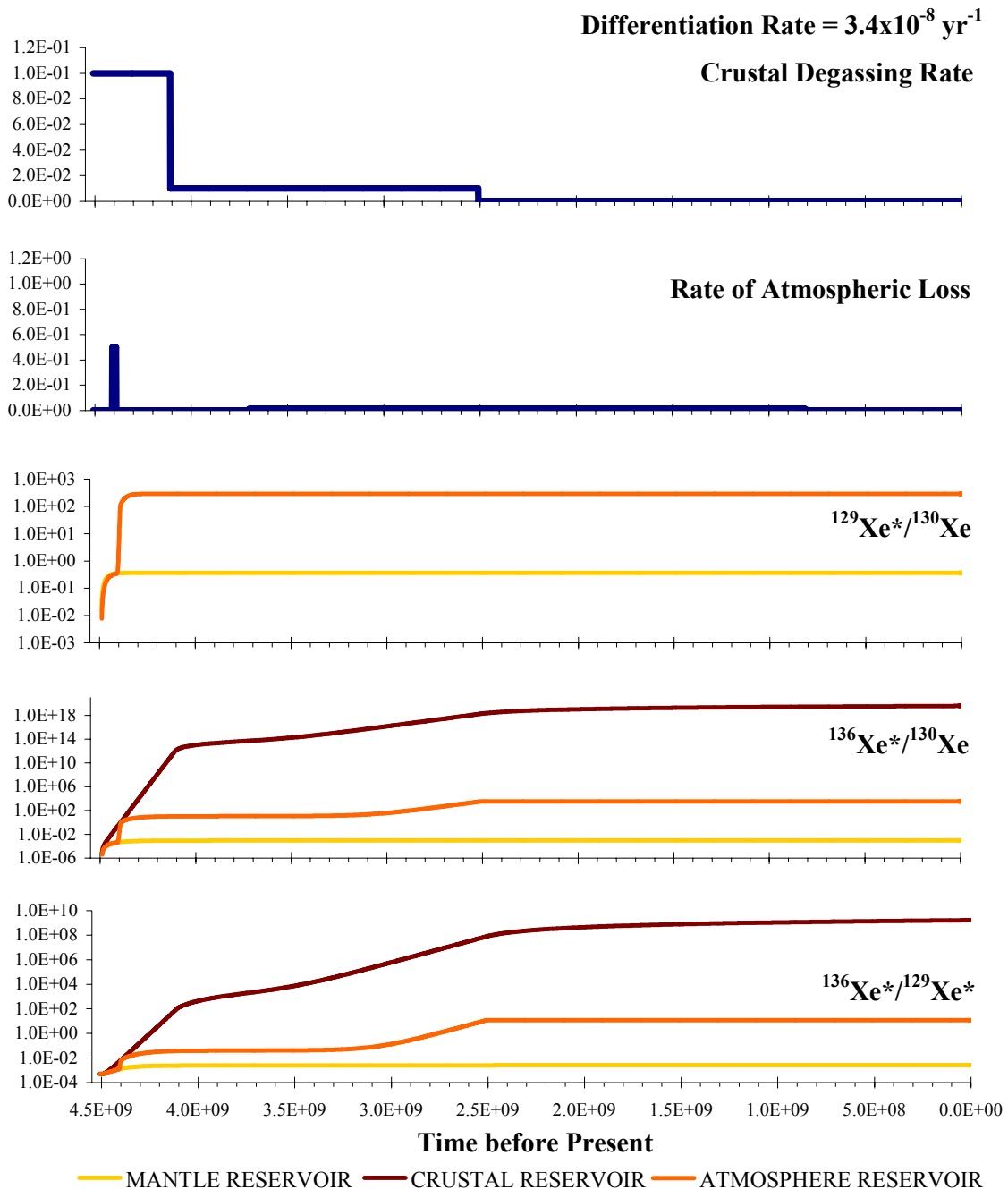

Figure IV-6. Graphical illustration of model 4 in Table IV-4. The workable model seems capable of producing $^{136}Xe^*/^{129}Xe_{xs}$ ratios low in the atmosphere and high in the crust and a source of gas close to solar in the mantle, as required by the present understanding of the martian components.

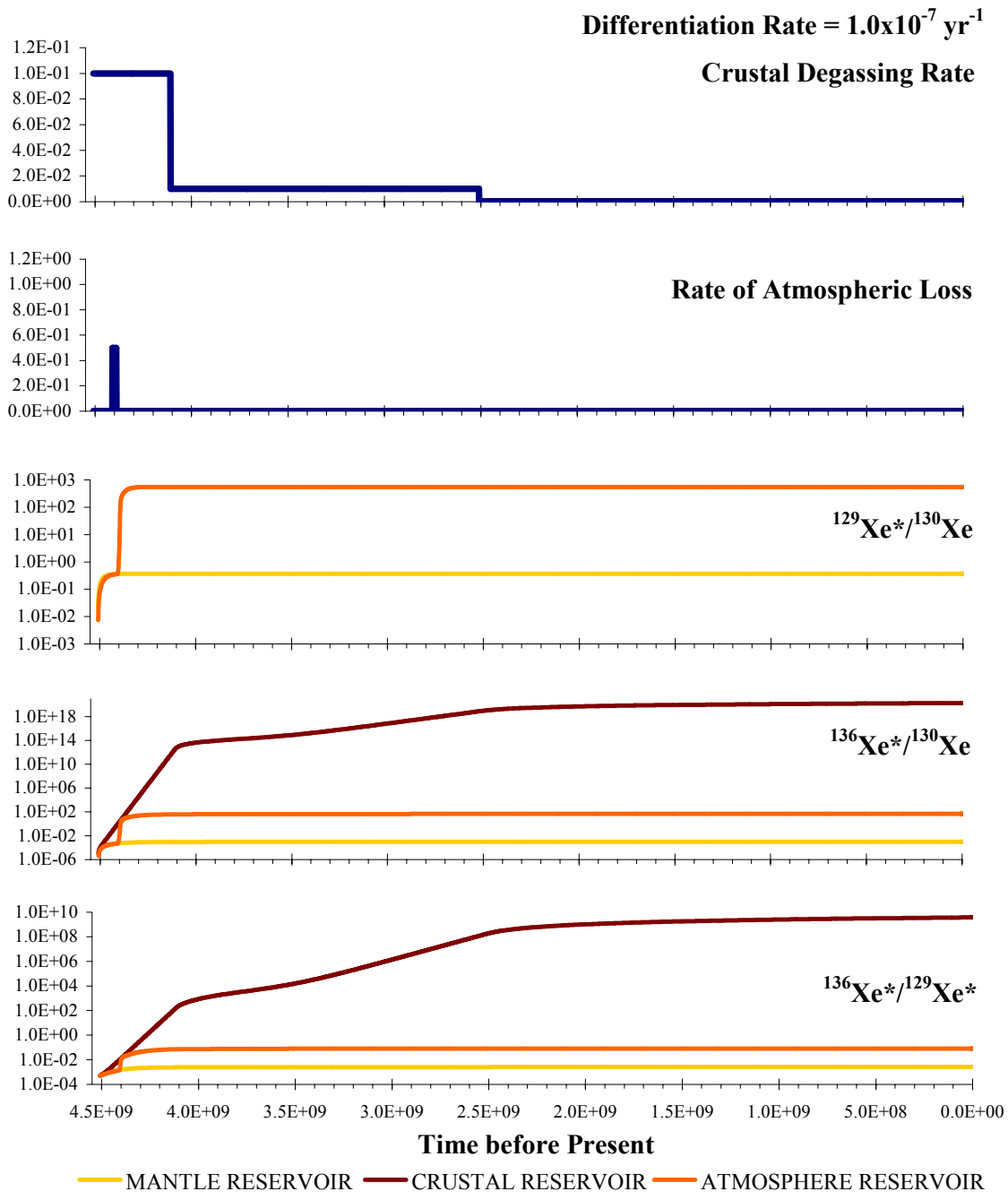

Figure IV-7. Graphical illustration of model 1 in Table IV-4. Similar to Figure IV-5 this model seems to meet the requirements of the present understanding of the martian components. Differentiation rate (α) differ between the two models in that more constituents are moved to the crust with this model.

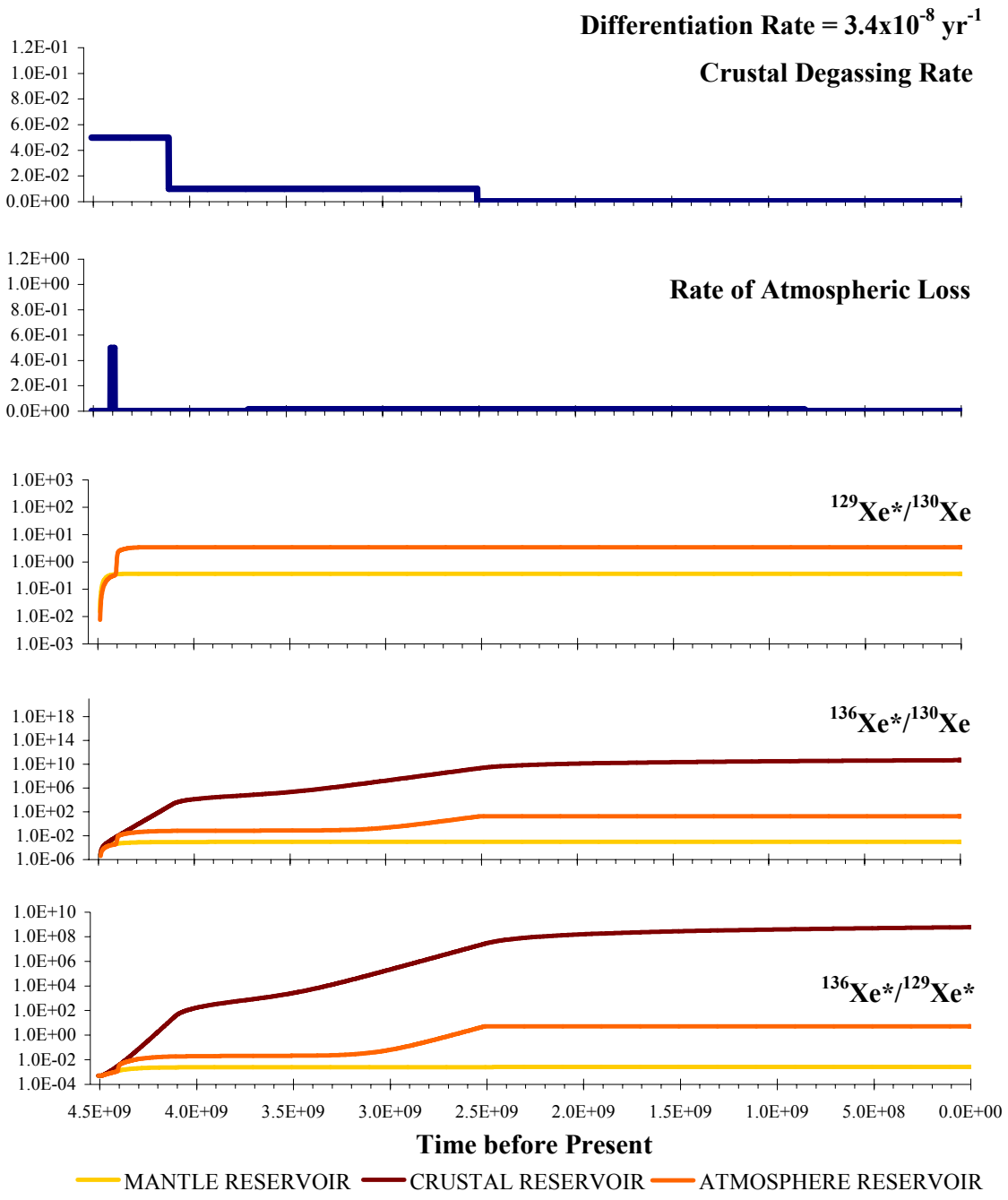

Figure IV- 8. Graphical illustration of model 7 in Table IV-4. Similar to Figure IV-5 this model seems to meet the requirements, however $^{129}Xe_{xs}/^{130}Xe$ ratio in the atmosphere is orders of magnitude smaller, and the $^{136}Xe^*/^{130}Xe$ ratio in the crust is several orders of magnitude smaller. This exemplifies the requirement of a major early degassing event.

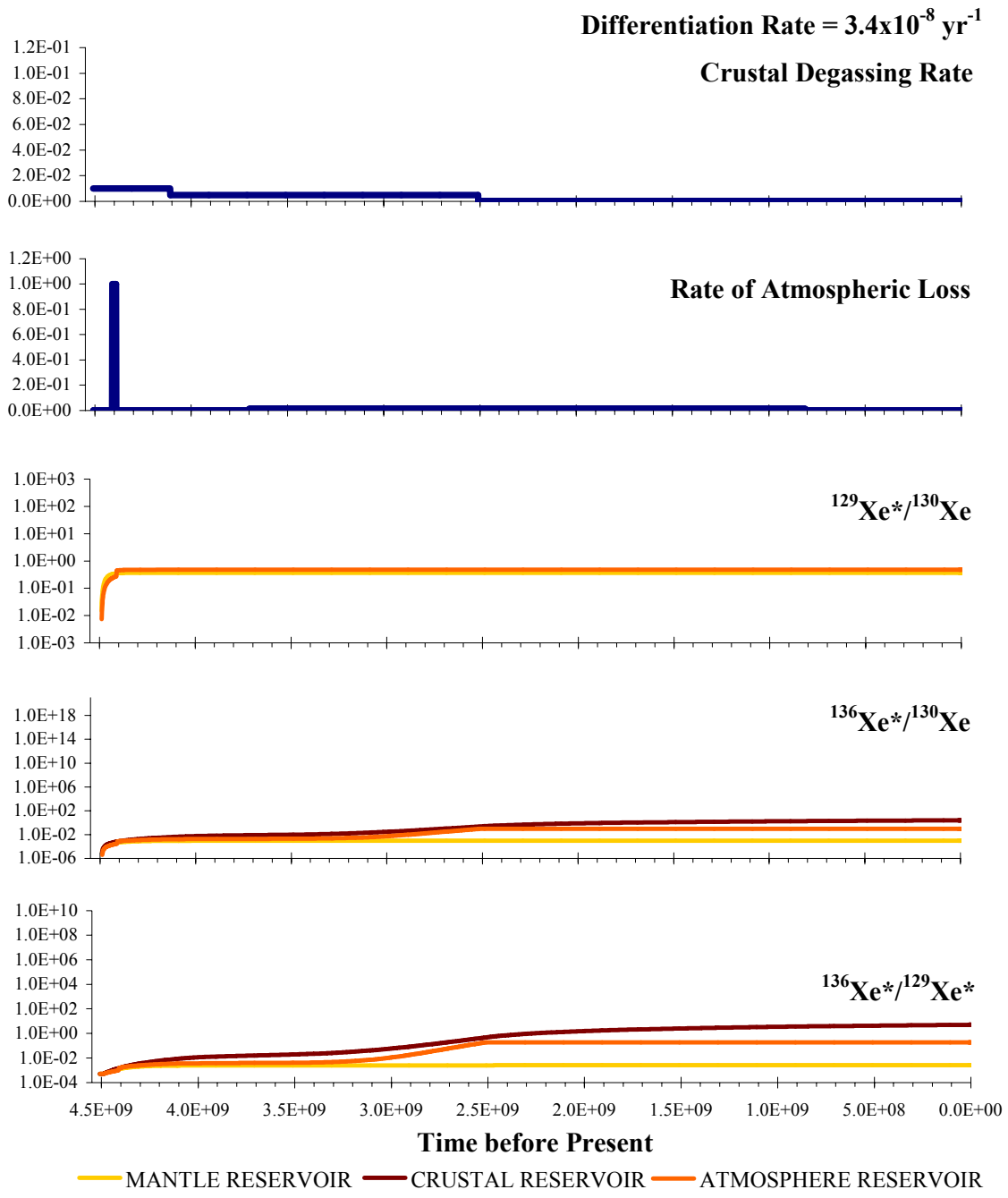

Figure IV- 9. Graphical illustration of model 10 in Table IV-4. Represented here is the worse-case scenario; too slow of early degassing, as well as extreme atmospheric loss during hydrodynamic escape.

in which the degassing rate changes is slightly arbitrary, with the one restriction that the major degassing lasts more than 100 Ma after accretion, based on the decay of ^{129}I, to allow a high ^{136}Xe*/^{129}Xe* ratio to evolve in the crust. The closure of the crust was chosen to allow the possible contribution of ^{136}Xe to the atmosphere reservoir, if the closure of crustal degassing is before 1.42 Ga, the model shows Pu-derived xenon as the dominant fission xenon in the atmosphere.

For hydrodynamic escape, μ is chosen for the maximum depletion of the early atmosphere in most models, while the late erosion rate is at most two orders of magnitude lower than that observed during hydrodynamic escape. The degree of early atmospheric loss has a limited range to provide suitable ratios for the atmosphere. If the rate is too high, all traces of ^{129}Xe* are lost; on the other hand, if the rate is too low, ^{129}Xe is replenished from the decay of ^{129}I and thus the ^{129}Xe*/^{130}Xe ratio is limited by the amount of iodine initially in the system. In either case, the resultant ^{129}Xe*/^{130}Xe ratio is indistinguishable from the mantle, opposing the requirement of a high ratio in the martian atmosphere.

The workable models seems capable of producing ^{136}Xe*/^{129}Xe* ratios low in the atmosphere and high in the crust and a source of gas close to solar in the mantle, as required by the present understanding of the martian components. For the shergottite relationship, this model supports Shergotty's parent magma as a mixture of mantle and crustal reservoirs as well as a contribution from the atmosphere reservoir. EETA's parent magma reflects a mantle reservoir mixed with lesser extent of crustal reservoir. This

supports the argument for crustal assimilation for the observed variations in the basaltic shergottites.

Extending the model to the other major radiogenic rare gas component has presented some problems. For the same properties that lead to elevated $^{136}Xe^*$ in the crust, lead to elevated $^{40}Ar^*$ excesses. This highlights an extreme form of an outstanding problem in the identification of anomalies due to ^{244}Pu decay in martian meteorites; the absence of identifiable excess of parentless ^{40}Ar from ^{40}K decay. A source region with substantial fission anomalies from ^{244}Pu decay must have closed to xenon loss within 500 Ma of the origin of the solar system, suggesting that ^{40}Ar should have accumulated over ~2.7 Ga before the formation event of the nakhlites. Nakhla has a well defined ^{40}Ar-^{39}Ar age of 1.33 ± 0.03 Ga and a bulk K-Ar age of 1.36 ± 0.03 Ga (Podosek, 1973). These are both identical to the accepted crystallization age of Nakhla, and indicate that the parent melt was substantially degassed on formation. Preservation of ^{136}Xe fission anomalies in the nakhlites and other young martian meteorites thus requires partition of xenon away from argon at some point during or shortly before formation, a process that is unlikely to have preserved total fission xenon contents in a way that allows ^{136}Xe/Pu ratios to be interpreted chronologically as closure ages of the source region.

Summary

Similar to the observations in Shergotty, maskelynite-dominate, opaque-dominate phases, and pyroxene-dominate separates contain uniquely identified martian atmospheric and interior xenon components. The opaques, the smallest grains, show martian atmospheric xenon (^{129}Xe excess over $^{129}Xe/^{132}Xe$=1) that is 5 times more

concentrated than observed in maskelynite and absent in pyroxene. This further supports the argument of gas concentrations related to grain size, in that the smallest grains present greater surface area for adsorption before shock incorporation of martian atmospheric xenon. Thus, the measured bulk Kr/Xe ratio in the shergottites may be the same elemental fractionations between EETA79001 melt glass and nakhlites, instead of a simple mixing of martian interior and atmosphere components.

The interior component consists of solar xenon with a fission contribution similar to that suggested by Chass-E (Mathew and Marti, 2001). The fission contribution is measured to be higher than Chass-E, but lower than that observed in Shergotty. The pyroxene-dominate separate best defines the interior component though it is present in all minerals analyzed. Pyroxene exhibits a consistent $^{129}Xe_{xs}$ ($^{129}Xe/^{132}Xe \sim 1.03$) that contrasts with the maskelynite and opaque minerals where $^{129}Xe/^{132}Xe$ increased with increasing release temperature. This interior component in pyroxene is thought to be ambient xenon, which is a mixture of solar and fission components, present in the magma in which the pyroxenes formed before incorporation. The fission contribution in the interior component is evidence of a crustal contribution to the melt, but not to the extent documented in Shergotty, or a preservation of a fission anomaly from ^{244}Pu in the source region of the interior component.

To address the different fission contributions in EETA79001 Lithology B and Shergotty, a model was devised to trace the course of xenon and its parent radiogenic isotopes ^{129}I, ^{244}Pu, and ^{238}U between the martian mantle, crust and atmospheric reservoirs and radioactive decay. The model produces $^{136}Xe^*/^{129}Xe^*$ ratios low in the

atmosphere and high in the crust and a source of gas close to solar in the mantle, as required by our present understanding of the martian xenon components.

The identification of a pure solar component in Chassigny argues that, if anything, the model underestimates the initial xenon to iodine/plutonium ratio chosen. Since degassing of the source region rich in plutonium is crucial to the model's success (decay of Pu can only increase $^{136}Xe/^{130}Xe$ once the original complement of solar xenon has been effectively removed), should the interpretation withstand further tests constraints are imposed on the location of this reservoir. Although labeled 'crustal', its identification with the martian crust remains controversial – a mantle reservoir rich in incompatible elements is also a candidate source region. However, the requirement for the source region to be degassed argues in favor of a location close to the surface, in effect strengthening the case for identification with the crust itself. The measurement of fission xenon in Shergotty and lesser extents in EETA79001 Lithology B supports the argument for crustal assimilation.

CHAPTER V

CONCLUSIONS

Xenon analyses of two basaltic shergottites have been presented. This research examined identifiable mineral separates to determine the presence and sites of the martian xenon components. Maskelynite-, opaque-, and pyroxene-dominate mineral separates from Shergotty and EETA79001 Lithology-B contain martian atmospheric and interior xenon components.

The opaques in both meteorites, which are the smallest grains in each meteorite, show martian atmospheric xenon (^{129}Xe excess over ^{129}Xe/^{132}Xe=1). For Shergotty, this concentration is 5-10 times more concentrated in opaque minerals than in maskelynite and pyroxene (on the assumption that excess ^{129}Xe in pyroxene was incorporated through the same mechanism). For EETA79001 Lithology-B it is 5 times more concentrated in the opaques than observed in maskelynite and absent in pyroxene. Atmospheric gas concentrations are argued to relate to grain size, in that the smallest grains present greater surface area for adsorption before shock incorporation of martian atmospheric xenon. This is the same mechanism thought to account for the incorporation of martian atmospheric xenon in Nakhla. Thus the measured bulk Kr/Xe ratio in the shergottites may be the same elemental fractionations between shock melt glass in the SNCs and not a simple mixing of martian mantle and martian atmosphere.

The interior component found in both meteorites consists of solar xenon with a fission contribution and is similar to that observed in Chassigny (Chass-E of (Mathew

and Marti, 2001). Though present in all minerals analyzed, it is best defined in the pyroxene-dominate separates. Pyroxenes from Shergotty and EETA79001 Lithology-B exhibit a consistent $^{129}Xe/^{132}Xe$ ratio (1.2 for Shergotty and 1.03 for EETA79001 Lithology-B) that contrasts with the maskelynite and opaque minerals, where $^{129}Xe/^{132}Xe$ increased with increasing release temperature. The fission contribution for both meteorites is higher than Chass-E, but EETA79001 Lithology-B fission contribution is lower than that observed in Shergotty. This interior component in the pyroxenes of both meteorites is thought to be ambient xenon, which is a mixture of solar, fission and atmosphere (for Shergotty) components, present in the magma in which the pyroxenes formed before incorporation. The fission contribution in the interior component is attributed to an assimilated crustal component to the melt. The extent of this crustal contribution differs for the two meteorites in that Shergotty exhibits a greater extent than that in EETA79001 Lithology-B.

To explain the different fission contributions in EETA79001 Lithology B and Shergotty, a model was constructed to trace the course of xenon and its parent radiogenic isotopes ^{129}I, ^{244}Pu, and ^{238}U between the martian mantle, crust and atmospheric reservoirs and radioactive decay. The model produced $^{136}Xe^*/^{129}Xe_{xs}$ ratios that are low in the atmosphere and high in the crust and a source of gas close to solar in the mantle, as required by our present understanding of the martian xenon components. Degassing of the source region rich in plutonium is crucial to the model's success, as decay of Pu can only increase $^{136}Xe/^{130}Xe$ once the original complement of solar xenon has been effectively removed. This constrains the location of this reservoir; the requirement for the source region to be degassed argues in favor of a location close to the surface, in

effect strengthening the case for identification with the martian crust rather than a mantle reservoir rich in incompatible elements as a candidate source region.

Further work on other basaltic shergottites is needed to establish whether the variation between Shergotty and EET79001 Lithology-B represents part of a wider trend. Work has already begun on the basaltic shergottite Dar al Gani 489. This meteorite is reported as having an even lesser extent of crustal contribution to its melt (Herd and Papike, 2000). If the trend holds true, DaG489 will have even a lesser extent of fission contribution in its interior component.

LIST OF REFERENCES

LIST OF REFERNCES

BART G. D., SWINDLE T. D., OLSON E. K. and TREIMAN A. H. (2001) Xenon and krypton in Nakhla mineral separates. *Abstracts Submitted to the Lunar and Planetary Science Conference* **XXXII**, CD#1363.

BECKER R. H. and PEPIN R. O. (1984) The case for a martian origin of the Shergottites: Nitrogren and noble gases in EETA79001. *Earth and Planetary Science Letters* **69**, 225-242.

BOGARD D. D., CLAYTON R. N., MARTI K., OWEN T. and TURNER G. (2001) Martian volatiles: Isotopic composition, origin, and evolution. *Space Science Reviews* **96**(1-4), 425-458.

BOGARD D. D. and GARRISON D. H. (1998a) Relative abundances of argon, krypton, and xenon in the Martian atmosphere as measured in Martian meteorites. *Geochimica Et Cosmochimica Acta* **62**(10), 1829-1835.

- (1998b) Trapped and radiogenic argon in Martian shergottites. *Meteoritics & Planetary Science* **33**(4), A19-A19.

BOGARD D. D., HORZ F. and JOHNSON P. H. (1986) Shock-Implanted Noble-Gases - an Experimental-Study with Implications for the Origin of Martian Gases in Shergottite Meteorites. *Journal of Geophysical Research-Solid Earth and Planets* **91**(B13), E99-E114.

BOGARD D. D., HUSAIN L. and NYQUIST L. E. (1979) Ar-40-Ar-39 Age of the Shergotty Achondrite and Implications for Its Post-Shock Thermal History. *Geochimica Et Cosmochimica Acta* **43**(7), 1047-1055.

BOGARD D. D. and JOHNSON P. (1983) Martian Gases in an Antarctic Meteorite. *Science* **221**(4611), 651-654.

BOGARD D. D., NYQUIST L. E. and JOHNSON P. (1984) Noble-Gas Contents of Shergottites and Implications for the Martian Origin of Snc Meteorites. *Geochimica Et Cosmochimica Acta* **48**(9), 1723-1739.

BORG L. E., NYQUIST L. E., TAYLOR L. A., WIESMANN H. and CHI-Y S. (1997) Constraints on Martian differentiation processes from Rb-Sr and Sm-Nd isotopic analyses of the basaltic shergottite QUE94201. *Geochimica Et Cosmochimica Acta* **61**(22), 4915-4931.

BREUER D., SPOHN T. and WULLNER U. (1993) Mantle Differentiation and the Crustal Dichotomy of Mars. *Planetary and Space Science* **41**(4), 269-283.

CLAYTON R. N. and MAYEDA T. K. (1983) Oxygen isotopes in eucrites, shergotties, nakhlites and chassignites. *Earth and Planetary Science Letters* **62**, 1-6.

DIXON E. T., HONDA M., MCDOUGALL I., CAMBELL I. H. and SIGURDSSON I. (2000) Preservation of near-solar neon isotopic ratios in Icelandic basalts. *Earth and Planetary Science Letters* **180**(3-4), 309-324.

DRAKE M. J., SWINDLE T. D., OWEN T. and MUSSELWHITE D. S. (1994) Fractionated martian atmosphere in the Nakhlites? *Meteoritics & Planetary Science* **29**(6), 854-859.

DREIBUS G. and WANKE H. (1985) Mars, a volatile-rich planet. *Meteoritics* **20**(abstract), 367-381.

- (1987) Volatiles on Earth and Mars - a Comparison. *Icarus* **71**(2), 225-240.

DUKE M. B. (1968) The Shergotty meteorite: Magmatic and shock metamorphic features. In *Shock Metamorphism of Natural Materials* (ed. F. a. Short), pp. 612-621. Mono Book Corp., Baltimore.

FANALE F. P., CANNON W. A. and OWEN T. (1978) Mars - Regolith Adsorption and Relative Concentrations of Atmospheric Rare-Gases. *Geophysical Research Letters* **5**(1), 77-80.

FRANCHI I. A., WRIGHT I. P., SEXTON A. S. and PILLINGER C. T. (1999) The oxygen-isotopic composition of Earth and Mars. *Meteoritics & Planetary Science* **34**(4), 657-661.

GARRISON D. H. and BOGARD D. D. (2000) Cosmogenic and trapped noble gases in the Los Angeles martian meteorite. *Meteoritics & Planetary Science* **35**, A58-A58.

GILMOUR J. D. (2000a) Discussion of xenon components (ed. K. D. Ocker), Knoxville.

- (2000b) The extinct radionuclide timescale of the early solar system. *Space Science Reviews* **92**(1-2), 123-132.

GILMOUR J. D., LYON I. C., JOHNSTON W. A. and TURNER G. (1994) Relax - an Ultrasensitive, Resonance Ionization Mass- Spectrometer for Xenon. *Review of Scientific Instruments* **65**(3), 617-625.

GILMOUR J. D., WHITBY J. A., BURGESS R. and TURNER G. (1998a) Xenon and argon isotopes in irradiated, etched Nakhla; characterizing the host of Martian atmospheric xenon. In *Workshop on the issue Martian meteorites: where do we stand and where are we going?*, pp. 18-20. Lunar and Planetary Institute, Houston, TX, United States.

GILMOUR J. D., WHITBY J. A. and TURNER G. (1998b) Xenon isotopes in irradiated ALH84001: evidence for shock-induced trapping of ancient Martian atmosphere. *Geochimica Et Cosmochimica Acta* **62**(14), 2555-2571.

- (1999) Martian atmospheric xenon contents of Nakhla mineral separates: implications for the origin of elemental mass fractionation. *Earth and Planetary Science Letters* **166**, 139-147.

- (2001) Disentangling xenon components in Nakhla: martian atmosphere, spallation and martian interior. *Geochimica Et Cosmochimica Acta* **65**(2), 343-354.

HALLIDAY A. N., WANKE H., BIRCK J. L. and CLAYTON R. N. (2001) The accretion, composition and early differentiation of Mars. *Space Science Reviews* **96**(1-4), 197-230.

HERD C. D. K. and PAPIKE J. J. (2000) Oxygen Fugacity of the Martian basalts from analysis of iron-titanium oxides: Implications for mantle-crust interaction on Mars. *Meteoritics & Planetary Science* **35**(5, Suppl).

HERD C. D. K., PAPIKE J. J. and BREARLEY A. J. (2001) Oxygen fugacity of martian basalts from electron microprobe oxygen and TEM-EELS analyses of Fe-Ti oxides. *American Mineralogist* **86**(9), 1015-1024.

HOHENBERG C. M., HUDSON B., M. K. B. and PODOSEK F. A. (1981) Xenon spallation systematics in the Angra dos Reis meteorite. *Geochimica Et Cosmochimica Acta* **45**, 1909-1915.

HONDA M., MCDOUGALL I. and PATTERSON D. (1993) Noble-gases in submarine pillow basalt glasses from Loihi and Kilauea, Hawaii--A solar component in the earth. *Geochimica Et Cosmochimica Acta* **57**(4), 859-874.

HURST G. S., PAYNE M. G., PHILLIPS R. C., DABBS J. W. T. and LEHMANN B. E. (1984) Developement of an Atom Buncher. *Journal of Applied Physics* **55**(5), 1278-1284.

JAGOUTZ E. (1991) Chronology of SNC meteorites. *Space Science Reviews* **56**, 13-22.

JAGOUTZ E., SOROWKA A., VOGEL J. D. and WÄNKE H. (1994) ALH84001: Alien or progenitor of the SNC family. *Meteoritics & Planetary Science* **29**(abstracts), 478-479.

JAKOSKY B. M. and JONES J. H. (1997) The history of Martian volatiles. *Reviews of Geophysics* **35**(1), 1-16.

JONES J. H. (1986) A discussion of isotopic systematics and mineral zoning in the shergottites: Evidence for a 180 m.y. igneous crystallization age. *Geochimica Et Cosmochimica Acta* **50**, 969-977.

- (1989) Isotopic relationships among the shergottites, the nakhlites and Chassigny. *Abstracts Submitted to the Lunar and Planetary Science Conference* **XIX**, 465-474.

LEE D. C. and HALLIDAY A. N. (1997) Core formation on Mars and differentiated asteroids. *Nature* **388**(6645), 854-857.

LODDERS K. (1998) A survey of shergottite, nakhlite, and Chassigny meteorites' whole-rock compositions. *Meteoritics & Planetary Science* **33**, A183-A190.

LONGHI J. (1991) Complex magmatic processes on Mars: Inferences from the SNC meteorites. *Abstracts Submitted to the Lunar and Planetary Science Conference* **XXI**, 695-709.

LUGMAIR G. W. and MARTI K. (1977) Sm-Nd-Pu Time-Pieces in Angra-Dos-Reis Meteorite. *Earth and Planetary Science Letters* **35**(2), 273-284.

MARTY B. and MARTI K. (2002) Signatures of early differentiation of Mars. *Earth and Planetary Science Letters* **196**(3-4), 251-263.

MATHEW K. J. (2000) Discussion of xenon components in Chassigny, ALH84001 and Nakhla (eds. J. D. Gilmour and K. D. Ocker).

MATHEW K. J., KIM J. S. and MARTI K. (1998) Martian atmospheric and indigenous components of xenon and nitrogen in the Shergotty, Nakhla and Chassigny group meteorites. *Meteoritics & Planetary Science* **33**, 655-656.

MATHEW K. J. and MARTI K. (2001) Early evolution of Martian volatiles: Nitrogen and noble gas components in ALH84001 and Chassigny. *Journal of Geophysical Research* **106**, 1401-1422.

MCSWEEN H. Y. and STOLPER E. M. (1979) Allan Hills 77005 : A new meteorite type found in Antarctica. *Science* **204**, 1201-1203.

MCSWEEN H. Y. J. (1994) What we have learned about Mars from SNC meteorites. *Meteoritics & Planetary Science* **29**, 757-779.

MCSWEEN H. Y. J. and JAROSEWICH E. (1983) Petrogenesis of the EETA79001 meteorite: Multiple magma pulses on the shergottite parent body. *Geochimica Et Cosmochimica Acta* **47**, 1501-1513.

MIKOUCHI T., MIYAMOTO M. and MCKAY G. A. (2001) Mineralogy and petrology of the Dar al Gani 476 martian meteorite: Implications for its cooling history and relationship to other shergottites. *Meteoritics & Planetary Science* **36**(4), 531-548.

MIURA Y. N., NAGAO K., SUGIURA N., SAGAWA H. and MATSUBARA K. (1995) Orthopyroxenite ALH84001 and Shergottite ALH77005 - additional evidence for a martian origin from noble gases. *Geochimica Et Cosmochimica Acta* **59**(10), 2105-2113.

MOHAPATRA R. K. and OTT U. (2000) Trapped noble gases in Sayh al Uhaymir 005: A new martian meteorite from Oman. *Meteoritics & Planetary Science* **35**, A113-A113.

MURTY S. V. S. and MOHAPATRA R. K. (1997) Nitrogen and heavy noble gases in ALH84001: Signature of ancient Martian atmosphere. *Geochimica Et Cosmochimica Acta* **61**(24), 5417-5428.

MUSSELWHITE D. S. and DRAKE M. J. (2000) Early outgassing of Mars: Implications from experimentally determined solubility of iodine in silicate magmas. *Icarus* **148**(1), 160-175.

MUSSELWHITE D. S., DRAKE M. J. and SWINDLE T. D. (1991) Early Outgassing of Mars Supported by Differential Water Solubility of Iodine and Xenon. *Nature* **352**(6337), 697-699.

MUSSELWHITE D. S. and SWINDLE T. D. (2001) Is release of martian atmosphere from polar clathrate the cause of the nakhlite and ALH84001 Ar/Kr/Xe ratios? *Icarus* **154**(1), 207-215.

NORMAN M. D. (1999) The composition and thickness of the crust of Mars estimated from rare earth elements and neodymium-isotopic compositions of Martian meteorites. *Meteoritics & Planetary Science* **34**(3), 439-449.

NYQUIST L. E., BOGARD D., WOODEN J., WIESMANN H., SHIH C. Y., BANSAL B. and MCKAY G. (1979a) Early Differentiation, Late Magmatism and Recent Bombardment on the Shergottite Parent Planet. *Meteoritics* **14**, 502.

NYQUIST L. E., BOGARD D. D., SHIH C. Y., GRESHAKE A., STOFFLER D. and EUGSTER O. (2001) Ages and geologic histories of Martian meteorites. *Space Science Reviews* **96**(1-4), 105-164.

NYQUIST L. E., WOODEN J., BANSAL B., WIESMANN H., MCKAY G. and BOGARD D. D. (1979b) Rb-Sr Age of the Shergotty Achondrite and Implications for Metamorphic Resetting of Isochron Ages. *Geochimica Et Cosmochimica Acta* **43**(7), 1057-1074.

OCKER K. D. and GILMOUR J. D. (2001) Martian atmospheric and 'interior' xenon components in Shergotty mineral separates. *Meteoritics* **36**(9 abstracts), A152.

OTT U. (1988) Noble gases in SNC meteorites: Shergotty, Nakhla, Chassigny. *Geochimica Et Cosmochimica Acta* **52**(7), 1937-1948.

OTT U. and LOHR H. P. (1992) Noble gases in the new shergottite LEW88516. *Meteoritics & Planetary Science* **27**(3, Suppl), 271.

OTT U., LOHR H. P. and BEGEMANN F. (1988) New noble gas data for SNC meteorites: Zagami, Lafayette and etched Nakhla. *Meteoritics & Planetary Science* **23**(3, abstracts), 295-296.

OWEN T., BIEMANN K., RUSHNECK D. R., BILLER J. E., HOWARTH D. W. and LAFLEUR A. L. (1977) The composition of the atmosphere at the surface of Mars. *Journal of Geophysical Research* **82**(28), 4635-4639.

OZIMA M. and POSOSEK F. A. (1983) *Noble gas Geochemistry*. Cambridge University Press, Cambridge. pp. 367.

PAYNE M. G., DENG L. and THONNARD N. (1994) Applications of Resonance Ionization Mass-Spectrometry. *Review of Scientific Instruments* **65**(8), 2433-2459.

PEPIN R. O. (1991) On the Origin and Early Evolution of Terrestrial Planet Atmospheres and Meteoritic Volatiles. *Icarus* **92**(1), 2-79.

- (1994) Evolution of the Martian Atmosphere. *Icarus* **111**(2), 289-304.

PODOSEK F. A. (1973) Thermal History of Nakhlites by Ar-40-Ar-39 Method. *Earth and Planetary Science Letters* **19**(2), 135-144.

PODOSEK F. A. and HUNEKE J. C. (1971) Isotopic Composition of Pu-244 Fission Xenon in Meteorites - Reevaluation Using Lunar Spallation Xenon Systematics. *Earth and Planetary Science Letters* **12**(1), 73-&.

PODOSEK F. A., HUNEKE J. C., BURNETT D. S. and WASSERBURG G. J. (1971) Isotopic composition of xenon and krypton in the lunar soil and in the solar wind. *Earth and Planetary Science Letters* **10**, 199-216.

PORCELLI D. and WASSERBURG G. J. (1995) Mass-Transfer of Xenon through a Steady-State Upper-Mantle. *Geochimica Et Cosmochimica Acta* **59**(10), 1991-2007.

SHIH C. Y., NYQUIST L. E., BOGARD D. D., MCKAY G. A., WOODEN J. L., BANSAL B. M. and WIESMANN H. (1982) Chronology and Petrogenesis of Young Achondrites, Shergotty, Zagami, and Alha77005 - Late Magmatism on a Geologically Active Planet. *Geochimica Et Cosmochimica Acta* **46**(11), 2323-2344.

SHUKOLYUKOV A. and BEGEMANN F. (1996) Pu-Xe dating of eucrites. *Geochimica Et Cosmochimica Acta* **60**(13), 2453-2471.

SMITH J. V. and HERVIG R. L. (1979) Shergotty meteorite: Mineralogy, petrology and minor elements. *Meteoritics & Planetary Science* **14**, 121-142.

STÖFFLER D., OSTERTAG R., JAMMES C., PFANNSCHMIDT G., SEN GUPTA P. R., SIMON S. B., PAPIKE J. J. and BEAUCHAMP R. H. (1986) Shock metamorphism and petrology of the Shergotty achondrite. *Geochimica Et Cosmochimica Acta* **50**, 889-904.

STOLPER E. M. and MCSWEEN H. Y. J. (1979) Petrology and origin of the shergottite meteorites. *Geochimica Et Cosmochimica Acta* **43**, 1475-1498.

SWINDLE T. D., CAFFEE M. W. and HOHENBERG C. M. (1986) Xenon and other noble gases in shergottites. *Geochimica Et Cosmochimica Acta* **50**(6), 1001-1015.

SWINDLE T. D., GRIER J. A. and BURKLAND M. K. (1995) Noble gases in orthopyroxenite ALH84001: A different kind of martian meteorite with an atmospheric signature. *Geochimica Et Cosmochimica Acta* **59**(4), 793-801.

SWINDLE T. D., HOHENBERG C. M., NICHOLS R. H., OLINGER C. T. and GARRISON D. H. (1989) Excess Fission Xenon in Meteorites. *Meteoritics* **24**(4), 330-330.

SWINDLE T. D. and JONES J. H. (1997) The xenon isotopic composition of the primordial Martian atmosphere: Contributions from solar and fission components. *Journal of Geophysical Research-Planets* **102**(E1), 1671-1678.

SWINDLE T. D. and KRING D. A. (1997) Implications of small comets for the noble gas inventories of Earth and Mars. *Geophysical Research Letters* **24**(24), 3113-3116.

SWINDLE T. D., TREIMAN A. H., LINDSTROM D. J., BURKLAND M. K., COHEN B. A., GRIER J. A., LI B. and OLSON E. K. (2000) Noble gases in iddingsite from the Lafayette meteorite: Evidence for liquid water on Mars in the last few hundred million years. *Meteoritics & Planetary Science* **35**(1), 107-115.

TERRIBILINI D. (2000) Edelgasisotopenanalysen und Bestrahlungsgeschichte von estraterrestrischen Gestein- und Metallproben. Doctoral thesis. Univerity of Bern.

THONNARD N., PAYNE M. G., WRIGHT M. C. and SCHMITT H. W. (1984) Noble-Gas Atom Counting Using Ris and Tof Mass-Spectrometry. *Institute of Physics Conference Series*(71), 227-234.

THONNARD N., WRIGHT M. C., DAVIS W. A. and WILLIS R. D. (1992) The 2nd-Generation Ris-Tof Noble-Gas Detector - Detection Limits Below 100 Atoms in Less-Than 5 Minutes. *Institute of Physics Conference Series*(128), 27-30.

WADHWA M. (2001) Redox state of Mars' upper mantle and crust from Eu anomalies in shergottite pyroxenes. *Science* **291**(5508), 1527-1530.

WASSON J. T. and WETHERILL G. W. (1979) Dynamical, Chemical and Isotopic Evidence regarding the Formation Locations of Asteroids and Meteorites. In *Asteroids* (ed. T. Gehrels), pp. 926-974. University of Arizona Press, Tucson.

WETHERILL G. W. (1986) Accumulation of the terrestrial planets and implications concerning lunar origin. In *Origin of the Moon* (eds. W. K. Hartmann, R. J. Phillips and G. J. Taylor), pp. 519-550. Lunar and Planetary Institute, Houston.

WIENS R. C. (1988) Noble gases released by vacuum crushing of EETA79001 glass. *Earth and Planetary Science Letters* **91**, 55-65.

WIENS R. C. and PEPIN R. O. (1986) Laboratory Shock Emplacement of Low Ambient Pressure Gases into Basalt - Relation to Eeta79001 Trapped Gas. *Meteoritics* **21**(4), 540-540.

- (1988) Laboratory Shock Emplacement of Noble-Gases, Nitrogen, and Carbon-Dioxide into Basalt, and Implications for Trapped Gases in Shergottie Eeta-79001. *Geochimica Et Cosmochimica Acta* **52**(2), 295-307.

APPENDIXES

APPENDIX A

THE STATUS OF KRYPTON ANALYSES AT THE INSTITUTE FOR RARE ISOTOPE MEASUREMENTS

The original dissertation research was to modify the resonance ionization spectroscopy system at the University of Tennessee's Institute for Rare Isotope Measurements (IRIM) for krypton isotope analysis from minute extraterrestrial samples. Previously the system had only been utilized for measurements of the rare ^{81}Kr and ^{85}Kr isotopes in environmental applications. As little work had been done with krypton in the planetary sciences, this project would compliment the pioneering work on xenon by the Manchester group with their ultra-sensitive resonance ionization mass spectrometer, RELAX. Because of delays due to technical difficulties in getting the IRIM system into full operation, and taking advantage of the presence of Dr. Gilmour from Manchester at IRIM during his sabbatical, it was decided to shift the dissertation to xenon research using the Manchester facilities. But, as considerable practical experience in resonance ionization and noble gas spectrometry applicable to xenon work was gained, progress on the krypton system is described below.

Completed work focused on upgrading and building the laser-microprobe resonance ionization spectroscopy time-of-flight mass spectrometry (LM RIS-TOF) system for the analysis of krypton isotopes. This work included: the purchase and installation of a new resonance ionization laser system; upgrade of the existing vacuum

system; the design and employment of a new sample chamber; design and employment of a new gas standard calibration system; and the design and installation of the laser microprobe. The complete LM RIS-TOF system is shown in Figure A-1. The main sections are (1) the time-of-flight mass spectrometer, (2) the resonance ionization spectroscopy laser system, (3) the vacuum system, (4) the sample chamber, and (5) the microprobe laser.

Mass Spectrometer

Noble gases are released into the static time-of-flight (TOF) mass spectrometry by the laser microprobe. The TOF has a unique feature called an "atom buncher," to concentrate the noble gas atoms in the region of space probed by the resonance ionization spectroscopy (RIS) lasers. This consists of a cold finger, which collects the atoms in the chamber, coupled to a pulsed laser fired a few microseconds before the RIS lasers, that heats the cold finger, causing the condensed atoms to desorb in synchronism with the RIS lasers (see Figure A-2).

The TOF employs second-order time focusing to achieve a resolution $M/\Delta M$ of greater than 1200. Data is collected with a transiet digitizer having 0.5 ns time resolution, while a real-time computer system allows simultaneous collection of all noble gas isotopes. For krypton at optimal tuning, in 10 minutes, typically more than 90% of the krypton atoms in the mass spectrometer have been counted. The entire system is contained in an all-metal ultra-high vacuum housing that is evacuated by ion pumps to pressures below $1x10^{-10}$ Torr when the system is not processing a sample. The vacuum is

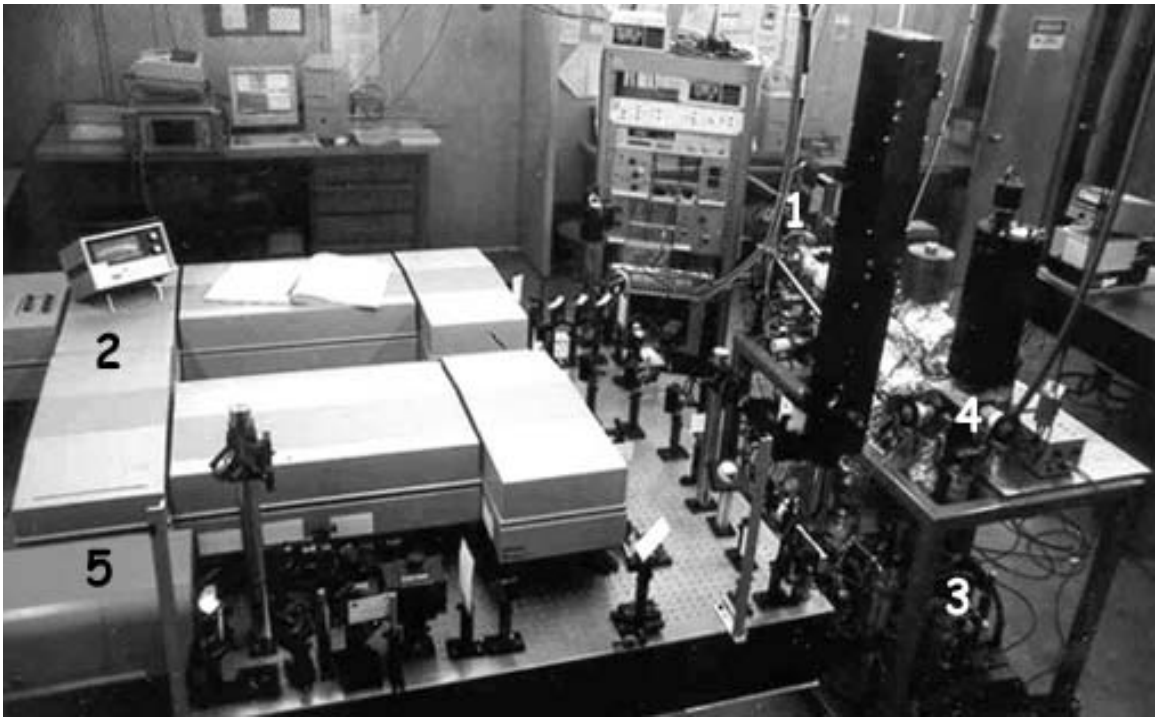

Figure A-1. The laser microprobe resonance ionization spectroscopy time-of-flight mass spectrometer (LM RIS-TOF) as housed at the Institute for Rare Isotope Measurements (IRIM). The numbers (1-5) correspond to the main sections as described in the text.

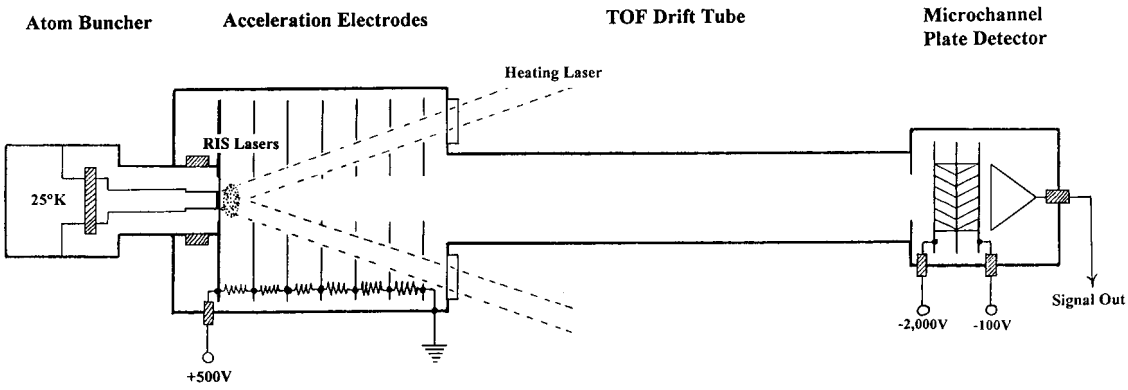

Figure A-2. Schematic of the time-of-flight mass spectrometer illustrating relative positions of the cold finger, heating laser, and the RIS lasers. The ionized atoms are accelerated and sent down the TOF drift tube to a microchannel plate detector. The resulting signal is digitized and processed by a dedicated computer.

monitored by the ion pump controller, as well as an additional ionization gauge attached to the TOF tube. Furthermore, the system can be heated to about 250°C for additional cleaning and low background maintenance. Modifications to the mass spectrometer included the addition of all metal bakeable values to the new sample chamber, and a new gas standard inlet system.

The gas standard inlet system, designed and added to the RIS-TOF system, utilizes a series of calculated and measured expansion ratios to introduce as few as 10^4 to 10^5 noble gas atoms. This new gas standard inlet system eliminated uncertainties due to the scattering that was noted from the previous $1{:}10^5$ Kr:Ar mixture calibration technique. This calibration system allows detail studies, thus determining the reproducibility and stability of the overall system necessary for accurate isotope ratio measurements and for reliable background subtraction.

Resonance Ionization Spectroscopy Laser System

The RIS-TOF system utilizes lasers tuned to specific atomic energy levels of the analyte element, thus producing only ions of the chosen element, which currently is krypton. The system includes two Continuum ND-6000 tunable dye lasers and one custom-built dye laser, all pumped by a Continuum PL-8010 Nd-YAG laser operating at 10 Hz repetition rate. Non-linear doubling and mixing crystals convert the dye laser output to the wavelength required for RIS. Purchase of the new more powerful Continuum lasers, combined with careful design, layout and alignment of the optics guiding the eight required wavelengths, provides simultaneous arrival of the photons at

the correct location within the mass spectrometer resulting in stable resonance ionization spectroscopy.

Resonance ionization of krypton and generation of the shortest wavelength is shown in Figure A-3. The first excitation step of the krypton RIS scheme requires a photon at 116.5 nm, and is achieved by a non-linear process known as four-wave mixing in a Xe/Ar gas mixture. This allows a single resonance transition of high oscillator strength, not only reducing the power required by many orders of magnitude, but greatly increases the element selectivity in the ionization process by elimination multiphoton nonresonant ionization of impurities. Two 252.5 nm photons excite xenon to the 6p state. Using a slightly higher energy than the energy difference to the 7s state, a third photon at 1507.3 nm is added which stimulates a transition to the ground state and emission of the 116.5 nm photon. Once excited to the 5s state, krypton is excited to the 6p state with a 558.1 nm photon and finally into the ionization continuum using a 1064.0 nm photon.

Vacuum Pumping System

In addition to the ion pumps attached to the TOF, an auxiliary pumping system is provided to evacuate the sample chambers after sample loading, and maintains a high vacuum (x 10^{-9} Torr) within the portions of the system that are not on line to the mass spectrometer. A wide-range turbo molecular vacuum pump has been installed to reduce the base pressure and permit baking of the ion pumps. A rotary pump backs this pump, with a molecular sieve trap in between to prevent any oil vapor back-flow from the rotary pump. In an attempt to further reduce background, copper gaskets were replaced with

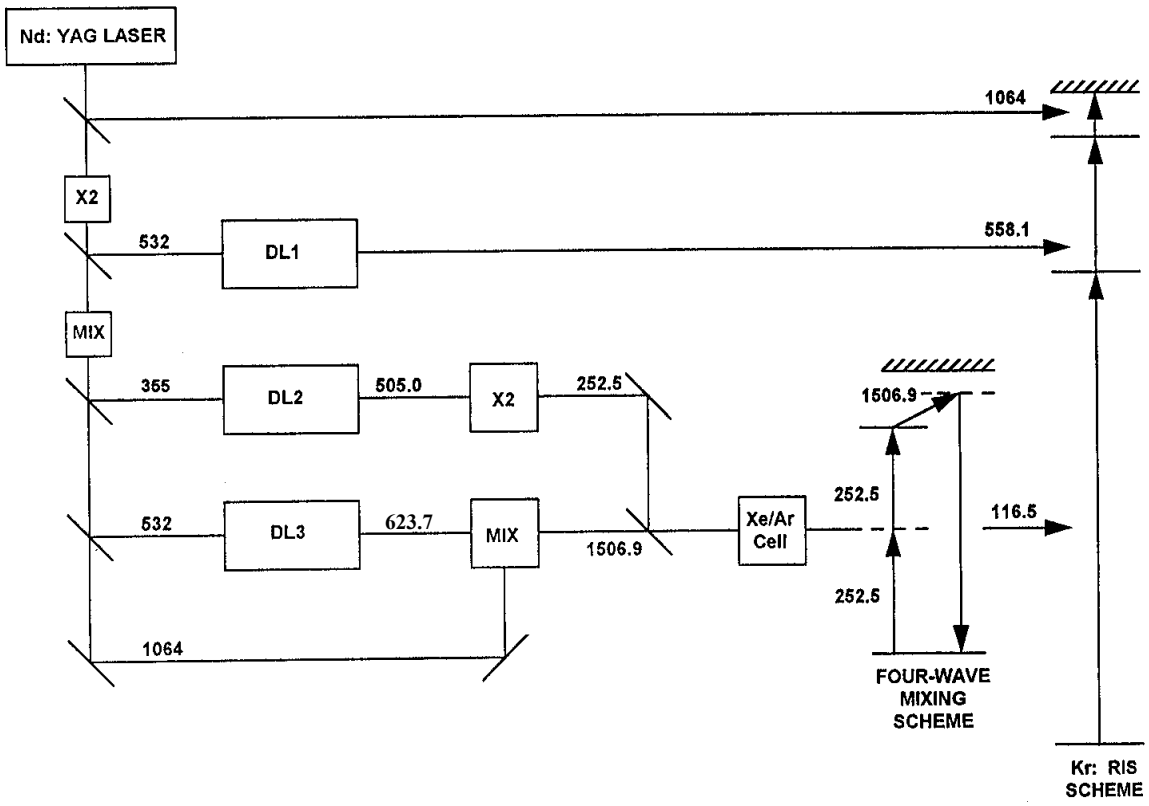

Figure A-3. Schematic of the resonance ionization spectroscopy (RIS) laser system. The Nd:YAG laser, operating at 1064 nm, pumps 3 dye lasers to generate the specific wavelengths required for the ionization of krypton. See text for further details of ionization sequence.

silver plated gaskets to maintain tighter seals. Likewise, much of the system's plumbing is configured to enable baking of the entire system at 250° to 300°C. To protect the vacuum during power failures, pneumatic values were installed to close and isolate various parts of the system.

Sample Chamber

The sample chamber is constructed from two stainless steel vacuum flanges. The chamber is mounted to the mechanical stage via a flexible welded bellows attached beneath the bottom flange, permitting ± 0.5 inch movement of the sample chamber in three orthogonal directions under the laser-probe microscope. The bellows is connected to a rigid cube that allows gas flow to the TOF and/or to the vacuum system through respective valves. The top flange of the chamber has an optical window, through which the sample can be viewed. The optical window is constructed of sapphire, which results in less krypton trapping than quartz and permits essentially all the laser's energy to pass without any absorption. The bottom flange is customized to hold optically thick samples, or small separated grains, depending on sample used. To prevent damage to the underside of the sapphire window, a thin sapphire cover slip is placed over the sample. The cover slip acts as a shield, becoming coated with material that would otherwise cover the window and is replaced each time the sample is changed. Direct lighting is provided by a light source that is reflected onto the sample by a pellicle beam splitter mounted in the laser microprobe viewing system. Diffuse light is from a series of miniature

incandescent bulbs mounted at the periphery of the sapphire window. These light sources can be adjusted independently to optimize the visibility of sample morphology.

Laser Microprobe

The microscope has been custom-built to accommodate the laser, a video camera, and the sample vacuum chamber. The video camera permits optical viewing of the sample before and after laser-desorption. An X-Y-Z translation stage permits proper focusing, alignment and rastering of the sample with the laser beam.

The 1064 nm wavelength beam of an Nd:YAG laser is doubled twice by nonlinear crystals to generate ultraviolet light at 266 nm for probing the sample. The collimated 266 nm beam is reflected by a dichroic beamsplitter set at 45° and focused onto the sample with a 40 mm focal length objective optimized for high-power UV laser pulses. Visible light from the sample surface passes through the dichroic beamsplitter to the video camera through a three position custom optical turret that provides overall field of views of 40 mm, 4.0 mm and 0.4 mm (See Appendix B).

APPENDIX B

VERSATILE SAMPLE VIEWING SYSTEM WITH LARGE MAGNIFICATION RANGE

This chapter is a slightly modified revision of a paper by the same name published in the journal *Review of Scientific Instruments* in 2000 by Katherine Ocker, Norbert Thonnard and Charles Joyner:

K. D. Ocker, N. Thonnard, and C. F. Joyner, Versatile sample viewing with large magnification range. *Review of Scientific Instruments* **71**(2), 581-582, (2002).

My contributions to the work reported in this paper include (1) detailed design of the viewing system, (2) assembly of the viewing system, (3) testing of the viewing system and laser microprobing gas extraction system, and (4) most of the writing.

Abstract

A sample viewing system has been designed and constructed to assist in the *in situ* analysis of terrestrial and extraterrestrial samples by laser microprobe gas extraction. The system provides sample-viewing fields of 36 mm, 3.3 mm and 370 μm, and combines and focuses the microprobing UV laser beam onto the sample being studied.

With the increased desire to obtain isotopic data from extremely small regions, or even from micron-sized single interstellar grains, an *in situ* gas extraction system

utilizing UV laser microprobing has been coupled to a resonance ionization spectroscopy time-of-flight (RIS-TOF) mass spectrometer system. The RIS-TOF mass spectrometer is an extremely fast analyzer having demonstrated a detection limit of ~100 ^{85}Kr atoms (Thonnard, 1995; Thonnard et al., 1992). This laser microprobing system consists of three components: 1) a sample viewing system (described here), 2) a Nd-YAG laser and associated optics, and 3) a noble gas extraction chamber.

The selection of a viewing system presents a considerable challenge, as it is desirable to see the entire 36 mm diameter sample region, while still having the option of zeroing in on few micron-sized interstellar grains. The system has to introduce, as well as focus, the UV microprobing beam collinearly with the viewing beam. And finally, it has to maintain a sufficient working distance (>35 mm) so that the separation between the vacuum window and the sample surface is sufficient to prevent damage to the window.

The adopted design, shown in Figure B-1, consists of three regions, all with lenses set at infinite conjugate ratio, which minimizes spherical aberration when using off-the-shelf achromatic lenses (Smith, 1997). In region I, the UV microprobing beam is combined with the visible viewing beam using a dichroic beam splitter reflecting 266 nm radiation. For the high (A) and medium (B) power modes, the beam is focused onto the sample surface with a 40 mm focal length (5X) triplet microscope objective optimized for diffraction limited performance (3 μm spot) at 266 nm. The microscope objective also serves as the first element of the viewing system. Region II contains three sets of relay lenses providing sample-viewing fields of 36 mm, 3.3 mm and 370 μm. The different

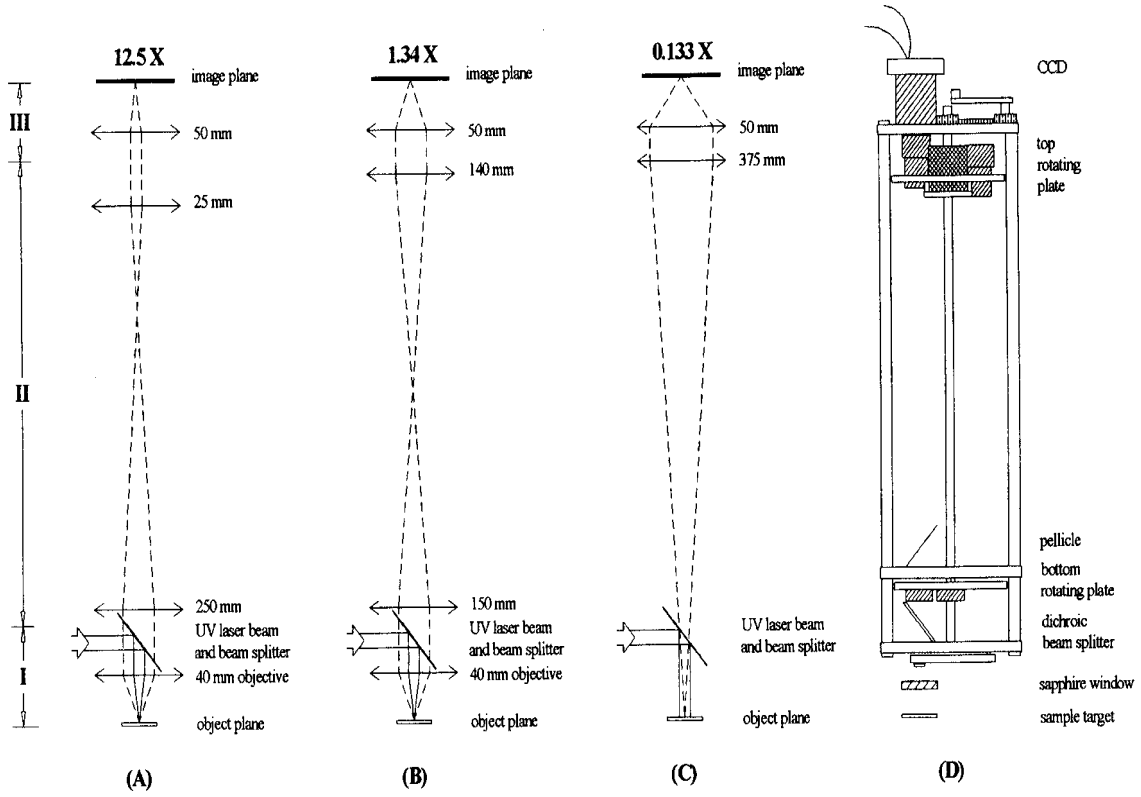

Figure B-1. Schematic of the viewing system and microprobing laser beam delivery system for *in situ* laser gas extraction at micron-sized scales showing high-power (A), medium-power (B) and low-power (C) viewing optics. The mechanical arrangement (D) consists of a central shaft that rotates two disks onto which the magnification changing optics of region II are mounted, permitting changing the viewing field by turning a single knob.

magnifications provide viewing of the entire sample chamber, Figure B-2 (A), thus allowing proper identification and location on the sample, down to details less than 2 μm, as shown in Figure B-2 (C inset). Region III focuses the collimated beam exiting region II onto a 1/3" format (4.8 x 3.6 mm) single-board, high resolution (768 x 494 pixels), monochrome CCD sensor with an F1.8, 50 mm f.l. camera lens.

The transfer of the image from regions I to II, and from II to III by collimated beams, results in significant flexibility in design and placement of the optics. In Figure B-1 (A), for example, the distance between the 40 mm objective in region I and the 250 mm lens in region II can be changed arbitrarily (except for vignetting problems) to accommodate other optics, such as the 266 nm beam splitter, without changing the magnification or having to adjust the focus of the lenses. Similarly, the distance between the upper relay lens of region II to the 50 mm camera lens in region III is also arbitrary. This permits selection of the magnification (set by the product of the focal length ratios of the lens pairs) to meet the viewing needs using stock, commercially available, two-element achromats. For the wide-field view, Figure B-1 (C), the image is relayed to the CCD camera by a single 375 mm f.l. achromat.

A simplified side-view of the viewing system is shown in Figure B-1 (D). The relay lenses of region II are mounted on two co-rotating disks. The shaft that operates the disks also operates a cam that swings the 40 mm objective that is mounted on an arm out of the optical path in the wide-field of view setting. The sample is illuminated by a combination of miniature incandescent lamps surrounding the optical axis at the bottom

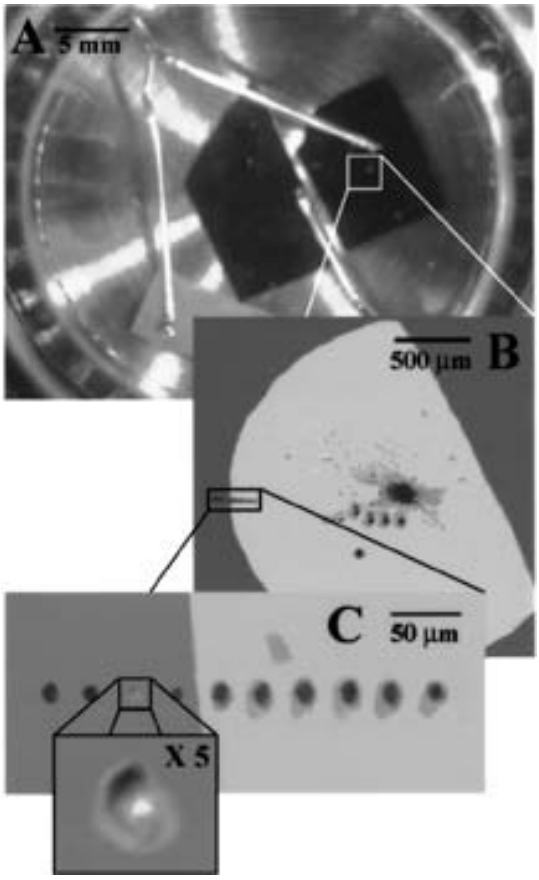

Figure B-2. Images captured by a digital frame grabber of krypton-implanted silicon samples used to test the laser microprobing gas extraction system. Due to alteration of the silicon structure, the implanted areas appear lighter. At the lowest magnification, the entire sample chamber showing three silicon samples is visible (A). At medium (B) and high (C) magnification, we zero in on a specific region of the sample. The string of craters in (C), separated by 30 μm, is due to single UV laser pulses. Their diameter depends on the pulse energy. To show details as small as 2 μm can be resolved, a portion of (C) has been enlarged by a factor of five, inset.

mounting plate, and a collimated beam from a 5 W quartz-iodide incandescent bulb that enters the system through a pellicle beam splitter.

The ablating laser beam is generated by a quadrupled Q-switched Nd-YAG laser, delivering up to 5 mJ per pulse at 266 nm. Although only 10-20 μJ pulse energy is sufficient in the microprobing mode (~10 μm typical crater size), the higher pulse energy is useful for extracting gas from larger areas (up to 200 μm diameter) with a single laser pulse. The beam passes through a continuously variable attenuator to adjust the laser pulse energy delivered to the sample, a spatial filter to smooth out the intensity distribution of the laser beam, and a beam expander to match the entrance aperture of the focusing lens. The beam expander can also be adjusted to increase the size of the beam spot on the sample when desired.

The viewing system and microprobing laser system beams are fixed relative to the mass spectrometer. Instead, the noble gas sample extraction chamber, which is sealed with a sapphire window and is connected to the mass spectrometer through a welded bellows, can be position to within 1 μm with a three-axis manipulator having 25 mm travel in each axis.

Tests of the laser microprobing gas extraction system and sample viewing system were performed using silicon wafers that had previously been ion implanted with known amounts of krypton (Ocker and Thonnard, 1999). The wide magnification range made it easy to identify both the general location and precise position of the region being

investigated. Once the lenses in region II were properly collimated, the registration of the images was excellent when switching from one magnification to the next. Overall, the system has been extremely useful in developing the *in situ* microsampling gas extraction protocols by providing instant feedback on the results of specific laser microprobe operating parameters.

This research was supported in part by a grant from the NASA Office of Space Sciences under Grant NAG5-3464.

List of References

OCKER K. D. and THONNARD N. (1999) The path to krypton and xenon isotope measurements from few-micron sized samples; II. Pulsed UV laser microprobing. *Abstracts Submitted to the Lunar and Planetary Science Conference* **XXX**, CD# 1622.

SMITH W. J. (1997) Practical Optical System Layout and Use of Stock Lenses, edited by Robert E. Fischer and Warren J. Smith (eds. R. E. Fisher and W. J. Smith). McGraw-Hill, New York.

THONNARD N. (1995) Resonance Ionization: Potential Application of Few-Atom Detection Techniques to Inter-Planetary Dust Particle and 'Stardust Studies. *Abstracts Submitted to the Lunar and Planetary Science Conference* **XXVI**, 1411-1412.

THONNARD N., WRIGHT M. C., DAVIS W. A. and WILLIS R. D. (1992) The 2nd-Generation Ris-Tof Noble-Gas Detector - Detection Limits Below 100 Atoms in Less-Than 5 Minutes. *Institute of Physics Conference Series*(128), 27-30.

VITA

Katherine D. Ocker Stone was born in West Monroe, Louisiana on April 6, 1972. She was raised in Texas, attending K-12 classes in the Conroe Independent School District. She graduated from Conroe High School in 1989, ranked 36 out of 698 students.

From there, she went to Sam Houston State University in Huntsville, TX and received a B. S. in physics in 1994. Continuing at Sam Houston, she obtained her M. S. in physics in 1995. She then transferred to Knoxville, TN to attend the University of Tennessee for her doctoral studies in geological sciences, specializing in planetary science. It was during this time that she met and married Chris Stone in June 1999. She received her doctorate in 2002.

Katherine has accepted a research associate position at the Institute for Rare Isotope Measurements affiliated with the University of Tennessee, Knoxville.